An Isotopic and Fluid Inclusion Study of the Rock Canyon Creek, Fluorite-REE Deposit, southeastern British Columbia

By

Lichun Zhu

A Thesis

Submitted to the College of Graduate Studies and Research

Through the Department of Earth Sciences

In Partial Fulfillment of the Requirements for

The Degree of Master of Science at the

University of Windsor.

Windsor, Ontario, Canada

2000

ABSTRACT

The Rock Canyon Creek fluorite-REE deposit is hosted by a Cambro-Ordovician to Devonian carbonate-dominated sedimentary sequence in southeastern British Columbia. The most widespread mineralization consists of disseminated, vein and breccia-matrix fluorite with associated barite and a variety of REE minerals, which indicate that the deposit is hydrothermal and epigenetic.

Mineralization is associated closely with hydrothermal alteration of carbonates as evidenced by the extensively dolomitized host rock and the common assemblage of saddle dolomite, fluorite, quartz and calcite in open space. Five types of dolomite have been identified: (1) microdolomite; (2) replacement, non-ferroan dolomite; (3) saddle dolomite I, (4) coarse, ferroan dolomite, and (5) saddle dolomite II. Some Ordovician microdolomite falls in the isotopic range of typical Ordovician marine carbonates. Non-ferroan dolomite, which predates mineralization, is more depleted in ^{18}O and ^{13}C than microdolomite. The precipitation of saddle dolomite I, which predates mineralization, is related to veins and vugs. Geochemical and petrographic evidence suggest that saddle dolomite I and non-ferroan dolomite were precipitated from a hot, slightly saline fluid. Pervasive coarse ferroan dolomite occurs in most host rocks to the fluorite-REE mineralization. Both oxygen and carbon isotopic values (-14.06 to -15.21‰ VPDB for $\delta^{18}O$, and -0.61 to -1.47‰ VPDB for $\delta^{13}C$) for ferroan dolomite are similar to those of other epigenetic dolomites from the southern Rocky Mountains, but their distinctive $^{87}Sr/^{86}Sr$ ratios (0.70340 to 0.70460) (Kerferg and Muehlanbaches, 1997) are comparable to mantle values and indicate that ferroan dolomite was precipitated from carbonatite-derived F-REE fluid. Saddle dolomite II occurs in open space associated with fluorite and quartz, has similar isotopic compositions to ferroan dolomite and is suggested to have precipitated from the same fluid as that which precipitated ferroan dolomite. Late calcite, which postdates mineralization, typically has low $\delta^{13}C$ values (-0.73 to −7.14 ‰ VPDB) and radiogenic $^{87}Sr/^{86}Sr$ ratios (0.70999) which is similar to those of Laramide vein carbonates along the Rocky Mountains and suggests the precipitation of late calcite from a hot, saline fluid. The recrystallization of limestone resulted from the water/rock interaction that occurred during the passage of this fluid through the study area. The

occurrence of fluorite to the west of the thrust fault indicates that the mineralization postdates the Laramide Orogeny. This contradicts the previous suggestion that the mineralization is Devonian-Mississippian to early Mississippian in age.

Acknowledgements

TABLE OF CONTENTS

LIST OF FIGURES

LIST OF TABLES

Table

LIST OF PLATES

Plate

CHAPTER I
Introduction

1.1 Introduction

The Rock Canyon Creek fluorite-REE deposit is located in southeastern British Columbia near the Alberta border in the Main Ranges of the Rocky Mountains Foreland belt. The deposit is hosted by a sequence of Ordovician to Devonian sedimentary rocks which are dominated by carbonate rocks with lesser amounts of shales and sandstones. The deposit lies just east of westwardly-dipping thrust faults which place Cambro-Ordovician rocks over Upper Ordovician and Middle Devonian rocks. The deposit is near the headwaters of Rock Canyon Creek, approximately 40 kilometres east of Canal Flats, B.C., at 50°12'N, 115°08'W. It can be accessed by conventional vehicles along the White River and Canyon Creek forestry roads, which join highway 3A, 2 kilometres south of Canal Flats.

Fluorite mineralization at Rock Canyon Creek was first discovered by Chris Graf in 1977 during a regional exploration program for Paleozoic, carbonate-hosted Mississippi Valley-type zinc-lead mineralization funded by Riocanex. Further exploration work for Zn, Pb, Ag, and fluorite was carried out in 1978 and 1979, which included trenching, soil and rock geochemistry. In 1980 the claims were returned to Chris Graf, who had several samples analyzed for REE, which were found to contain up to 2.3 wt. % total REE. Between 1985 and 1991, exploration focused on the search for rare elements, such as REE and Nb. This exploration work, which extended the soil sampling coverage and included detailed structural mapping, outlined an elongate zone of hydrothermal alteration and mineralization that is over 2 km in length and up to 200 m wide (Fig.1.1). No drilling has been carried out so that the subsurface extent of the mineralization is still unknown. Access is excellent, but exposure is poor due to thick glacial drift cover.

1.2 Previous Studies

The study area has been mapped at various scales by Bending (1978), Leech (1979), Norsford (1981), Mott et al. (1986), Pell and Hora (1987) and Dix (1991). There

1
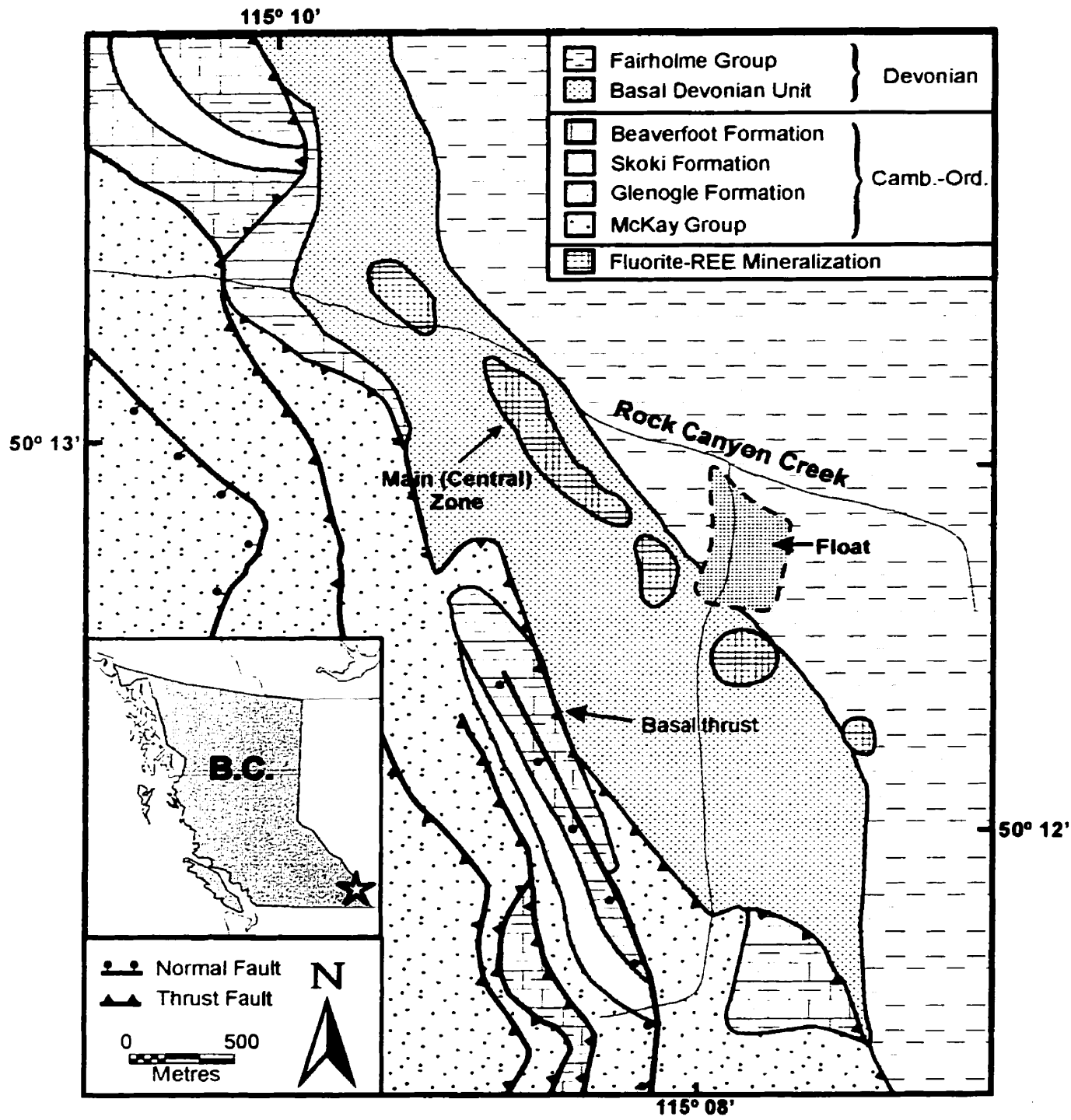
Fig. 1.1. Geology of the Rock Canyon Creek Fluorite-REE Deposit from Samson et al. (1999)
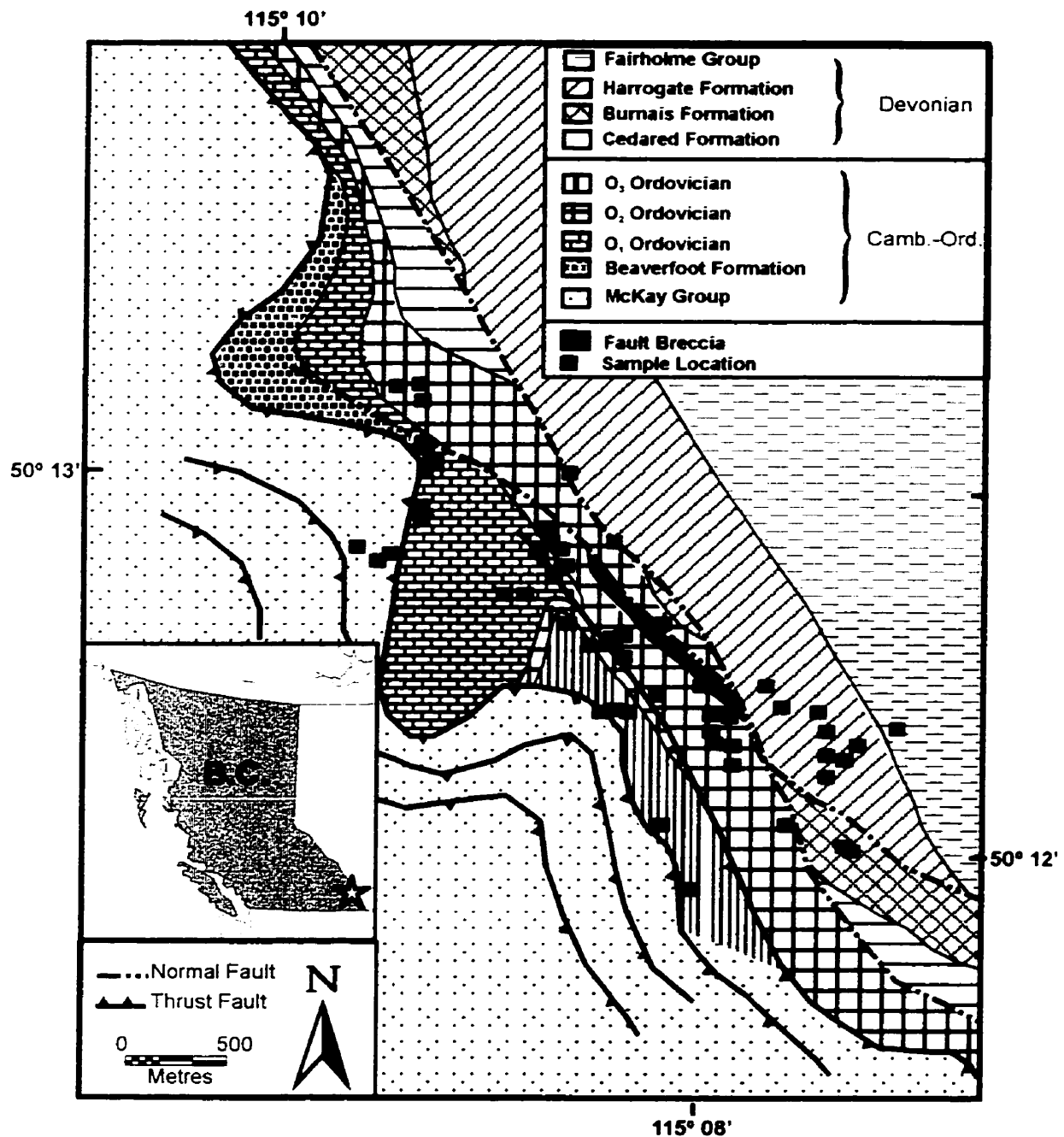
Fig. 1.2. Geology of Rock Canyon Creek Fluorite-REE Deposit also Showing the Sample Location, Modified from Dix (1991).

have been no detailed studies to date, however, that concentrate on the stratigraphy of the Rock Canyon Creek area. Rocks immediately east of the most easterly (basal) thrust, and which host the deposit, are considered by most authors to be a basal Devonian unit (Fig.1.1). The basal Devonian unit regionally rests on a major unconformity. Dix (1991), however, interpreted these rocks to be, at least in part, Ordovician in age (Fig.1.2). The difficulty in interpreting the age results from the complicated structure, caused by faulting and overturning of the sequence, and similar fossil contents in the rocks, as well as the intense alteration associated with the mineralization. One of the major differences between the interpretation of Dix (1991) and earlier workers is that Dix (1991) suggested that the mineralization is fault controlled and bounded and cut by high-angle reverse faults, whereas earlier authors believed it to be stratabound and unrelated to high-angle faulting (Pell and Hora, 1987; Hora and Kwong, 1986; Pell and Fontaine, 1988; Pell; 1992).

An understanding of the processes affecting the distribution and concentration of the rare earth elements (REE) is important in many respects. Only a few primary magmatic occurrences of REE are known (e.g. Mountain Pass, California) whereas a number of REE deposits are interpreted to be hydrothermal in origin (e.g. Bayan Obo, China). In carbonatites, which have the highest REE contents (ΣREE = 72 – 15515 ppm) and the highest LREE/HREE ratios (La/Lu = 7.1 - 1240) of any rock type (Schofield and Haskin, 1964; Kapustin, 1966; Barber, 1974; Eby, 1975; Mitchell and Brunfelt, 1975), most REE minerals have been precipitated from hydrothermal fluids (Mariano, 1989). The mineralization in the Rock Canyon Creek fluorite-REE deposit is characterized by fine-grained, disseminated, vein and breccia-matrix fluorite in brown-weathering, ferroan carbonates. Several REE minerals have been identified (Pell, 1992), including bastnäesite [Ln(CO$_3$)F], parisite [Ln,Ca(CO$_3$)$_2$F$_2$], gorceixite (Ba, Ca, Ln)Al$_3$(PO$_4$)$_2$(OH)$_3$H$_2$O, synchysite (LnFCO$_3$.CaCO$_3$) and goyazite [SrAl$_3$(PO$_4$)$_2$(OH)$_5$.H$_2$O] (Samson et al., 1999). The mineralization has been suggested to be hosted by carbonate rocks that have been fenitized by fluids evolved from a deep-seated carbonatite (Pell and Hora, 1987). This conclusion is based on chondrite-normalized REE patterns characterized by light REE enrichment and no Eu anomaly, which is similar to the patterns seen in carbonatites from

4

British Columbia. The mineralization is enriched in F, Ba, Nb, Sr, Y and P, which is also consistent with carbonatite-derived fluids (Pell, 1992).

Carbonatites are defined as igneous rocks containing at least 50 volume per cent carbonate minerals, and are normally associated with alkaline silicate rocks (Woolley and Kempe, 1989). Even though the magmatic origin of carbonatites is beyond dispute as a general principle, and is indeed an essential part of the definition of these rocks, the evidence supporting such an origin is all too commonly ambiguous and circumstantial. The origin of carbonates becomes more complicated when carbonatites occur among sedimentary carbonate rocks. In this case, and particularly in the substantially altered varieties of carbonates, sedimentary carbonate forms very gradual transitions to the carbonatite carbonate. Some uncertainty then occurs over the boundary between the carbonatite carbonates and the sedimentary carbonate rocks, and the contacts become particularly difficult to identify if the carbonatites are formed metasomatically. A combination of evidence from field relations, associated rock types, texture, mineralogy, trace elements, and isotopes are required to distinguish sedimentary carbonates from carbonatite carbonates because no single criterion is decisive if volcanic features are not present (Barker, 1989).

Dolomitization in Western Canada has been the subject of study of many researchers. It has been suggested that dolomitization occurrs during exposure to a variety of environments with different physical and chemical characteristics. It has also been suggested in many case studies that dolomites could have precipitated from the injection of hydrothermal fluids. Examples of hydrothermal dolomitization in Western Canada include the Devonian Presqu'ile Barrier dolomites (Qing and Mountjoy, 1994), the Wabamun of the Peace River Arch (Packard et al., 1990), the Manetoe dolomite (Morrow et al., 1986), dolomites from the Keg River Formation (Aulstead and Spencer, 1985), and Mississippian dolomites from the Debolt Formation (White and Al-Aasm, 1997). The slow infiltration of basinal fluids into permeable strata during burial is one of models suggested for dolomitization (Machel, 1985, 1986, Machel and Mountjoy, 1987). As temperature increases, the Mg/Ca ratio required for dolomitization decreases, thus making most warm solutions capable of converting limestone to dolostone. Several case studies of dolomite in

the southern Rocky Mountain have been reported (Nesbitt and Muehlenbachs, 1994; Yao and Demicco, 1997) that document the dolomitizing fluid. Preliminary work (Zhu et al, 1999; Samson et al., 1999) suggests that several different types of carbonates are associated with the Rock Canyon Creek fluorite-REE deposit. The relationship between the mineralization and dolomitization is still unknown. Understanding this relationship could provide important clues to the evolution and history of the hydrothermal fluids which deposited the REE and fluorite.

1.3 Objectives

Dolomitization is a common feature of the Paleozoic strata of Western Canada. The origin and nature of the fluids that cause such dolomitization are a source of debate and intensive research. The genesis of hydrothermal rare earth element deposits is also a topic which has received considerable attention recently. Little is known about the source of the fluids responsible for such deposits. Such information is critical in understanding the genesis of these deposits. The Rock Canyon Creek deposit will provide a unique opportunity to integrate the relationships between dolomitization and Fluorite-REE mineralization. The genesis of the Rock Canyon Creek fluorite-REE deposit is controversial. Earlier workers suggest a relation to carbonatitic magmatism, but any affiliation to igneous activity is hypothetical. Dolomitization is widespread and closely associated with the mineralization. The exact age of the host rock is unclear, as is the structure in the area hosting the deposit. The primary objectives of this study are therefore:

- To determine the nature of the wall rock alteration associated with the deposit.
- To evaluate the relationship between alteration (dolomitization) and fluorite-REE mineralization
- To gain insight into the origin and nature of the mineralizing and dolomitizing fluids.
- To determine the sources and composition of diagenetic fluids and their evolutionary history.

6

1.4 Methodology

Twenty five samples were provided by Chris Graf of the Ecstall Mining Corporation, B.C.. Fifty samples were collected from Rock Canyon Creek by I.M. Samson and I.S. Al-Aasm in 1995 and 1997 (Fig. 1.2). Thin and polished thin sections were prepared for almost all of the samples. Twenty doubly polished wafers were also made for microthermometric measurements of fluid inclusions. Forty thin sections were stained by a mixture of Alizarin Red-S and Potassium Ferricyanide to distinguish dolomite from calcite according to the method described by Dickson (1965). All thin sections were examined under a standard microscope for petrographic analysis. Cathodoluminescence (CL) microscopy was performed using a Technosyn cold cathodoluminescence stage with a 12-15 Kv beam and a current intensity of 0.42-0.43 mA. Fluorescence characteristics of carbonates were studied with a Nikon EPI fluorescence attached to a petrographic microscope.

Oxygen and carbon isotopes were analyzed from different generations of calcite and dolomite. The powdered samples were obtained using a microscope-mounted drill assembly and then reacted with 100% pure phosphoric acid for four hours at $25°$ and $50°C$ for calcite and dolomite, respectively according to the method outlined by Al-Aasm et al. (1990). Evolved CO_2 samples were analyzed for their oxygen and carbon isotope ratios at the University of Ottawa using a SIRA-12 mass spectrometer. Precision was better than 0.05 ‰ for both $\delta^{18}O$ and $\delta^{13}C$. Strontium ($^{87}Sr/^{86}Sr$) isotopes were analyzed on a Finnigan MAT 262 with 5 fixed collectors. NBS and ocean water were used as standard references and $^{87}Sr/^{86}Sr$ ratios were normalized to $^{87}Sr/^{86}Sr = 8.375209$. The mean standard error was 0.00003 for NBS-987.

Fluid inclusions were used to obtain information on the chemistry and temperatures of the hydrothermal fluids at Rock Canyon Creek. Inclusion microthermometry was conducted with a LINKAM THM-600 heating-freezing stage attached to a polarizing microscope fitted with a video camera at the University of Windsor. The stage was calibrated using H_2O and CO_2-H_2O synthetic inclusions. Laser

7

Raman Spectroscopy (LRS) was used to identify the solid phases in fluid inclusions of the host minerals as well as to test for the presence of CO_2 and CH_4 in the fluid inclusions. LRS was performed at the University of Windsor on double-polished wafers. Bulk analysis of fluid inclusion gases was carried out at McGill University, using an HP5890 series II gas chromatograph equipped with a micro-thermal conductivity detector. The apparatus employed for gas extraction consists of a heat-treated stainless crusher operated by hydraulic ram. Details of the procedure are given by Salvi et al. (1997).

CHAPTER II
Geologic Setting

2.1 Introduction to Regional Geology

The Rock Canyon Creek fluorite-REE deposit occurs within the Kananakis Lakes map area (NTS 82J/W1/2) (Leech, 1979). This area lies within the Southern Rocky Mountains (Fig.2.1), and occurs at the eastern boundary between the Main and Front Ranges in the Foreland belt. The Southern Rocky Mountains and adjacent Purcell Anticlinorium are characterized by a series of easterly-verging thrust faults and flexural-slip folds that formed within Upper Proterozoic to Tertiary sedimentary sequences during the Laramide Orogeny (Late Jurassic to Tertiary) (Bally et al., 1966; Price and Mountjoy, 1970; Price, 1981; Yao and Demico, 1997). Upper Proterozoic and Lower Cambrian units are dominantly composed of sandstone, conglomerate, and shale units. Middle Cambrian through Upper Jurassic units are characterized by a sequence of platformal carbonates in the east and a thick sequence of shales in the west, which were deposited along a passive margin of western Ancestral North America that formed as a result of rifting in Late Proterozoic time (Nesbitt and Muehlanbachs, 1994). The boundary between these lithofacies trends northwest and lies just west of the British Columbia-Alberta boundary. Late Jurassic through Tertiary sedimentation was dominated by sandstone and shales (Ricketts, 1989). The study area lies just within the lithofacies change belt, just west of the British Columbia-Alberta boundary. Laramide structural features are dominant in this area.

2.2 Regional Stratigraphy

The study area is underlain by a carbonate-dominated sedimentary sequence spanning Ordovician through Upper Devonian strata (Fig. 2.1). The Kananakis Lakes map area has been studied by Bending (1978), Leech (1979), Norsford (1981), Mott et al. (1986). Pell and Hora (1987) and Dix (1991) have studied the deposit area. The summary given below is based on their observations.

9
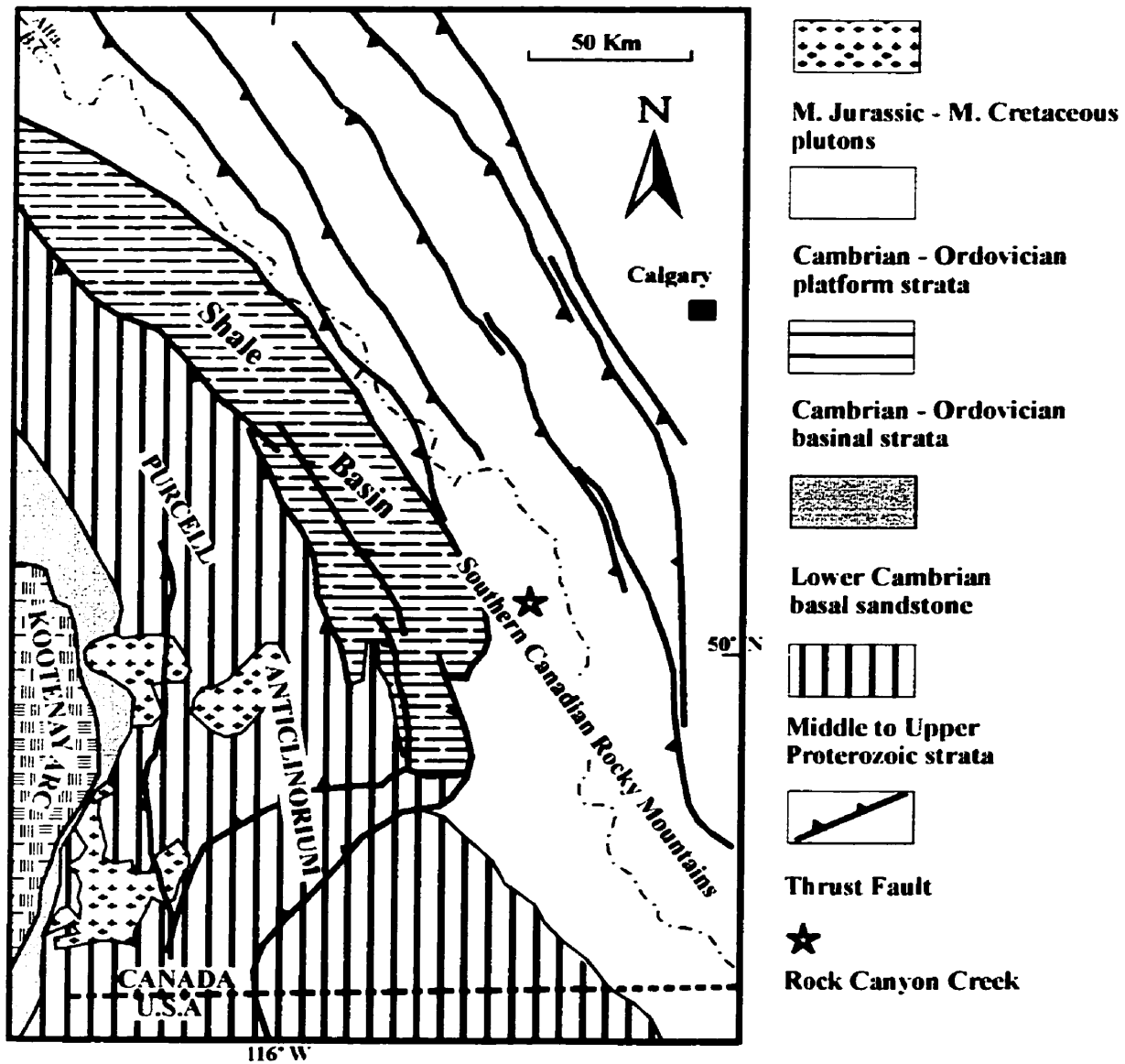
Fig. 2.1. Geology of Southern Canadian Rocky Mountains, simplified from Yao et al. (1997).

	West of the Southern Rocky Mountains	Study Area	East of the Southern Rocky Mountains
Middle Silurian			
Lower Silurian	Tegart Fm		
Upper Ordovician	Beaverfoot Fm Whiskey Trail Mem. Mount Wilson Fm	Beaverfoot Fm	Beaverfoot Fm Whiskey Trail Mem. Mount Wilson Fm
Middle Ordovician	Glenogle Fm	Skoki Fm	Owen Creek Fm Skoki Fm
Lower Ordovician	McKay Gp	Glenogle Fm McKay Gp	Tipperary Fm Outram Fm Survey Peak Fm
Cambrian			Mistaya Fm

Fig. 2.2 Schematic summary of the stratigraphy of the
Rock Canyon Creek area. A: Cambrian to Middle Silurian.
B. Middle-Late Devonian. Fm: Formation, Mem: member, Gp: Group

B

Stratigraphic column showing Middle-Late Devonian units: Frasnian (Fairholme Gp), Givetian, and Eifelian (Harrogate Fm, Burnais Fm, Cedared).

Legend:

Erosional Strata		Argillaceous Limestone	
Dolostone		Sandstone	
Quartzite		Aphanitic Dolomite	
Silty Dolostone		Shale	
Calcareous Shale		Shaly Limestone	
Dolomitic Limestone		Evaporites	
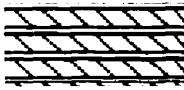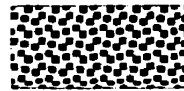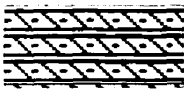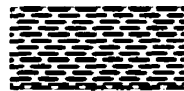
12

The McKay Group is a thick sequence of shaly limestones, limestones and shales, which is late Cambrian to early Ordovician in age, although in some occurrences it extends up to Middle Ordovician. The McKay Group is lithologically similar to the Survey Peak and Outram formations as developed east of the Southern Rocky Mountains, which are mainly composed of calcareous shales, mudstone, microcrystalline limestones, and some conglomerates.

In the western part of the Southern Rocky Mountains, the Middle Ordovician McKay Group and Glenogle formations are found to interfinger, the transitional Outram Formation is not present. The Glenogle Shales (previously termed the "Graptolite Shales"), which contains minor amounts of siltstone and limestone, conformably overlies the McKay Group. In the eastern part of the Southern Rocky Mountains, the Middle Ordovician Skoki Formation is dominated by thinly-bedded dolostone and overlies the Glenogle shales. The Owen Creek Formation underlies the Mount Wilson Quarzite and overlies the Skoki Formation. The most common Owen Creek rocks are very-fine grained dolostones. The Mount Wilson Quarzite comprises pure, resistant quartzites, which are conformable on the Owen Creek Formation or on the Glenogle Shales.

The Beaverfoot Formation of late Ordovician to early Silurian age conformably overlies the Mount Wilson Quarzite and consists of light grey to pale orange-brown, thickly bedded, massive dolostone. The lowest part of the Beaverfoot Formation is the Whiskey Trail Member, which contains dolomitic quartz sandstones. The lower part of the Beaverfoot Formation contains about five percent large fragments of solitary or colonial corals with lesser crinoid and brachiopods debris. The corals are always present and make it a very distinctive marker unit. Minor erosion surfaces indicate that the base of the Beaverfoot Formation is an unconformity that is characterized by local conglomerates with rounded dolomite and chert clasts, and a layer of coarse-grained dolomitic sandstone that varies from centimetres to metres in thickness.

Middle and Upper Silurian rocks are absent from the Southern Rockies and Devonian rocks rest directly on Precambrian to Lower Silurian strata. This gap

corresponds to the sub-Devonian unconformity, marking a major feature of the geology of western Canada. The overlying Cedared and Burnais formations were probably deposited within a very shallow sea with restricted circulation, which was constrained by the Purcell Arch and the Western Alberta Ridge in Eifelian time (Norsford, 1981). The Cedared Formation is the basal Devonian unit and basically consists of well-bedded dolostone and dolomitic quartz sandstone. Fossils are very rare, mostly poorly preserved and abraded, and include charophytes and fragments of fish, brachiopods, gastropods and ostracodes. Bedded and laminated gypsum is the principle constituent of the Burnais Formation, which also includes limestone, dolostone and breccias. In some occurrences, the Burnais and Cedared formations are found to interfinger, with the Burnais Formation completely bounded by the Cedared both vertically and laterally.

The Harrogate Formation overlies the Cedared Formation and consists of dolostone, shaly and nodular limestones. Mudstones and shales are predominant in the lowermost beds, limestone and dolostone in the middle part, and mudstone in the upper part. This sedimentary sequence reflects intermediate-deep water depositional environments. The Harrogate Formation is overlain by Upper Devonian (Frasnian) limestone, correlative with the Fairholme Group. The contact between these two units is not exposed, although, elsewhere in the Rocky Mountains, there is an unconformity separating the Upper and Middle Devonian strata. The Fairholme Group is a thick sequence of thin bedded, fossiliferous limestones with minor dolostone and greenish-grey and black shale.

2.3 Local Geology and Mineralization at Rock Canyon Creek

2.3.1 Local Structure

The Rock Canyon Creek area is underlain by a Cambrian-Ordovician to Middle-Upper Silurian carbonate-dominated sedimentary sequence (Fig. 1.1). The sequence to the southwest of the deposit is cut by a series of west-dipping thrust faults, and the area to the east of the deposit is underlain by an overturned to upright homoclinal sequence, younging to the east (Fig.1.1) (Pell and Hora, 1987, 1992; Dix, 1991). A NNW-SSE-trending fold

14

axis occurs just west of the mineralized zone that has been variably interpreted as an overturned syncline (Pell and Hora, 1987) and as a anticline (Dix, 1991) (Fig.1.2). Mineralization occurs in an elongate, approximately strata-parallel zone immediately east of the basal thrust (Fig. 1.1). Earlier workers (Pell and Hora, 1987, 1992) indicate that the mineralization is restricted to the Basal Devonian unit so that the mineralization is stratabound. Dix (1991), however, suggested that the mineralization is bounded and cut by high-angle faults which lie just east of the mineralization zone. Several fluorite occurrences have been found to the south west of the thrust along fractures and in breccias (Dix, 1991).

2.3.2 Local Stratigraphy

West of the Basal thrust, light grey to orange-brown fine-grained dolostones are interpreted to be the McKay Group (Norford, 1969; Leach, 1979) and probably part of the upper part of that Division (Mott et. al., 1986) (Fig. 1.1). Dix (1991) found a well exposed basal dolostone conglomerate along the western slope of the creek west of Candy Creek, suggesting a possible channel on an irregular paleotopography. The basal conglomerate represents either the Ordovician-Devonian unconformity or the unconformity between the Ordovician Owen Creek Formation and the underlying Skoki Formation. Glenogle Shales and Skoki Formation dolostone and limestone are found in the northwestern part of the study area (Fig.1.1). The Mount Wilson quartzite and Whiskey Trail Member dolomitic quartz sandstones are absent in the vicinity of the deposit. Coral-rich Skoki Formation limestone and dolostone rest on the Skoki Formation to the west of the deposit.

The central part of the study area (the deposit area) mainly comprises orange to buff coloured siliceous to silicified dolostone, with minor fine-grained limestone. These rocks were interpreted as basal Devonian units (Cedared Formation) by early workers (Bending, 1978; Leech, 1979; Norsford, 1981; Mott et al, 1986; Pell and Hora, 1987), whereas Dix (1991) interpreted these rocks to be Ordovician in age.

Burnais evaporites are locally found. Dix (1991) reported the existence of Burnais evaporites along a ridge north of the Rock Canyon Creek, however, no evaporite minerals have been found in the samples used in this study.

East of the main mineralized zone (Fig.1.1), the basal Devonian (Pell, 1990) is overlain by Harrogate Formation rocks, which contain well-exposed dark argillaceous limestone, nodular limestone with brachiopods and argillaceous dolostone. Dix (1991) documented a thin layer of quartz arenites overlying the Harrogate Formation, and he suggested that sedimentation continued within the basin west of the West Alberta Arch, during exposure and erosion of equivalent strata in the east. This quartz arenite layer is overlain by the Upper Devonian Fairholme Group, which is a thick sequence of thin-bedded, nodular to lenticular limestones with minor dolostones. The Fairholme Group strata display thick interbedded intervals of dolostone and limestone.

2.3.3 Fluorite-REE mineralization

The fluorite-REE mineralization at Rock Canyon Creek has been studied by Hora and Kwong (1986), Pell and Hora (1987), Pell and Fontaine (1988), Dix (1991), Pell (1992), Kerr (1995), and Samson et al. (1999). Based on their studies, four types of fluorite-REE mineralization have been identified.

The first and most widespread type of mineralization consists of disseminations and veinlets of dark-purple fluorite in a dark brown to dark orange-brown-weathering dolomitic matrix. Contacts between the mineralized and unmineralized host rocks are gradational. Fluorite content varies from 2 to greater than 10 per cent of the rock. Common accessory minerals include pyrite, barite, calcite, limonite, illite, bastnäesite and gorceixite. This type of mineralization contains the highest REE concentrations of the various styles of mineralization.

The second type of mineralization is characterized by massive, fine-grained, colourless and purple fluorite mineralization and by the presence of alumino-fluoride minerals such as prosopite and cryolite (Samson et al, 1999). This type of mineralization has lower REE concentrations and is only found as float in the southeastern part of the property (Fig. 1.1).

The third type of mineralization consists of fine-grained, purple fluorite in fine-grained limestone, which is locally inter-bedded with buff-weathering dolostone and forms

the matrix of solution breccias. Fluorite concentrations vary from trace amounts to a few per cent. Minor enrichment of REE is also reported (Graf, 1985). This type of mineralization is located relatively far away from the main mineralization zone and randomly distributed throughout the basal Devonian rocks.

The fourth type of mineralization was found (Pell and Hora, 1987) in one locality and is characterized by massive purple fluorite which forms the matrix of a carbonate breccia and locally replaces the host rock. The fluorite constitutes greater than 20% of the rock. Accessory minerals include barite, pyrite and magnetite.

.

CHAPTER III
Petrography and Mineralogy

3.1 Lithofacies

3.1.1 Introduction

A facies is a body of rock defined by specific sedimentary characteristics such as composition, lithology, texture, fossil contents, and sedimentary structures (Reading, 1986; Tucker and Wright, 1990). In the samples studied several lithofacies have been identified based on their petrographic and mineralogic characteristics. The limestone classification employed is that of Wright (1992), which is modified from the schemes of Dunham (1962). These lithofacies are: mudstone, wackestone, and packstone/grainstone. The limestone and dolomitic limestone in the Rock Canyon Creek area are composed predominantly of brachiopods, crinoids, ostracods and other skeletal particles. Most of the limestones are dolomitized to variable extents. In spite of the fact that some indication of pre-diagenetic fabrics is evident, or even clear in some phases, limestone fabrics are so obliterated by dolomitization that they can be described only by their crystalline texture.

3.1.2 Mudstone Facies

Mudstone facies rocks are abundant and are easily recognizable in both hand sample and under the microscope. In hand sample, they generally appear grey to black in color. There are two groups of mudstone in the study area; one is a black, very fine-grained laminated limestone, which is abundant in the Harrogate Formation and the lowest part of the Fairholme Group (Dix, 1991), east of the deposit. The mudstones usually do not have skeletal fragments (Plate A-B), but in some cases, there are a few well-preserved brachiopods and ostracodes. Small amounts of planar-euhedral, fine-coarse, unimodal to polymodal replacement dolomites are also present. The other group of mudstones is in the McKay Group, west of the deposit. This group of rocks is light gray to dark gray and is completely dolomitized with very fine-grained planar-e, unimodal replacement dolomites (Plate A-A). Some detrital quartz grains are also present in this facies. These rocks are mostly regular and laminated. Skeletal fragments are

uncommon and represented by ostracodes and brachiopods. There is also a minor amount of very fine-grained crystalline limestone in the centre of the study area just west of Candy Creek (Pell and Hora, 1987).

3.1.3 Wackestone Facies

In the sample suite used in this study, wackestone facies is the most abundant and widespread facies type. Rocks of this facies are generally gray to dark gray. The skeletal fragments are predominantly fossils, and include crinoid, brachiopods and ostracodes; most are well preserved. Lime mud composes up to 90% of these rocks. Evidence of compaction includes the presence of stylolites (Plate A-D) and broken shells. The lower part of the Fairholme Group displays thick interbedded intervals of dolostone and limestone (Dix, 1991), and the limestones are mainly of wackestone facies (Plate A-C, D). Wackestone is completely dolomitized in the Cedared Formation (Basal Devonian). Late ferroan calcite cement fills in vugs and fractures, and, in some cases, calcite replaces dolomite crystals (Plate B-C). Most host rocks around the mineralized zone are strongly to completely dolomitized and depositional fabrics of these rocks are obliterated. In some cases, however, some crinoids and fragments of brachiopods and ostracodes are preserved (Plate A-E), which indicates that the host rocks are wackestone facies. The faunal assemblage is typically marine and the absence of framebuilding organisms suggests that deposition probably occurred in a low-energy, deeper water conditions in a mud-dominated environment.

3.1.4 Packstone/Grainstone facies

This facies was only observed in one sample, immediately east of the thrust fault, and is a crinoid and brachiopod-rich limestone (Plate A-F). It is dark grey in colour. The skeletal fragments comprise up to 90% of the rock. The inner and wall structure of fossils are generally well-preserved and have a micrite envelope. Dolomitization has selectively affected micrite and stylolites. The lithology and faunal assemblage of this packstone is very similar to that of Beaverfoot Formation rocks. The abundant normal marine fauna of crinoids and brachiopods suggest that the sediments that formed this rock was deposited in a broad, stable and moderate to shallow marine carbonate platform (Tucker and

Wright, 1990).

3.2 Diagenesis, Mineralization and Alteration

3.2.1 Early Diagenesis

3.2.1.1 Introduction

Diagenesis is defined as all the processes that occur in and affect sediments immediately after deposition, and continuing until the realms of incipient metamorphism at elevated temperatures and/or pressures (Tucker, 1981; Tucker and Wright 1990). The carbonate sequence in the study area underwent a complex diagenetic history, represented now by many different types of diagenetic fabrics. Major early diagenetic events include micritization, compaction, cementation, dolomitization, silicification, and brecciation. Dolomitization is the most significant diagenetic process that has occurred in the carbonate rocks of Rock Canyon Creek, and has affected all facies to varying degrees. Almost all limestones in the study area are partially to completely dolomitized. Five types of dolomite have been identified and are: (1) pervasive microdolomite, (2) dolomite cement, (3) replacement non-ferroan dolomite, (4) saddle dolomite I, (5) coarse ferroan dolomite, and (6) saddle dolomite II. The classification of dolomite is based on texture, luminescence and composition, and is summarized in Table 3.1. The textural description is based on the classification of Sibley and Gregg (1987). The first four dolomite types are the products of diagenetic processes and formed during the pre-mineralization stage. The last two dolomite types are associated with the mineralization and will be described later in Section 3.2.2.

3.2.1.2 Micritization

Micritization represents the first diagenetic event to occur within the carbonate rocks of the study area. The packstone facies contains well-developed micrite envelopes on shell fragments (Plate A-F). Some wackestone facies rocks also have micrite envelopes on fragments (Plate B-A, B). Micritization represents an early marine diagenetic process involving algae, cryanobacteria and fungi boring into skeletal fragments, these bores are then filled with micritic calcite (Tucker and Wright, 1990).

Table 3.1 Characteristics of Dolomite

Dolomite Type	CL	Size(μm)	Texture	Origin
Microdolomite	Non-lum.	1-20	Planar-e, -s, nonmimic	Replacement
Dolomite Cements	Dull-red	20-200	Planar-e, -s	Cement
Saddle Dolomite I	Zoned: red and dull red	50-300	Euhedral to planar-s	Cement
Non-Ferroan Dolomite	Dull red to non-lum.	50-500	Nonplanar to -s, clear overgrowth rim, mimic to nonmimic	Replacement
Ferroan Dolomite	Dull red	20-500	Nonplanar to -s, nonmimic	Replacement
Saddle Dolomite II	Red	50-500	Euhedral to planar-s	Cement and replacement

Note: lum.:luminescent; planar-e: planar-euheral; planar-s: planar-subheral.

3.2.1.3 Microdolomite

Microdolomite usually shows as a grey, brown, and even black colour in hand samples. It generally consists of 1 - 20 μm crystals with planar-e and planar-s fabrics (Plate A-A). Larger crystals are generally turbid but many display small, clear overgrowth rims which are most obvious on larger crystals. Under cathodoluminescence, microdolomite is non-luminescent. Microdolomite occurs in mudstone and wackestone facies. Clasts in intraformational breccia (McKay Group, west of the deposit) are mudstone and wackestone facies and are completely dolomitized while the matrix consists of quartz and coarse dolomite cements and, in some cases, saddle dolomite. Microdolomite is common in the samples used in this study, especially in McKay group rocks.

3.2.1.4 Dolomite Cement

Dolomite cement is widespread in rocks from the central and western part of the study area. It consists of coarse, clear, planar-e to planar-s crystals varying from 20 to 200 μm in size. Dolomite cement occurs in veins, vugs and the matrix of intraformational breccias. It also occurs as isopachous rims on clasts in intraformational breccia and conglomerate (Plate G-A), and in pores of fossil molds (Plate B-A, B) in wackestone facies. It is non-ferroan and non- to dull-red cathodoluminescent.

22
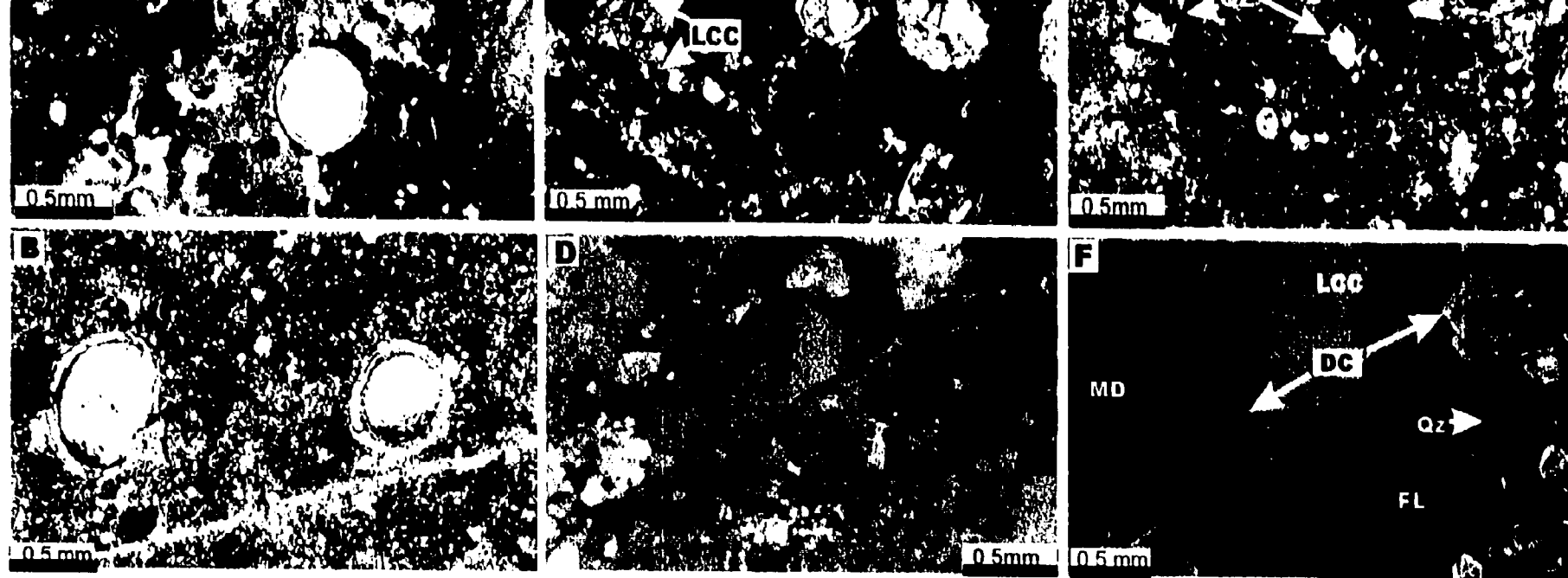
A) Peloids and fossil fragments showing micritization and dolomite cementation in packstone facies, Beaverfoot Formation, Upper Ordovician, east of the deposit (PPL). B) Photomicrograph of wackestone facies with geopetal texture showing a micrite envelope and dolomite cementation in pore of fossil and in a veinlet (PPL). C) Photomicrograph of dolostone. The fossil fragments have micrite envelopes and dolomite cements. Late ferroan-rich calcite lining a vug (PPL). D) Photomicrograph of mineralized dolostone with a vein of dolomite, quartz and zoned fluorite. Quartz (QZ) pseudomorphing dolomite (PPL). E) Photomicrograph of limestone showing quartz (QZ) pseudomorphing dolomite (PPL). F) Photomicrograph of intraformational breccia with fragments of massive microdolomite (MD) in matrix of dolomite cement (DC), fluorite (FL), quartz (QZ) and late calcite (LCC) (XPL).

3.2.1.5 Compaction

In the study area, evidence of mechanical compaction is best observed in wackestone and packstone facies rocks. For example, fossil grains with micrite envelopes have been broken into several pieces (Plate B-B). Condensed packstone/grainstone facies were initially produced during mechanical compaction of wackestone by the closer packing of grains. Fractures are also widespread developed in the study area, probably resulting from mechanical compaction. Veinlets are usually filled by dolomite or calcite cement (Plate B-B). These veinlets are crosscut by late veins and vugs of dolomite, fluorite, quartz and late calcite.

Chemical compaction develops under increased pressure associated with lithostatic stresses as would be found in deep burial environments. In the study area, the most commonly recognized chemical compaction features are stylolites (Plate A-D). Other evidence of chemical compactions, such as dissolution seams and fitted fabrics, were not observed.

3.2.1.6 Dissolution

Petrographic evidence suggests that dissolution occurred early in the diagenetic history. Fossils were dissolved, leaving voids which have geopetal texture, were later filled by dolomite spar (Plate B-A, B, C). Micrite envelopes on some grains help to preserve these structures. Some fossils (e.g. crinoids, brachiopods) have not been affected by dissolution, but in the same sample, some fossils do, which suggests that the unaffected fossils were stablized prior to dissolution (Plate A-D, F).

3.2.1.7 Calcite Cementation

Calcite cementation is a common diagenetic feature in the carbonate rocks of Rock Canyon Creek. These cements include poikilotopic calcite, coarse calcite spar and vein calcite. All these type of calcite cements are non-ferroan. Poikilotopic calcite cement occurs in condensed packstone facies. It comprises coarse crystals, up to a few millimetres in diameter, and usually engulfs several skeletal grains, such as crinoids and brachiopods. These cements are non-luminescent under CL. Where well-developed cements in packstone occur, dolomites are rarely present, which indicate that the presence

of these cements might have prevented some later diagenetic events. Coarse calcite spar usually consists of coarse, equant crystals and is non-luminescent and non-ferroan. They occur mainly in interparticle pores and cavities in packstone or wackestone facies. They may show a drusy texture of increasing crystal size toward the centre of the cavity.

3.2.1.8 Saddle Dolomite I

Saddle dolomite in the study area is characterized by its coarse crystal size, curved crystal surfaces, and sweeping extinction (Plate H-C, D, E, F). There are two stages of saddle dolomite in the study area. The first stage of saddle dolomite (saddle dolomite I) appears to predate the mineralization, as this saddle dolomite is replaced by fluorite in a few cases and no close relationship exists between mineralization and saddle dolomite I (whereas some other saddle dolomite are closely associated with mineralization, and will be described later in section 3.2.2.4). Saddle dolomite I is widespread and is abundant in some samples. Crystals of saddle dolomite I range in size from 50 to 300 μm. Generally, crystals of saddle dolomite I are clear, planar-e to planar-s, and they normally display red to dull red CL. Some of the crystals are, however, zoned, with red to bright red cores and several outer bands of alternating non-luminescence and red CL (Plate H-E, F). These zoned dolomites occur at the margins of veins and vugs, with the centres of cavities filled by nonluminiscent saddle dolomite (Plate H-E, F).

3.2.1.9 Replacement Non-ferroan Dolomite

Replacement non-ferroan dolomite includes large isolated replacement dolomite crystals, selective dolomite in the matrix of wackestone and packstone facies rocks, and pervasive dolomite in coarse crystalline dolostone. All these dolomites are non-ferroan and are dull red to non-luminescent under CL. Some planar-e isolated dolomite crystals have a thin red rim under CL. These isolated crystals of dolomite range in size from 50 to 500 μm. Dolomite that selectively replaces the matrix of wackestone and packestone facies is nonplanar to planar-s and ranges in size from 50 to 100 μm.

Replacement non-ferroan dolomite is the most common type of dolomite in the samples examined in this study and is located mainly in the central part of the study area (the deposit area). This dolostone is generally grey in hand sample, and is orange where it has been silicified. Most of these pervasive dolomites are nonplanar to planar-s,

25

nonmimical to mimimical, and exhibit polymodal textures with crystals ranging in size from 20 to 300 μm. Some of these pervasive dolomite crystals have inclusion-rich cores and clear, inclusion-free overgrowth rims (Plate G-C).

3.2.1.10 Silicification

Multiple stages of silicification have been recognized in the study area, although this type of alteration is not very common in the samples. Silica occurs as both a cement and as a replacement of mudstone facies, wackestone and grainstone facies rocks in both mineralized and unmineralized rocks. Petrographically, it includes megaquartz, microquartz and length-fast chalcedony. There are at least three recognizable generations of silicification. The earliest generation includes microquartz laminae in laminated mudstone and megaquartz in pores of dissolved fossil fragment. These quartz crystals are anhedral to subhedral and were probably precipitated in the early diagenetic history as these quartz crystals are replaced by fluorite, barite, saddle dolomite and late calcite.

3.2.1.11 Brecciation

There are several different types of breccia present in the study area. According to the timing of the brecciation, there are at least three stages of brecciation. Intraformational breccia occurs in mudstone and wackestone facies west of the deposit with insitu mudstone fragments (Plate I-A, B). The fragments are poorly-sorted, angular and surrounded by an isopachous dolomite cement. These textures indicate that the breccia might be a solution collapse breccia due to the subsurface exposure. The matrix comprises saddle dolomite, quartz, fluorite and late, coarse calcite. Some solution collapse breccias have also been reported in Burnais Formation (Dix, 1991).

3.2.2 Mineralization and Related Alteration

3.2.2.1 Mineralization

Based on mineralogy, texture and the fluorescence characteristics of fluorite, three major styles of mineralization have been identified (Samson et al., 1999) and are summarized in Table 3.2. The disseminated fluorite style and massive fluorite are the same as those described by Hora and Kwong (1986), Pell and Hora (1987), Pell and Fontaine (1988), Dix (1991) and Samson et al. (1999). The breccia-matrix fluorite style is

similar to the fourth type of mineralization described in section 2.3.3, which Samson et al. (1999) incorporated into the disseminated fluorite style rocks. Since the host rocks to the breccia-matrix fluorite are replacement non-ferroan dolomite and are different from those to disseminated fluorite rocks, in this study, the breccia-matrix fluorite style are separated from the disseminated fluorite style. The fine-grained purple fluorite in fine-grained limestone described in section 2.3.3 is not very common and only found in one sample, so it was incorporated into the disseminated fluorite style.

Table 3.2 Summary of Mineralized Rock types

Type	Mineralogy and Texture
Disseminated fluorite	Disseminated, veinlets and matrix of fluorite, barite and REE
Breccia-matrix fluorite	Dark purple breccia-matrix zoned fluorite
Massive fluorite	Massive fluorite-alumino-fluoride

(1) Disseminated Fluorite

The disseminated fluorite style is primarily characteristic of the main mineralized zone which defines a northwest-trending zone mappable for over a kilometer, sub-parallel to strike (Fig. 1.1). Fluorite-barite-REE mineralization occurs in veins, in breccia matrices, and disseminated through massive and laminated dolostone. Most mineralized samples are characterized by thin veins, vugs and small, disseminated patches (aggregates) containing colourless to purple fluorite, barite, dolomite, quartz, and REE minerals (Plates C, D). This type of fluorite, barite and REE mineralization is reported to be the most widespread and occurs most frequently within the Basal Devonian unit (Hora and Kwong, 1986; Pell and Hora, 1987; Pell and Fontaine, 1988). Fluorite in this style of rocks constitutes mostly less than 10 percent of the rock.

The host rocks to this mineralization weather to dark grey to orange-brown colour, and dark purple fluorite can be easily seen in veins and vugs in hand specimen (Plate C-A). They are mostly medium-grained crystalline ferroan-rich dolostones. Away from the main mineralized zone, this type of mineralization is hosted in fine-grained limestone (which is similar to the third type mineralization described in section 2.3.3),

very-fine grained, massive or laminated dolostone west of the deposit and even west of the basal thrust (Plate B-F, I-B). These rocks are weakly altered. Fluorite, barite and REE minerals vary from trace amounts to a few per cent of the rock away from the mineralization zone, and occur mainly in veins and vugs.

The mineralization is dominated by fluorite. Barite is the next most abundant mineral, and can be the dominant mineral in some samples. Dolomite and quartz are less common. The dolomite typically occurs around the edge of the veins and vugs (Plate C-C, D, G-E, F) and is, in many cases, coarser than the surrounding carbonate host rock. Isolated dolomite crystals also occur in the fluorite, which indicate that this dolomite precipitated earlier than fluorite. All of these dolomites are generally euhedral to subhedral with weak, sweeping extinction and are red under cathodoluminescence. In some cases zonation is visible under CL (Plate C-C, D). Some dolomite crystals are pseudomorphed by quartz (Plate D-C), which is in turn replaced by fluorite. Fluorite commonly replaces barite, and euhedral barite crystals may be surrounded by massive fluorite. In contrast barite also occurs interstitially to euhedral, colourless-purple fluorite in some samples (Plate C-B, Samson et al., 1999). This indicates that there is more than one stage of barite deposition and/or fluorite deposition.

Five generations of fluorite are recognizable in these rocks. The characteristics of the different type of fluorite are summarized in table 3.3.

Table 3.3. Characteristics of fluorites of disseminated style rocks.

Stage	Fluorite type	CL	Characteristics
1	Colourless fluorite I	Bright blue	High relief
2	Colourless fluorite II	Dark blue	Low relief, replaces colourless fluorite I
3	Purple fluorite	Dark blue	Replaces colourless fluorite II
4	Colourless fluorite III	blue	Replaces colourless fluorite II with purple fluorite
5	Zoned fluorite	Zoned: bright blue and dark blue	Zoned fluorite of colourless and purple fluorite, coated by dark purple rims.

The first comprises fine-grained colourless fluorite with lesser purple fluorite, which

29

occurs mainly as disseminations. This type of fluorite is the most common in samples used in this study and exhibits bright blue to dark-blue cathodoluminescence (Plate C-C, D). Luminescence studies indicate that this kind of colourless fluorite can be separated into two generations based on different CL characteristics (Plate D-A, B). The earlier stage of colourless fluorite (I) is cloudy, and has a higher relief than the later stage of colourless fluorite, exhibits bright blue CL, and is zoned. This is veined or brecciated and replaced by a later stage colourless fluorite (II) with lower relief and dark blue CL. The third type of fluorite is dark-purple and occurs as patches or veinlets in the colourless fluorite (II), and exhibits blue to dark-blue CL. In some samples, the dark-purple fluorite crosscuts and replaces the colourless fluorite. The fourth type of fluorite is colourless fluorite (III) and bright blue CL which crosscuts and replaces colourless fluorite II and the purple fluorite.

Some samples contain zoned fluorite crystals in vugs that have purple cores surrounded by alternating colourless and purple fluorite zones and that are coated by a dark-purple rim (Plate D-C, D). The zonation is also seen in CL and comprises alternating pale-blue and bright-blue zones. The dark-purple rim shows dark blue CL. The REE contents of zoned fluorite crystals decrease from the cores to the purple rims (Kerr, 1995). These euhedral zoned fluorite crystals are probably later than the colourless fluorite III since these crystals normally occur in veins or vugs where they are surrounded by colourless fluorite. In some samples dark purple fluorite dominates, and in others, colourless fluorite dominates.

The REE minerals are generally difficult to recognize with transmitted light microscopy so that their abundance is difficult to estimate. However, SEM analysis (Samson et al., 1999) show that the REE minerals are very fine-grained (individual crystals typically have maximum dimensions of 10 to 40 μm) and are either disseminated through the host carbonate adjacent to fluorite-barite patches or veins, or, less commonly, occur within patches and veinlets (Plate D-E). There appear to be no REE minerals associated with later stage colourless fluorite (colourless fluorite III), which probably indicates that the REE minerals were mainly precipitated during the earlier stages of disseminated fluorite style mineralization. The REE minerals generally occur as small

31

yellow to brown aggregates of crystals (<100 μm) that comprise syntaxial intergrowths of two Ca-REE fluorcarbonates with different Ca/REE ratios (Plate D-F) (Samson et al., 1999). Semi-quantitative EDS analyses suggest that these are probably synchisite $(CaREE(CO_3)_2F)$ and parisite $(CaREE_2(CO_3)_3F_2)$ (Samson et al., 1999). Bastnäesite $(REECO_3F)$ and gorceixite $((Ba,Ca,REE)Al_3(PO_3OH)_2(OH)_6)$ have also been reported from the deposit (Hora and Kwong, 1986).

(2) Breccia-Matrix Fluorite

This type of mineralization consists of dolostone breccia fragment (Plate E-A) in a matrix dominated by dark-purple fluorite (over 40 percent in volume), with lesser amounts of colourless, zoned fluorite. This style of mineralization is different from fluorite in breccia-matrices in the disseminated style in that it has ferroan dolostone fragments, and has noly a few zoned fluorites. Samples containing the breccia-matrix fluorite type of mineralization are located in the main mineralized zone near the centre of the anticline. The fragments are fine to medium-grained replacement non-ferroan dolostone. In most cases, the fragments contain no fluorite, or only a few thin veins or small vugs. The fragments are gray to dark gray in hand specimen. Dolomite crystals exhibit non-planar to planar-s, nonmimical textures. As shown in Plate E-C, these dolomites have cloudy cores and clear rims, and the cloudy cores are distinguished by lots of very tiny inclusions. Under cathodoluminescence, these dolomites exhibit a dull red to red colour. The matrices comprise massive, dark-purple fluorite and euhedral, zoned fluorite associated with minor barite. The earliest fluorite in the matrix is yellowish and typically euhedral (Plate E-C), forming crystals up to 0.5 mm in size that probably represents a generation of fluorite which is not seen in the disseminated mineralization. Some of these early-formed crystals contain pinkish-red growth bands (Plate E-B), but most are optically homogeneous. This earliest fluorite invariably also contains abundant fine-grained, euhedral dolomite crystals that may form larger aggregates which resemble dismembered, relict dolostone fragments, but might have been altered by the mineralizing fluid as evidenced by pinkish red CL. In contrast, dolostone fragments exhibit dull red to red CL. The early, yellow fluorite occurs as individual crystals, as aggregates and as fragments of crystals that have been overgrown, replaced and veined by colourless and

Plate E: Photomicrograph of Mineralization III
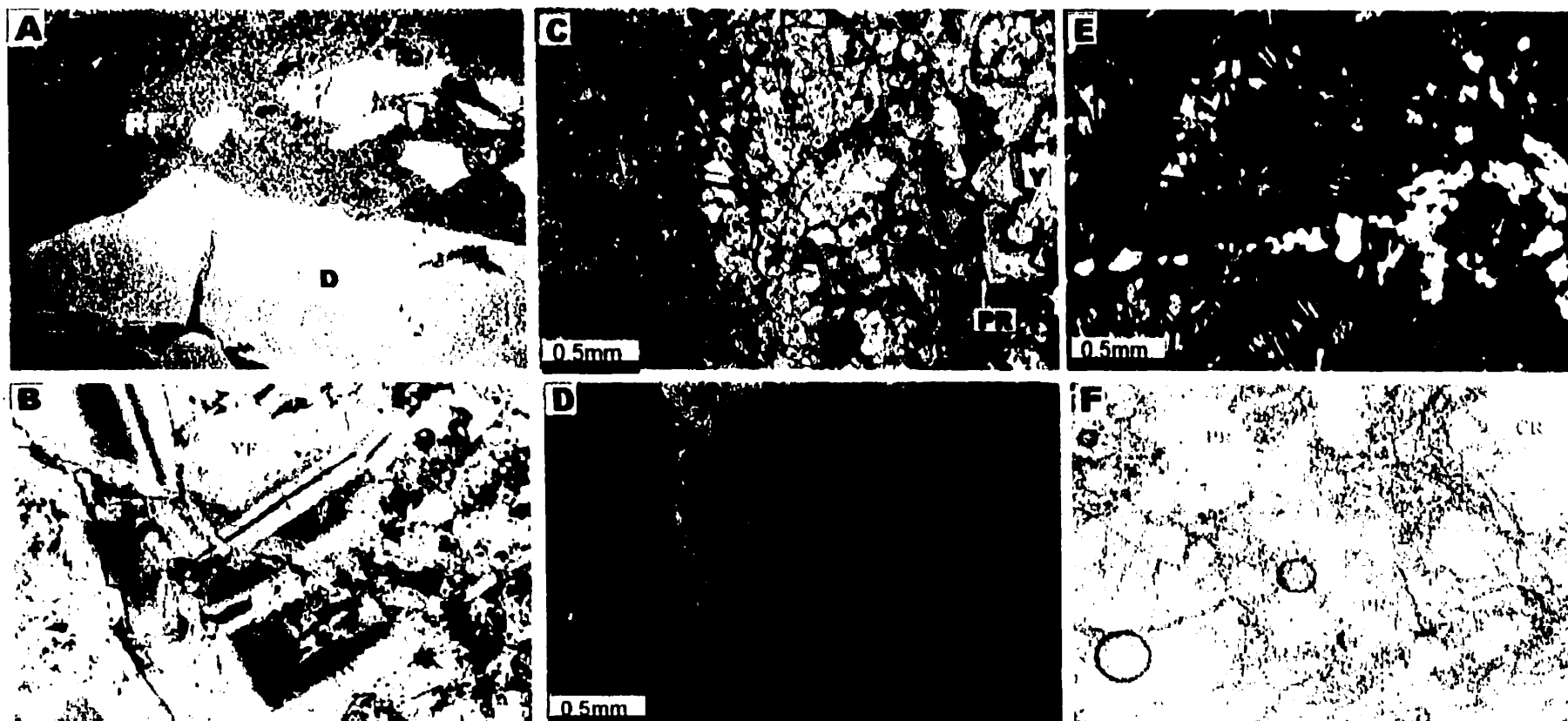
A) Breccia-matrix fluorite mineralization with fragments of dolostone (D) in matrix of purple fluorite (PF); Hand Specimen; Width 3.3 cm; (From Kerr, 1995). B) Breccia-matrix fluorite showing early, euhedral cores of yellow fluorite (YF) with overgrowths of zoned, purple and colourless fluorite. The early yellow fluorite and zoned fluorite are crosscut, brecciated and replaced by later clear and purple fluorite (PF); width 1 mm; (from Kerr, 1995) (PPL). C) Zoned breccia matrix fluorite. Crystals have a yellow core (Y), an intermediate zone of colourless and purple fluorite, and dark purple rim (PR); PPL. D) CL image of area shown in photo C showing the CL zonation of colourless and purple fluorite. E) Mineralization style III with a large crystal of cryolite crosscut and replaced by prosopite (white) (XPL). F) Breccia-matrix fluorite showing a vein of prosopite (PR) crosscuting cryolite (CR); width 2.43 mm; (from Kerr, 1995) (PPL).

purple fluorite. Where this later colourless to purple fluorite has grown into open space, it forms euhedral, zoned overgrowths around the yellow crystals (Plate E-C) that are up to 0.5 mm in size. The zonation is characterized by alternating bands of colourless and purple fluorite, coated by the dark purple rims. Under cathodoluminescence (Plate E-D), the early, yellow and euhedral fluorite crystals exhibit a grey to light blue colour. The later colourless and purple fluorite zonation in this type of rock exhibits similar CL zonation as that seen in zoned fluorite in the disseminated mineralization (disseminated fluorite type rocks). The REE contents of this type of fluorite also decrease from the yellow cores, through the zoned overgrowth bands, with late purple fluorite rims having the lowest REE contents (Kerr, 1995).

(3) Massive Fluorite

The float samples from the southeastern part of the property (Fig. 1.1) consist of a very distinctive style of mineralization that contains abundant alumino-fluoride minerals. The mineralization is massive, comprising up to 40 % purple and colourless fluorite with lesser quartz, barite, phlogopite, cryolite (Na_3AlF_6), prosopite ($CaAl_2(F,OH)_8$), goyazite ($SrAl_3(PO_4)(PO_3OH)(OH_6)$), and elpasolite ($K_2NaAlF_6$). Gorceixite has also been reported by Hora and Kwong (1986).

There are no carbonate fragments, relicts, or any isolated carbonate crystals in this type of sample and therefore it presumably represents a more pervasive alteration or part of a large vein. The earliest minerals in the paragenesis of this type of mineralization appear to be cryolite, phlogopite and barite (Plate E-E, F, F-A, B). These minerals occur as coarse-grained (up to ~ 1 cm) corroded single crystals or massive aggregates in a finer-grained matrix comprising variable proportions of fluorite, prosopite, goyazite, quartz, elpasolite and kaolinite. The matrices are dominated by fluorite and prosopite, which also occur in veins within the cryolite and barite. Cryolite occurs as highly fractured crystals, which are crosscut and replaced by prosopite and colourless fluorite. Phlogopite occurs as euhedral crystals surrounded by fluorite and prosopite. Barite, cryolite and phlogopite do not occur in contact, making their relative timing uncertain. Quartz appears to post-date the barite, cryolite and phlogopite because it occurs as veins within, and as a matrix to, some barite crystals. Most quartz occurs as anhedral crystals, in veins, and as isolated,

34

Plate F: Photomicrograph of Mineralization IV
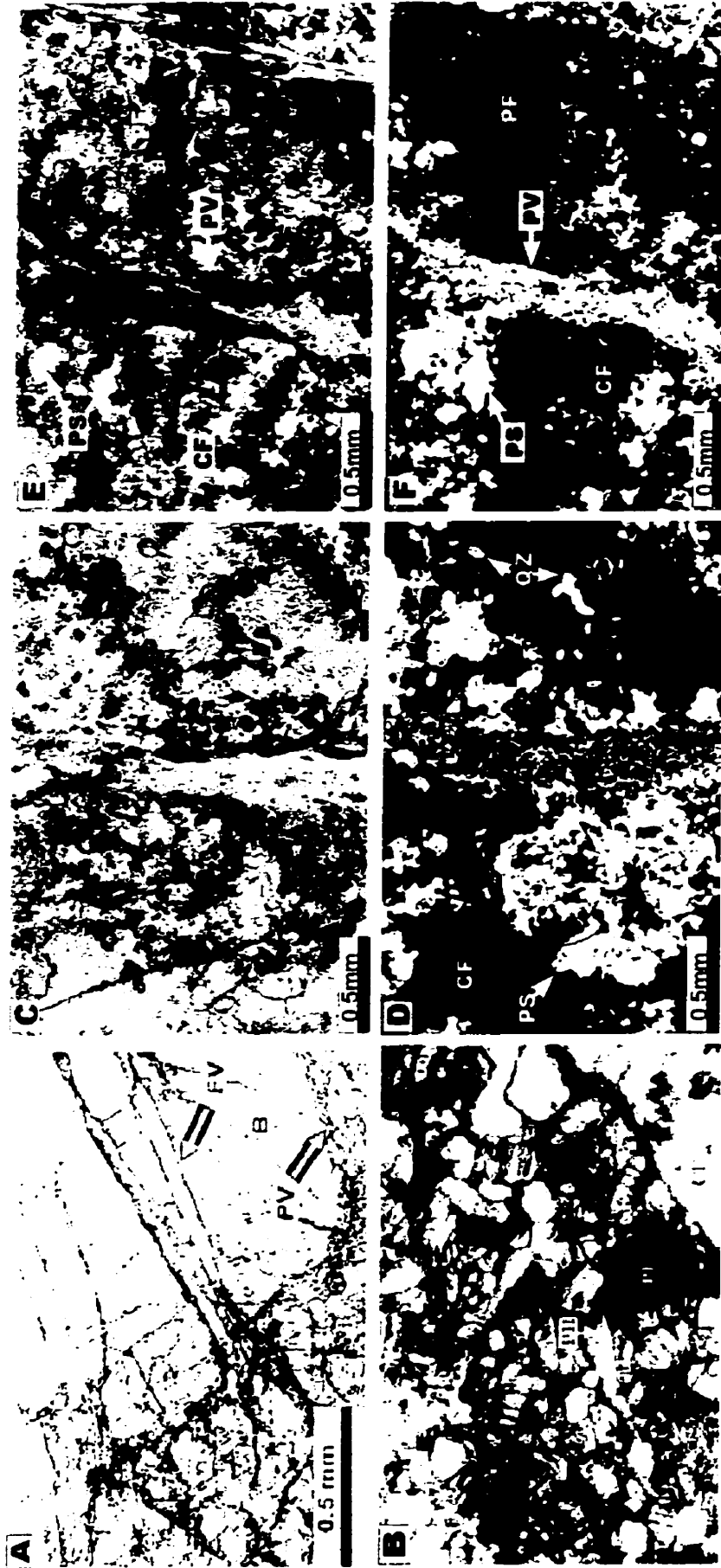
A) Mineralization style III. The large barite crystal (B) is cut by fluorite veins (FV) and a parisite vein (PV), (provided by Samson, I.M.) (PPL). B) Mineralization style III. Phlogopite (PH) is being replaced by colourless fluorite (CF) and purple fluorite (PF); width 2.43cm; (from Kerr, 1995) (PPL). C) Mineralization style III. The coarse prosopite (PS) aggregates replaced by massive colourless fluorite (CF). The euhedral quartz crystals float in fluorite. Later fine-grained prosopite vein (PV) crosscutting prosopite and fluorite (PPL). D) Image in polarized light of area shown in photo C. E) Mineralization style III. A vein of later purple fluorite (PF) crosscutting prosopite (PS) and colourless fluorite (CF). A fine-grained prosopite vein (PV) crosscuts all other minerals. F) Image in polarized light of area shown in photo E.

35

euhedral but corroded single crystals in a fluorite or prosopite matrix (Plate F-C, D).

Prosopite occurs as aggregates of coarse-grained anhedral to euhedral crystals, sometimes with fibrous texture, and as veinlets of fine-grained prosopite with minor quartz. Coarse-grained prosopite is extensively replaced by fluorite (Plate F-C, D). Fine-grained prosopite veins are probably the latest stage, as they crosscut all other minerals (Plate F-C, D, E, F). There are at least three separate stages of fluorite mineralization. An early purple fluorite stage consists of thin, discontinuous veins which are crosscut by colourless fluorite. Massive, colourless fluorite is the most abundant type, comprising up to 40 % of the rocks in volume, which are crosscut by later dark purple fluorite veins (Plate F-E). Later dark purple fluorite also occurs interstitially to or as veinlets in the colourless fluorite, sometimes along fractures. Under cathodoluminescence, all fluorites are homogeneous and dark blue and all other minerals are non-luminescent. Goyazite occurs as fine-grained aggregates that appear to postdate the massive prosopite and fluorite. Elpasolite occurs as a fine-grained alteration product of cryolite. Some unusual minerals have also been identified from this assemblage including Nb- and Sn-bearing rutile (Samson et al., 1999) and an Ag-Sn-Te-S phase. The latter was reported by Muller (1986), and microprobe analyses indicate a stoichiometry of approximately $Ag_8Sn(TeS_2)_2$, which correlate with no known mineral species. No REE fluorocarbonates have been identified from this style mineralization. All fluorites have low REE concentrations (Kerr, 1995).

3.2.2.2 Coarse Ferroan Dolomite Alteration

Four main types of alteration are found in the study area: dolomitization, silicification, Fe-Mn alteration and felspathization. Most of the studied samples are altered to varying degrees. A major alteration is the formation of ferroan dolomite.

Coarse ferroan dolomite is closely associated with the fluorite-REE mineralization, which indicates that dolomitization is related to the mineralization. These dolostones are distributed mainly along the main mineralized zone. In hand sample, these rocks are dark grey to orange-brown colour. Coarse ferroan dolomite consists of nonplanar to planar-s, crystals with a nonmimical texture. It is light yellow in transmitted

light. Crystals range in size from 20 to 500 μm. Coarse, ferroan dolomites normally exhibit dull red colour under CL. Some samples contain very minor amount of skeletal grains replaced by ferroan dolomite, which shows that coarse ferroan dolomite is a replacement product. Coarse ferroan dolomite is the second most common type of dolomite in the samples used in this study after replacement non-ferroan dolomite.

3.2.2.3 Saddle Dolomite II

Saddle dolomite II in the study area is closely associated with fluorite, and is characterized by its coarse crystal size, curved crystal surfaces, and sweeping extinction. Crystals of saddle dolomite II range in size from 50 to 500 μm. Saddle dolomite II occurs primarily as a fracture- and vug-filling cement, however, it is also found replacing limestone where it is associated with fine-grained purple fluorite (Plate H-A, B). In rocks containing the fluorite-REE disseminated style of mineralization hosted by pervasive ferroan dolomite, coarse saddle dolomite II typically occurs around the edges of veins and vugs and may line the cavities with minor quartz and abundant fluorite (Plate G-E, F). The contact between saddle dolomite crystals and coarse ferroan dolomite of the host rocks, is, in some cases, gradational, but in most cases, it can be distinguished by the presence of brown REE mineral aggregates around the boundary of the original vug (Plate G-E), which indicates that saddle dolomite postdates the REE minerals. The boundary can also be distinguished by the contrast in CL characteristics; the red CL of the saddle dolomite versus the non- to dull red luminescence of the ferroan dolomite. The saddle dolomite is clearer and is coarser grained than the coarse ferroan dolomite.

3.2.3 Late Diagenesis

3.2.3.1 Late Calcitization

Late calcite refers to calcite precipitated in late veins, vugs and breccia matrices, or to calcite that occurs as a replacement of earlier rocks but which post-dates the fluorite mineralization. These calcites are the most common calcite type in the samples used in this study. There are at least three recognizable generations of late calcite as evidenced by crosscutting relationships (Plate I-E, F). The first generation of calcite is common in disseminated fluorite type rocks, and generally fills in veins and vugs containing

dolomite, quartz, and fluorite (Plate B-F, I-A, B). The dolomite, quartz and fluorite are replaced by the calcite, which comprises coarse, clear crystals that increase in crystal size towards the centre of the vugs, veins or pores.

Recrystallization of calcite is also an important feature in the study area, and has resulted in an increase in crystal size in mudstone facies and in the matrix of wackestone facies, to 5-20 μm or greater and these calcites normally replace saddle dolomite, fluorite, quartz and ferroan dolomite. These calcites generally have light red CL but in some cases exhibit zonation with alternating light red and red bands under CL.

A second generation of calcite occurs in wide veins and in the matrix to dolostone breccias. These calcite crystals are fibrous and non-luminescent and post-date the fluorite mineralization, as evidenced by the replacement of fluorite fragments by the matrix calcites. The latest calcite is calcite in veinlets which crosscut all other minerals. This calcite shows red luminescence and is ferroan in some cases.

3.2.3.2 Silicification

In rocks containing disseminated fluorite, late silicification occurs as aggregates of fine-grained quartz and length-fast chalcedony which replace fluorite and associated minerals. This silicification represents the latest stage of silicification in the study area.

3.2.3.3 Brecciation

Some breccias occur along the western margin of the property area just south of Rock Canyon Creek. These breccias are polymictic. Clasts are lithologically similar to rocks of Ordovician age. Their matrix is mainly composed of late coarse calcite (up to 95 % of the matrix), and the contact between this late calcite and fragments is sharp (Plate I-C). The late calcite matrix exhibits a fibrous texture. In these breccias, fluorite is only present in fragments. Some other breccias occur along the eastern side of the mineralization zone which has minor fluorite (up to 5 %) fragments. These fluorite fragments are replaced by late coarse calcite (Plate I-D).

CHAPTER IV
ISOTOPE STUDY

4.1 Carbon and Oxygen Isotope Results

4.1.1 Introduction

Several different carbonate minerals and phases have been analyzed to determine their isotopic composition. This section summarizes data on the carbon and oxygen isotopic composition of the carbonates in the study area. Details of the analyses can be found in Appendix I. According to their timing relative to mineralization, three groups of carbonates are described: pre-mineralization limestone and dolostone, syn-mineralization dolomites and post-mineralization calcites.

4.1.2 Pre-mineralization

(1) Ordovician Limestone:

Two samples of calcitic crinoid fragments in an Upper Ordovician packstone/grainstone facies limestone have $\delta^{18}O$ values of -9.8 and -9.6 ‰ VPDB, and $\delta^{13}C$ values of -1.5 and -1.2 ‰ VPDB. These values are somewhat (about 2‰) depleted in ^{18}O relative to typical data for Ordovician calcite (Veizer et al., 1997) (Fig. 4.1A).

(2) Devonian Limestone

Four samples from Devonian mudstone facies rocks have $\delta^{18}O$ values ranging from -9.4 to -8.1 ‰ VPDB (average = -8.5, σ = 0.6) and $\delta^{13}C$ values varying from -1.4 to 1.0 ‰ VPDB (average = -0.2, σ =1.1). These values are also somewhat depleted in ^{18}O relative to typical values of Devonian calcite (Fig. 4.1A), whereas the carbon isotopic values fall in the range of typical value of Devonian calcite.

(3) Microdolomite

Microdolomites (n = 7) from Upper Ordovician mudstone facies rocks have $\delta^{18}O$ values ranging from -7.8 to -3.2 ‰ VPDB (average = -5.6, σ = 0.2), and $\delta^{13}C$ values
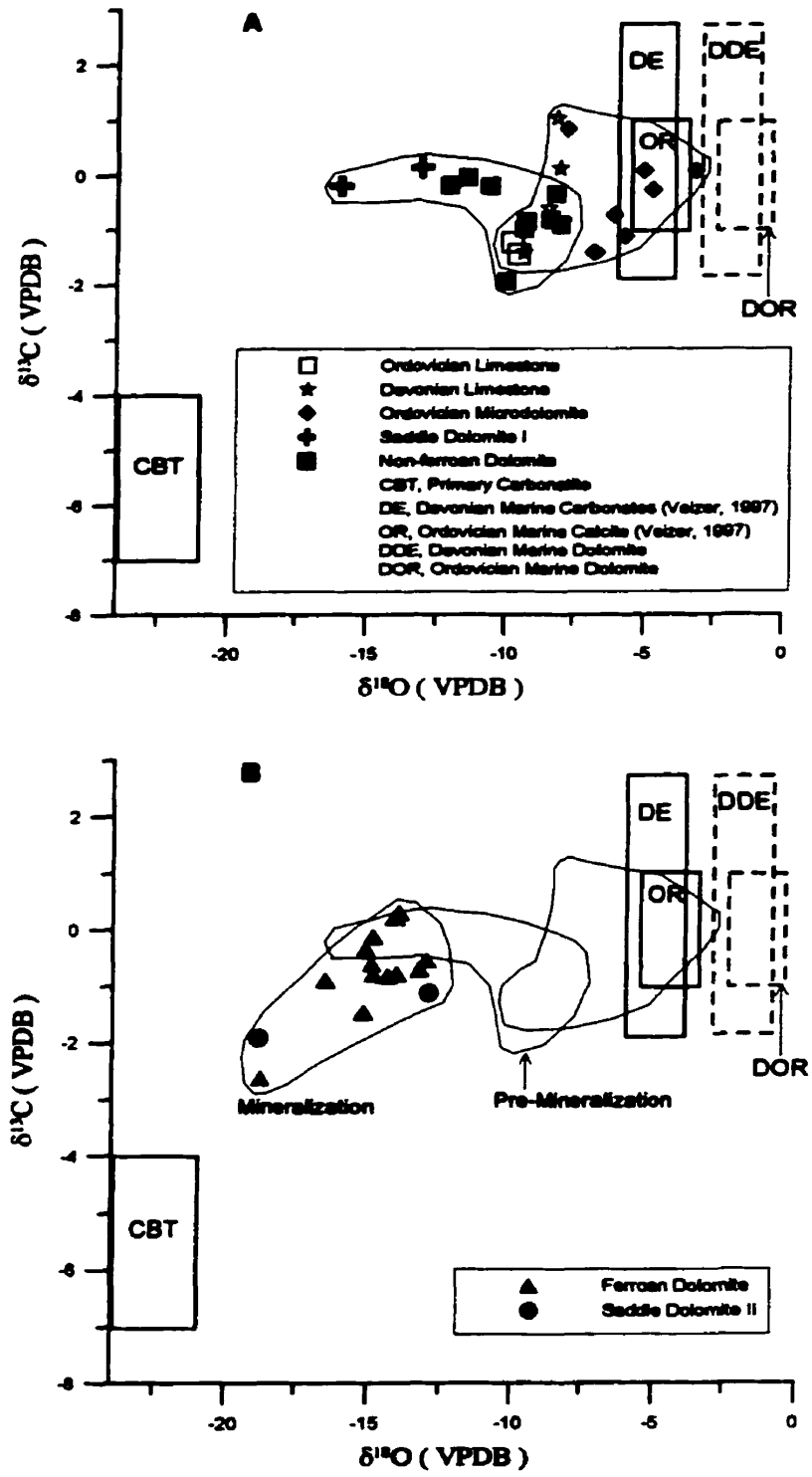
Fig. 4.1 Oxygen and carbon isotopic composition of different carbonate minerals.
A: Pre-mineralization carbonate phases.
B: Syn-mineralization carbonate phases.

varying from -1.4 to 0.8 ‰ VPDB (average = -1.4, σ = 0.2). This range of values overlaps the typical range for Ordovician dolomites (Fig. 4.1A). A dolomite cement value also falls in this range (Fig. 4.1A).

(4) Saddle Dolomite I

Two saddle dolomite I samples yielded values of -15.9 and -13.1 ‰ VPDB in $\delta^{18}O$ and -0.2 and 0.1 ‰ VPDB in $\delta^{13}C$, respectively. These values are significantly depleted in both ^{18}O and ^{13}C relative to those of Ordovician and Devonian marine dolomites.

(5) Coarse Non-ferroan Dolomite

Coarse, non-ferroan dolomites (n = 9) yielded $\delta^{18}O$ values ranging from -12.1 to -8.0 ‰ VPDB (average = -9.7, σ = 1.4) and $\delta^{13}C$ values varying from -2.0 to -0.1 ‰ VPDB (average = -0.7, σ = 0.6). Both ^{18}O and ^{13}C are more depleted than Ordovician and Devonian limestone and microdolomites (Fig. 4.1A).

4.1.3 Syn-mineralization

(1) Ferroan Dolomite

Samples (n = 13) from the ferroan dolomite which hosts the fluorite-REE mineralization are considerably more depleted in both ^{18}O and ^{13}C than the non-ferroan dolomite. The $\delta^{18}O$ values range from -18.8 to -13.0 ‰ VPDB (average = -14.9, σ = 1.5) and $\delta^{13}C$ values vary from -2.6 to -0.3 ‰ VPDB (average = -0.7, σ = 0.8) (Fig. 4.1B). The coarser-grained ferroan dolomites are more depleted in both ^{18}O and ^{13}C in general.

(2) Saddle Dolomite II

Two saddle dolomites, which are closely associated with the fluorite-REE mineralization, are also significantly more depleted in both ^{18}O and ^{13}C than non-ferroan dolomite and share the same range as that of the ferroan dolomite. The $\delta^{18}O$ values range from -18.9 to -13.0 ‰ VPDB and $\delta^{13}C$ values vary from -1.9 to -1.1 ‰ VPDB (Fig. 4.1B). Saddle dolomite II values are significantly more depleted in ^{13}C than those of saddle dolomite I.
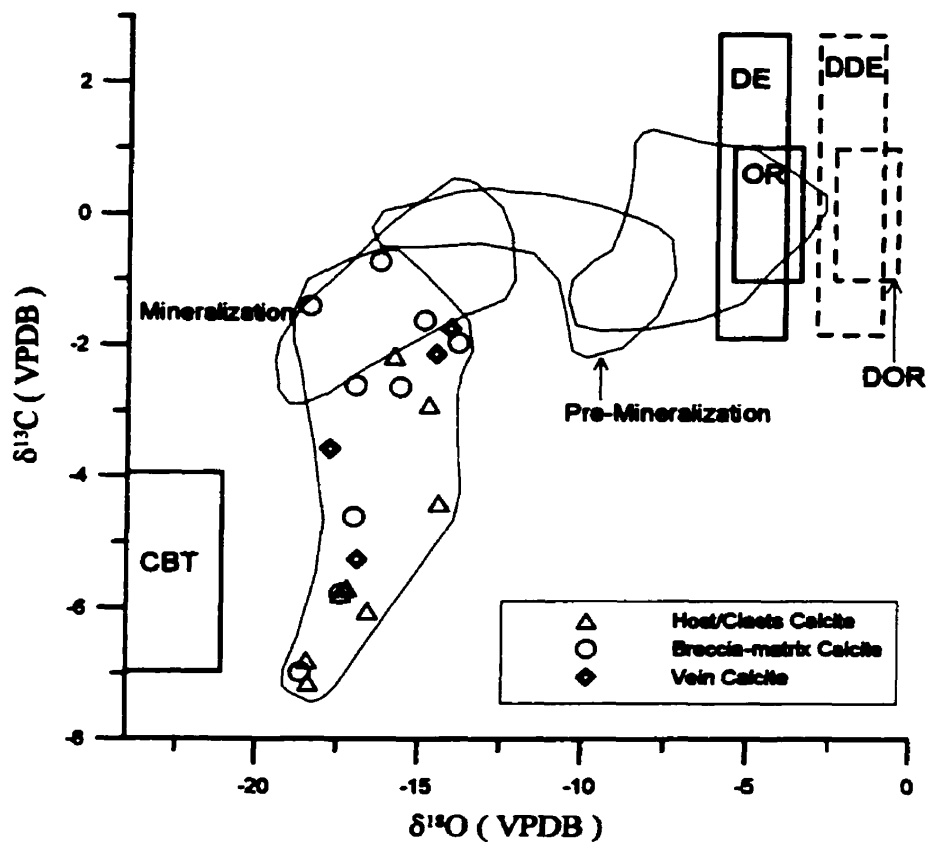
Fig. 4.2 Carbon and oxygen isotopic composition of post-mineralization calcites.

4.1.4 Post-mineralization

(1) Late Calcite Vein

Calcite (n = 4) from late calcite veins has $\delta^{18}O$ values ranging from -17.8 to -14.1 ‰ VPDB (average = -15.8, σ = 1.8) and $\delta^{13}C$ values varying from -5.3 to -1.8 ‰ VPDB (average = -3.2, σ =1.6). The $\delta^{18}O$ values fall in the same range as those of syn-mineralization dolomites, whereas the $\delta^{13}C$ values are highly variable and significantly more depleted (Fig. 4.2).

(2) Late Calcite Matrix

Calcite (n = 10) in breccia matrices yielded $\delta^{18}O$ values ranging from -20.7 to -13.8 ‰ VPDB (average = -17.0, σ = 2.0) and $\delta^{13}C$ values varying from -7.0 to -0.7 ‰ VPDB (average = -3.0, σ = 2.1). The $\delta^{18}O$ values fall in the same range as those of syn-

mineralization dolomites and late calcite veins, whereas the $\delta^{13}C$ values are more variable, and significantly more depleted (Fig. 4.2).

(3) Recrystallized Calcite Clasts and Host Rocks

Calcite from recrystallized breccia clasts and host rocks to the fluorite mineralization, which postdate the fluorite mineralization, (n = 8) have the same isotope composition as the late calcite veins and calcite from breccia matrices. They show significant ^{13}C depletion relative to pre- and syn-mineralization carbonates. The $\delta^{18}O$ values range from -18.4 to -14.4 ‰ VPDB (average = -16.6, σ = 1.5) and $\delta^{13}C$ values vary from -7.1 to -2.2 ‰ VPDB (average = -5.1, σ = 1.8).

4.2 Strontium Isotope Results

4.2.1 Introduction

In order to constrain the chemistry, environments and possible sources of the mineralizing and dolomitizing fluids, several samples have been analyzed for their strontium isotopic composition ($^{87}Sr/^{86}Sr$). These are: limestone, microdolomite, coarse ferroan dolomite, saddle dolomite, replacement non-ferroan dolomite and late calcite. A completed compilation can be found in Appendix I.

4.2.2 Strontium Isotope Results

Figure. 4.3 illustrates the $^{87}Sr/^{86}Sr$ ratio of the analyzed samples plotted against $\delta^{18}O$ for calcite and dolomite from the study area. Microdolomite in Ordovician mudstone facies rock has a value of 0.70809 and falls in the range for postulated Ordovician seawater. Very fine-grained Devonian calcite, east of the deposit, shows a slightly enriched value of 0.70862 with respect to Middle Devonian seawater. Late calcite in a breccia matrix has values of 0.70998 and 0.70822 which are a more radiogenic than Devonian calcite. Saddle dolomite II, associated with the fluorite mineralization, has a value of 0.707839, which is similar to that of Ordovician or Devonian seawater, whereas saddle dolomite I which is not evidently associated with fluorite mineralization yields a

value of 0.70995. The ferroan dolomites yield very low $^{87}Sr/^{86}Sr$ ratios ranging from 0.70462 to 0.70336.
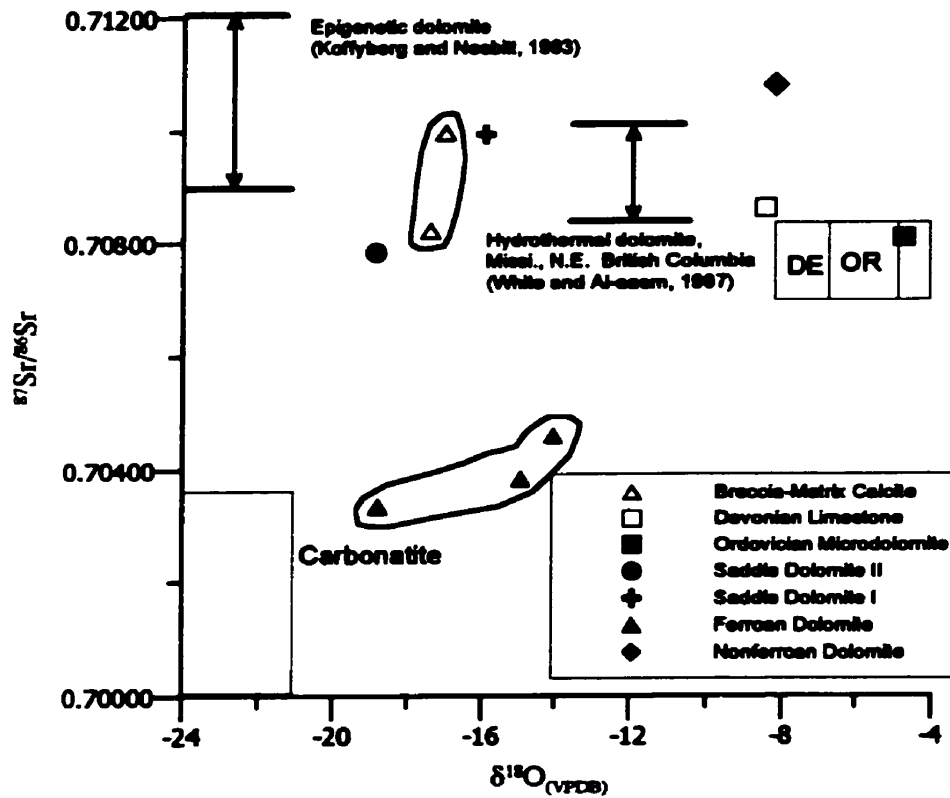
Fig. 4.3 $^{87}Sr/^{86}Sr$ and oxygen isotopic composition for calcite and dolomite phases comparing with published data for Rocky Mountains carbonates.

CHAPTER V
Fluid Inclusion Study

5.1 Fluid Inclusion Characteristics

5.1.1 Fluid Inclusion Types

In the study area, minerals suitable for fluid inclusion study include late calcite and a variety of dolomite and fluorite types. Fluid inclusions were classified according to the type and proportion of phases present at room temperature. Inclusions, which were interpreted to have undergone necking, were not included in this classification. Three types of fluid inclusions have been identified (Fig. 5.1)

Type L: Aqueous Liquid.

Type LV: Aqueous Liquid-Vapour.

Type LVS: Aqueous Liquid-Vapour-Solid.
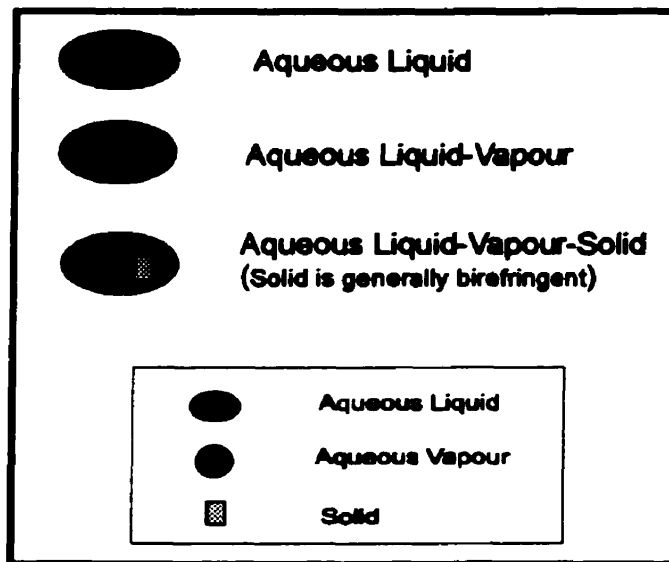
Fig. 5.1 Schematic Summary of Fluid Inclusion Types

Aqueous type (L) inclusions are widespread in the study area, though not very abundant, occurring in carbonates, quartz and a variety of the fluorite types. The liquid

48

only inclusions in carbonates are typically less than 2 μm in size, whereas those in fluorite are highly variable in size, ranging from 1 to 20 μm.

The aqueous liquid-vapour inclusions (LV) are by far the most abundant, occurring in different types of carbonates and all variety of fluorite types. LV inclusions in the different types of dolomite are mostly very small, ranging from 1 to 4 μm in size. LV inclusions in late calcite are typically between 2 and 15 μm in size. LV inclusions in fluorite range in size from 5 to 30 μm. Vapour/liquid ratios of LV inclusion are highly variable, ranging from about 1:5 to up to 6:1.

Aqueous liquid-vapour-solid inclusions (LVS) are typically between 10 and 30 μm in size. This type of inclusion has only been found in fluorite and late calcite. The solids within fluorite-hosted LVS inclusions are generally birefringent, euhedral, and in most cases occur as aggregates of fine-grained crystals. The solids are considered to have been trapped, rather than be daughter minerals because they are irregularly distributed in the inclusions and form aggregates rather than single crystals. In some cases, the solids within LVS inclusions are birefringent and square or rectangular in shape.

5.1.2 Distribution and Origin of Fluid Inclusions

5.1.2.1 Primary Fluid Inclusions

The origins of the fluid inclusions from Rock Canyon Creek were assessed using the criteria of Roedder (1984). Primary fluid inclusions are present in fluorite, ferroan dolomite, non-ferroan dolomite, saddle dolomite and late calcite.

Primary fluid inclusions in dolomite

Most of the ferroan dolomite crystals contain fluid inclusions. More than 80 % of the inclusions are type L and secondary, but some LV inclusions away from planes of secondary inclusions are interpreted as primary inclusions. These primary inclusions are isolated from other inclusions and are irregular in shape. They are typically very small (< 5 μm), and make up less than 1 % of the volume of the host ferroan dolomite. It's difficult to measure these inclusions due to the yellow colour of the host crystals and small size of

the inclusions. No solid-bearing inclusions have been found in ferroan dolomite. The characteristics of the inclusions in saddle dolomite and non-ferroan dolomite are the same as those of ferroan dolomite.

Primary fluid inclusions in fluorite

Inclusions in fluorite are more complex. Most of the fluorite contains abundant inclusions, however, dark purple fluorite rims of zoned fluorites are basically inclusion-free. The inclusions make up 5 to 10 % of the volume of the host crystals. Fluorite in the massive fluorite samples is inclusion free. Based on their distribution and characteristics, four groups of fluid inclusions in fluorite have been identified: (1) LV inclusions in zoned fluorite; (2) LV inclusions in yellow cores of the breccia-matrix fluorite; (3) LVS inclusions in yellow cores of the breccia matrix fluorite; and (4) LV inclusions in disseminated fluorite.

1) The aqueous liquid-vapour inclusions (LV) in zoned purple-colourless fluorite of the breccia-matrix fluorite are elongate and distributed along growth bands in the zoned fluorite (Plate J-B, C). Such inclusions are considered to be primary. They range from 5 to 20 μm in size. The vapour bubbles occupy about 15 per cent, on average, of the volume of these inclusions. No solids have been observed in the inclusions in zoned fluorite.

2) Aqueous, liquid-vapour inclusions in the yellow cores of breccia-matrix fluorite occur either as isolated inclusions (Plate J-C) or in three-dimensional arrays. The inclusions normally make up to 2 to 5 % of the volume of the host crystals. The size of the inclusions is highly variable, ranging between 2 and 30 μm. They are mostly irregular in shape. In some cases, vapour bubbles make up about 40 % of the volume of the inclusions (Plate K-A, B, C), and these high vapour/liquid ratio inclusions tend to decrepitate during microthermometric measurement.

3) In the yellow cores of the breccia-matrix fluorite, some inclusions contain an unidentified solid crystal along with a vapour bubble and a liquid phase. These inclusions occur as clusters. In crystals where LVS inclusions present, there are fewer LV inclusions. The size of these crystals is consistent relative to the volume of the

Plate J INCLUSION TYPE (I)

LVS inclusion in late calcite, solid minerals are birefregent.

LV inclusion in zoned breccia-matrix fluorite, note that the inclusion distributed along the growth zone.

LV inclusion in zoned breccia-matrix fluorite, same view as the box in photo B, but different magnification.

Plate K INCLUSION TYPE (II)

C

LV inclusion in yellow cores of breccia-matrix fluorite

B
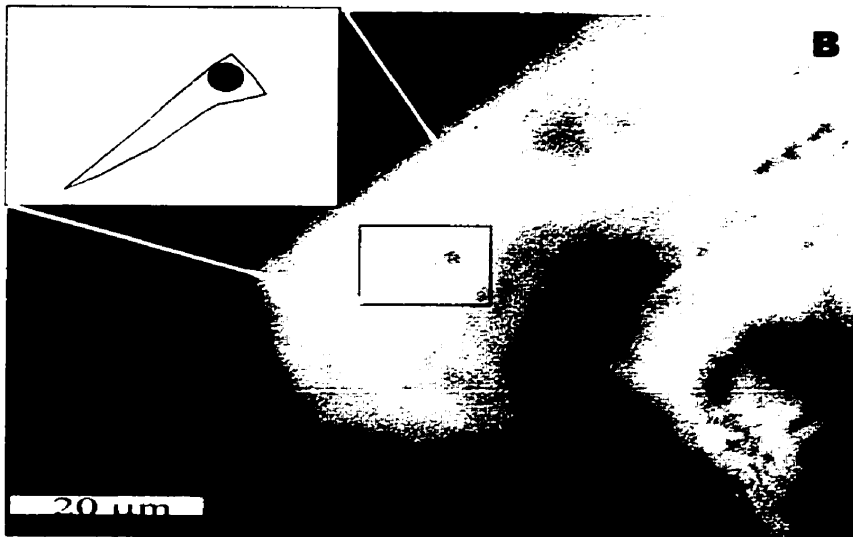
LV inclusion in yellow cores of breccia-matrix fluorite. The box shows the schematic map of the inclusion.

C

LV inclusion in yellow cores of breccia-matrix fluorite

52

inclusion (about 10 % of the volume of the inclusions), and their occurrence as single crystals (Plate L-A) rather than aggregates indicates that they are daughter minerals. Their identities could not be determined by Raman spectroscopy due to the intense fluorescence of the host fluorite. The vapour/liquid ratio in these LVS inclusions is also relatively consistent with the vapour bubble comprising about 15 to 20 per cent of the volume of the inclusions.

4) In the disseminated fluorite type rocks, fluid inclusions are mainly in colourless fluorite (II and III), most of these inclusions are secondary or pseudosecondary. Inclusions that do not appear to be related to planes have, however, been considered as primary inclusions. These inclusions are LV and occur either as isolated inclusions or in three-dimensional arrays. They are highly variable in size and irregular in shape. This type of inclusion is rare and make up about 2 % of the volume of the host crystals. The vapour bubble occupies about 10 to 20 % of the volume of the inclusions. Some of the higher vapour/liquid ratio inclusions tend to be decrepitated during microthermometric measurement.

Primary inclusions in late calcite

Most of the late calcite is inclusion free. In some cases, however, late calcite crystals have abundant inclusions including LV and LVS types, making up to 40 % of the volume of the host calcite (Plate J-A). The inclusions are mostly LV inclusions. LV inclusions in late calcite are generally rounded, but in some cases are elongate, and range between 2 and 10 μm in diameter. These inclusions usually have wide, dark edges. The vapour bubble, on average, occupies approximately 30 % of the volume of these inclusions. Some large inclusions contain a solid phase. These LVS inclusions are typically larger than the LV inclusions. They occur as rounded to elongate inclusions and range between 5 and 15 μm in size. The solid minerals are typically birefringent. Overall, the elongate inclusions are oriented along the growth direction as defined by abundant small inclusions (Plate J-A).

Plate L INCLUSION TYPE (III)

A
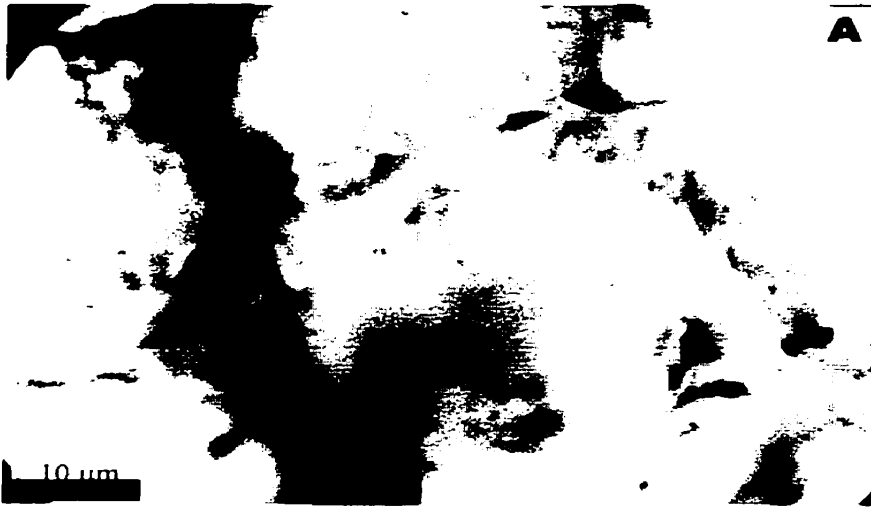
LVS inclusion in yellow cores of breccia matrix fluorite, solid minerals are birefregent.

B
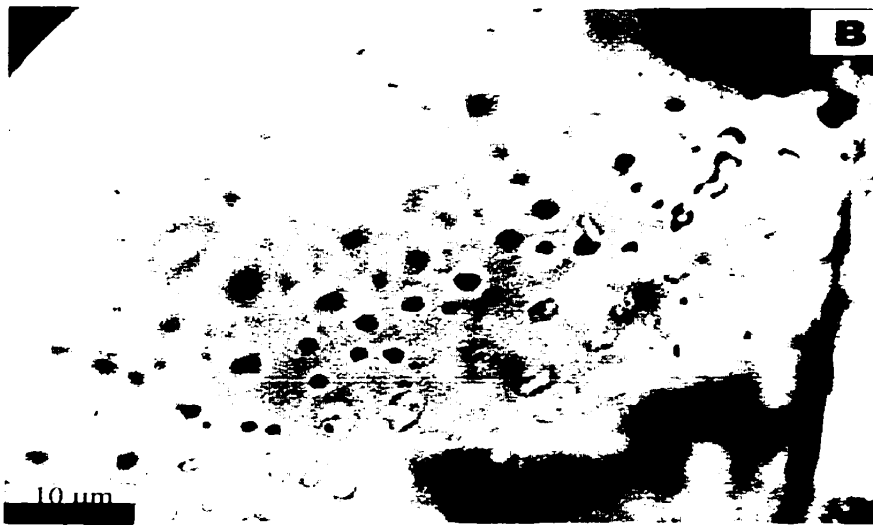
Secondary LV inclusions in disseminated fluorite, note that secondary inclusions occur in obvious planes.

C

Microphotograph of fluid inclusions during crushing test, note that the vapor bubbles in inclusions expanded rapidly.

54

5.1.2.2 Secondary inclusions

Secondary fluid inclusions are present in all minerals. In disseminated fluorite, secondary inclusions are more abundant than primary inclusions. In most cases, secondary inclusions were easy to identify, as they normally occur in obvious planes (Plate L-B). Most of the secondary inclusions in fluorite are LV inclusions; rare LVS inclusions are also present. The solid crystals occur either as single crystals or as aggregates. These crystals are birefringent and may be trapped carbonates.

5.2 Microthermometry of Fluid Inclusions

5.2.1 Introduction

Freezing and heating experiments were performed on different minerals including ferroan dolomite, non-ferroan dolomite, saddle dolomite, late calcite and the various variety of fluorite. Temperatures of initial freezing (Tn), initial melting (Te), final ice-melting (Tm ICE), hydrohalite-melting (Tm HH), inclusion homogenization (Th L-V) and inclusion decrepitation (Td) were made on liquid-vapour and solid-liquid-vapour inclusions. The small size of most inclusions (5 – 10 μm) prevented accurate measurements of the initial melting temperature. Although some of the inclusions yielded initial melting temperature of around -20 °C, most inclusions are halite undersaturated and Te values are lower than -20.8 °C (The eutectic temperature for the H_2O-NaCl system). The NaCl-$CaCl_2$-H_2O system has been used to convert the TmICE to salinity (Bodnar, 1993). This is reasonable in fluorine-rich hydrothermal system (Ca-rich) and because of the carbonate wall rock environment. The detailed data can be found in Figure 5.2 to Figure 5.4 and in Appendix II.

5.2.2 Results

5.2.2.1 Ferroan Dolomite

Upon cooling, liquid-vapour inclusions in ferroan dolomite froze to a dark, microcrystalline mosaic at temperatures between -58 and -47°C. Eutectic temperature (Te) ranges from -20 to -21 °C. Th LV values range from 158 to 203 °C (Fig. 5.2) (mean
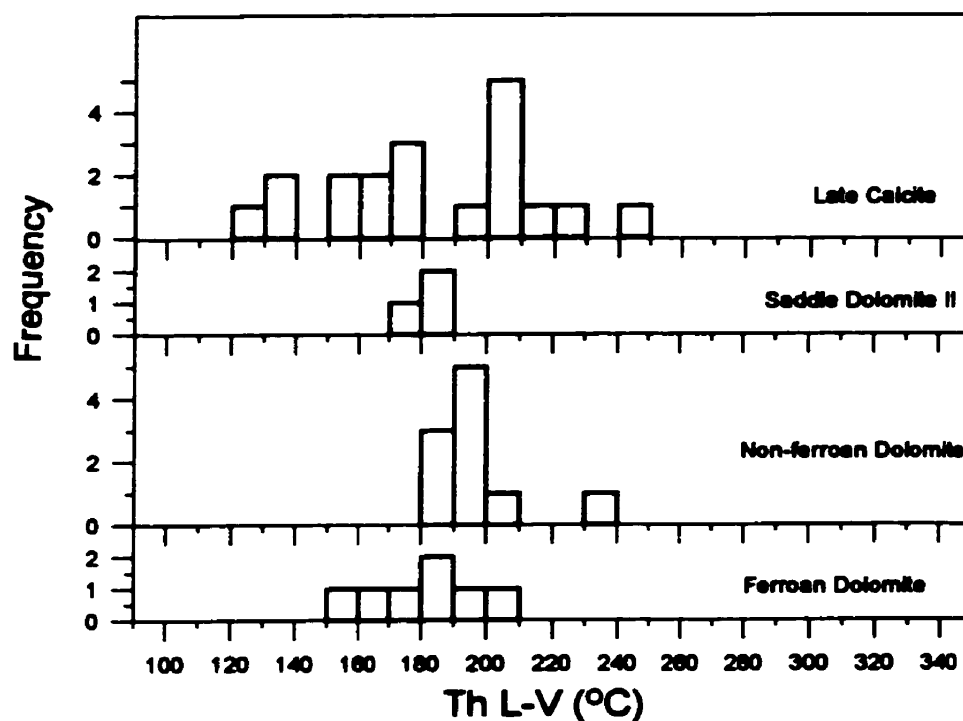
Fig 5.2 Histogram of Th L-V for fluid inclusion from different carbonates

= 181, σ = 15) with the mode at approximately 180 °C. Final ice-melting temperatures are highly variable, ranging from −22.1 to −6.7 °C (mean = -12 °C, σ = 7).

5.2.2.2 Non-ferroan Dolomite

Liquid-vapour inclusions from non-ferroan dolomite yielded homogenization temperatures ranging from 182 to 233 °C with a mode at approximately 195 °C (Fig. 5.2) (mean = 197 °C, σ = 15), which falls in the same range as the values for ferroan dolomite. A final ice-melting temperature measured on one good LV inclusion was −10.7 °C. No eutectic temperature was measured.

5.2.2.3 Saddle Dolomite II

Due to the small size of the inclusions from saddle dolomite II, no eutectic temperature and final ice-melting temperature have been measured. Homogenization temperatures of LV inclusions from saddle dolomite lie between 172 and 189 °C with the

mode at approximately 180 °C (Fig. 5.2) (mean = 181 °C, σ = 8), which are similar to the values for ferroan dolomite and non-ferroan dolomite.

5.2.2.4 Disseminated Fluorite

As indicated in section 5.2.2.1, LV inclusions are mainly found in colourless fluorite II and III of disseminated fluorite style rocks. During cooling, the aqueous liquid-vapour inclusions in disseminated fluorite started to freeze to a microcrystallime mosaic and/or the vapour bubble disappeared at temperatures between -30 and -73 °C. During heating from room temperature, some high vapour/liquid ratio inclusions decrepitated at temperatures between 146 and 272 °C. Eutectic temperatures were measured at around -27 °C. Homogenization temperatures are highly variable, ranging from 114 to 274 °C (mean = 183 °C, σ = 42.8) (Fig. 5.3). Final ice-melting temperatures (Tm ICE) range from -23.8 to -8.9 °C (mean = -15.3 °C, σ = 5.77). Within this range, two populations are evident, with modes at approximately -25 and -11 °C (Fig. 5.4, salinities are 25 and 11 wt % NaCl+CaCl₂ equiv).

5.2.2.5 Yellow Cores in Breccia-Matrix Fluorite

Initial freezing temperatures for liquid-vapour inclusions in the yellow fluorite cores were between -65 and -45 °C During heating from room temperature, some high vapour/liquid ratio inclusions decrepitated at temperatures between 84 and 247 °C. No eutectic temperatures were measured. Solid phases in LVS inclusions do not dissolve on heating (> 400 °C). Homogenization temperatures (Th LV) for all LV and LVS inclusions are also highly variable, ranging from 110 to 347 °C (mean = 191.7°C, σ = 55.08), with the mode at approximately 170 °C (Fig. 5.3). Final ice-melting temperatures (Tm ICE) range from -26.7 to -8.9 °C (mean = -13.9 °C, σ = 5.34), with most of the data clustered around -11 °C (Fig. 5.4), which is equivalent to a salinity of 11.3 wt % NaCl+CaCl₂.

5.2.2.6 Zoned Breccia-Matrix Fluorite

Inclusions in zoned fluorite yielded relatively good micorthermometric data due to their larger size. Initial freezing temperatures for liquid-vapour inclusions in zoned fluorite

are between –56 and –35 °C, which is lower than those of other fluorites. During heating from room temperature, some high vapour/liquid ratio inclusions decrepitated at temperatures of between 122 and 202 °C. Eutectic temperatures lie between –28 and –17 °C. Solid phases in LVS inclusions do not dissolve on heating (> 400 °C). One good inclusion yielded a hydrohalite-melting temperature of –2.8 °C after ice had melted at –4.2 °C. Homogenization temperatures (Th LV) for all LV and LVS inclusions are also highly variable, ranging from 97 to 290 °C (mean = 160.5 °C, σ = 73.8), with a mode at approximately 110 °C (Fig. 5.3), which is lower than those of other fluorites. Final ice-melting temperatures range from –9.5 to –2.0 °C (mean = -5.6 °C, σ = 2.2), and are higher than those of the other fluorite types (Fig. 5.4). The mode for this group (-6 °C) is equivalent to a salinity of 6.1 wt % NaCl+CaCl$_2$.
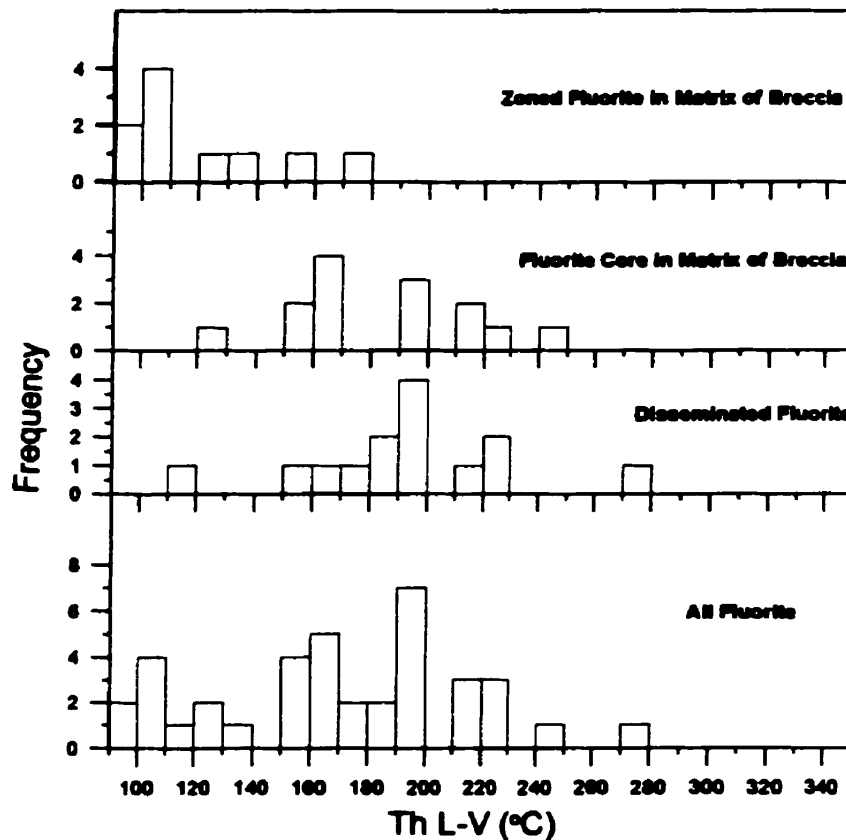
Fig 5.3 Histogram of Th-LV of fluid inclusions for variety of fluorites.
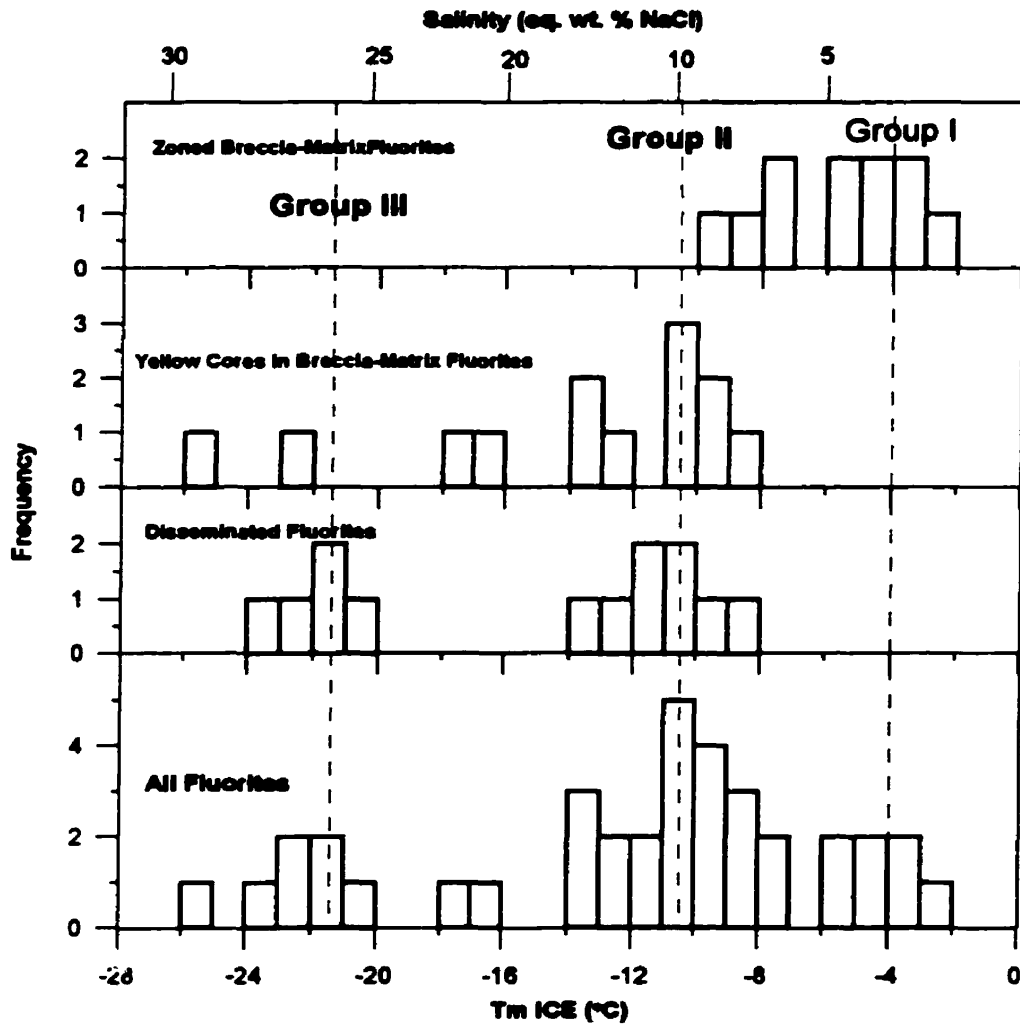
Fig. 5.4 Histogram of salinity of fluid inclusions for variety of fluorites

5.2.2.7 Late Calcite

Upon cooling, liquid-vapour inclusions from late calcite froze to a dark microcrystalline mosaic and the vapour bubble disappeared suddenly at temperatures between −59 and −66 °C. One sample has a eutectic temperature of −23.1 °C. Liquid-vapour-solid inclusions yielded initial freezing temperatures ranging from −60 to −48 °C. Solid phases in LVS inclusions do not dissolve on heating (> 400 °C). Final ice-melting temperatures for all inclusions in late calcite lie between −21.9 and. −13.6 °C (mean = − 17.4 °C, σ = 3.3). Homogenization temperatures are scattered, and range from 130 to 241 °C (mean = 183 °C, σ = 34) with the mode at approximately 200 °C (Fig. 5.2).

5.3 Gas Chemistry

Laser Raman spectroscopy, gas chromatography and crushing tests were used in an attempt to characterize the gases present and the pressure in the fluid inclusions from the Rock Canyon Creek fluorite.

Several inclusions from samples in which decrepitation was common at low temperature were tested by crushing. The vapour bubbles in the inclusions expanded into large bubbles during the crushing (Plate L-C), which indicated that the pressure in the inclusion is higher than atmospheric pressure.

Several inclusions in fluorite with relatively large vapour bubbles were analyzed for CO_2, CH_4, H_2S, and SO_2 using laser Raman spectroscopy. None of these gases were detected. This indicates that these gases are absent in the inclusion or their concentration are below detection limits, which are likely to be high because of the intense fluorescence of the host fluorite.

Three fluorite samples with abundant LV inclusions were analyzed by gas chromatography. One of the samples was lost during analysis. In the two others, N_2, CO_2, CH_4, $i-C_4H_{10}$, and H_2O were measured. Their abundances and mole fractions are given in Table 4.1. Basically, these two sets of data are very similar. Carbonic gas is an important constituent of the inclusions. X_{CO_2} values of 5.03 and 5.37 seem high given the absence of CO_2-related phase changes during the microthermometric measurement.

Table 4.1 Gas Chromatographic Data.

Sample #	Water	N_2		CH_4		CO_2		$i-C_4H_{10}$	
	mol	Mol	(%)	Mol	(%)	Mol	(%)	mol	(%)
RCC95-5	1511.75	2.20	0.15	1.26	0.08	76.09	5.03	N/A	N/A
RCC37	1951.61	4.95	0.25	1.56	0.08	104.72	5.37	0.34	0.02

CHAPTER VI
DISCUSSION AND INTERPRETATION

6.1 Paragenetic Sequence

Interpretation of the paragenesis for Rock Canyon Creek rocks is based on the preceding petrographic, mineralogic and geochemical results. The products and timing of the diagenetic and hydrothermal events are divided into three major stages: early diagenesis, mineralization and post-mineralization, and are summarized in Figure. 6.1.

6.1.1 Early Diagenesis

In the Rock Canyon Creek area, early diagenetic events refer to those that predate the fluorite-REE mineralization and includes micritization, microdolomite formation, compaction, dissolution, calcite cementation, dolomite cementation, silicification and brecciation.

Micritization:

Petrographically, the dark micrite rims surrounding grains represent the first diagenetic event in the study area. Micritization is an early marine process that involves endolithic algae, cyanobacteria and fungi boring into skeletal fragments; these bores are then filled with micrite, a microcrystalline calcite (Tucker, 1981; Tucker and Wright, 1990). Repeated boring and in-filling results in the formation of micrite envelopes around grains (Tucker, 1981). Poikilotopic calcite and calcite spar fill in the intraparticle porosity and surround the micrite envelopes, indicating that micritization predates calcite cementation.

Microdolomite

Microdolomite precipitated before the onset of mechanical and chemical compaction because early stylolites and veinlets crosscut the microdolomites, and stylolites in the same sample are dolomitized by later replacement non-ferroan dolomite. Chemical compaction begins after a few metres of burial and continues to a depth of several hundred metres (Shinn and Robbin, 1993; Choquette and James, 1987), which indicates that the microdolomite was precipitated either at the sediment-water interface or prior to burial in excess of 10 m. Other studies have shown that microdolomite occurs in

Fig. 6.1 Paragenetic Sequence of Rock Canyon Creek Fluorite-REE Deposit

Events	Early ⟶ Late
Micritization	▬
Microdolomite	▬
Early Calcite Cementation	▬▬▬▬▬
Compaction	▬▬▬
Dissolution	▬▬▬
Silicification	▪ ▪ ▪ ▪ ▪ ▪ ▪ ▪ ▪ ▪ ▪
Brecciation	▬▬▬ ▬▬ ▬▬
Dolomite Cement	▪ ▪ ▬▬▬
Replacement Non-ferroan Dolomite	▪ ▪ ▪ ▪ ▪ ▪ ▪
Ferroan Dolomite	▬▬
Saddle Dolomite (I, II)	I ▬▬ ▬▬ II
Fl, REE-Mineralization	▬▬▬▬
Late Calcite	▬▬

Mineralization ⟷

62
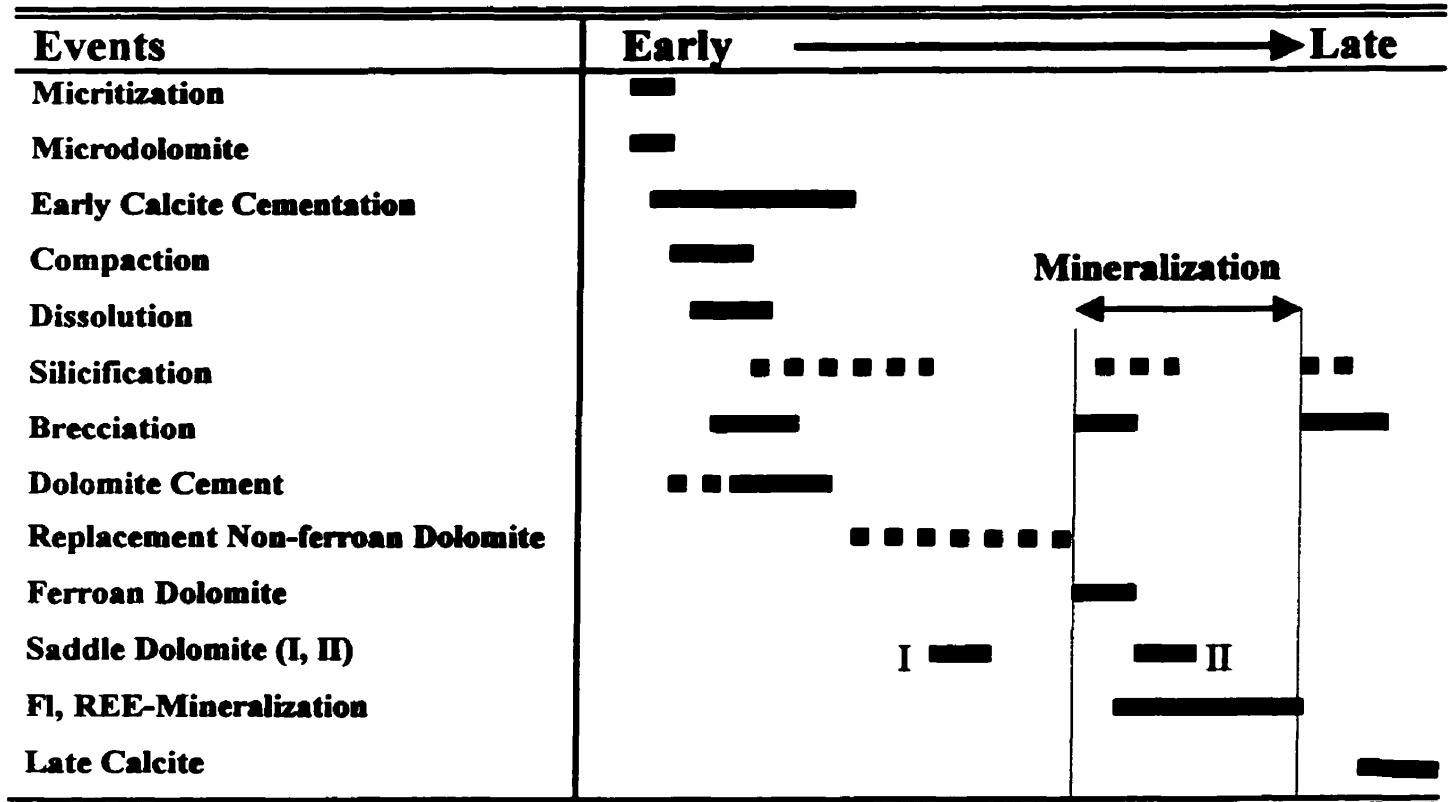
Fig 6.2A Paragenetic Sequence of Fluorite-REE Mineralization Stage
for Disseminated Fluorite and Breccia Matrix Fluorite type Rocks.

Events	Early —————————————→ Late
Ferroan Dolomite	▬
REE Minerals	▬
Saddle Dolomite II	▬
Colourless Fluorite I	▬
Colourless Fluorite II	▬
Purple Fluorite	▬
Colourless Fluorite III	▬
Yellow Cores	▬
Zoned Fluorite	▬
Silicification	▬
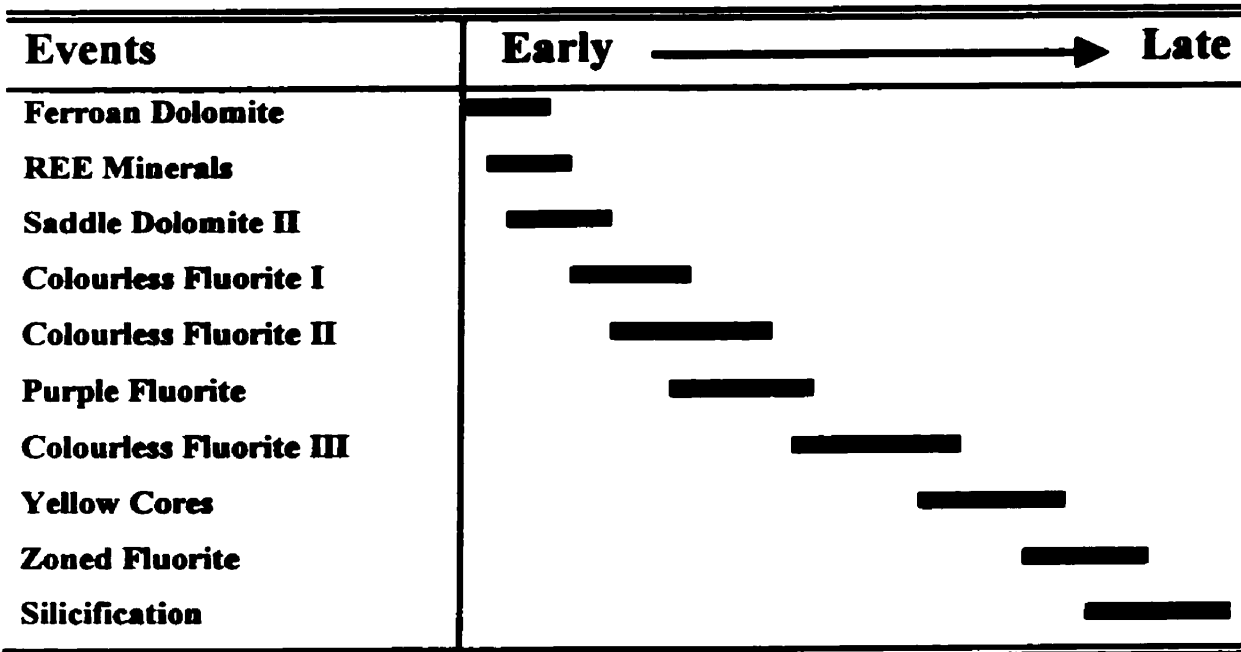
Fig 6.2B Paragenetic Sequence of Fluorite-REE Mineralization Stage
for massive fluorite type rocks

Events	Early —————————————→ Late
Cryolite, Phlogopite	▬
Quartz	■ ■ ■ ■ ■ ■
Coarse Prosopite	▬
Low REE Purple Fluorite	▬
Colorless Fluorite	▬
Purple Fluorite	▬
Fine Prosopite Vein	▬
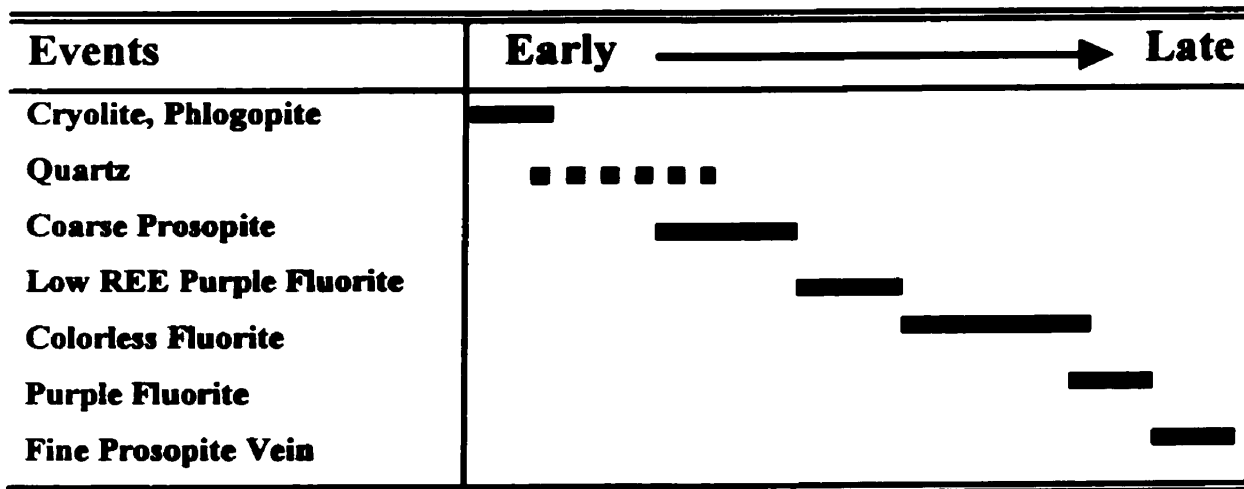
mudstone and wackestone facies that were originally precipitated in upper intertidal to supratidal settings (Tucker and Wright, 1990). The presence of clear rims around cloudy cores in the microdolomites indicate that they have been undergone a recrystallization.

Early Calcite Cementation

Calcite cementation is an important aspect of the diagenetic history of Rock Canyon Creek rocks, and it began in marine environments, continued through deep burial environments to later diagenetic events. Early calcite cementation includes pokilotopic calcite, coarse calcite spar and early calcite veining. All these types of calcite cements are non-ferroan and composed entirely of low-Mg calcite. The pokilotopic calcite cements formed during a relatively early diagenetic stage, either in a marine environment or in early burial stage. The calcite spar calcite veining occur as coarse crystals and in interparticle pores, cavity and veinlets, indicate that these calcites postdate dissolution and compaction.

Compaction:

After deposition of the carbonate sediments, various compactional textures and fabrics were developed due to overburden stresses. Particle reorientation and sediment dewatering begins at a depth of approximately one metre below the sediment-water interface (Choquette and James, 1987, 1990), so that mechanical compaction affects sediments relatively early in their diagenetic history. Although compaction occurs early in diagenesis, it is later than micritization and microdolomitization as evidenced by broken micrite envelopes and that microdolomites were crosscut by veinlets and stylolites.

Dissolution

Dissolution textures are also a common feature and are thought to have developed early in the diagenetic history of the Rock Canyon Creek rocks. Dissolution may occur in several different environments including sub-seafloor, meteoric and deep burial (Tucker, 1981). Examples of dissolution include: dissolution of metastable fossil grains, formation of stylolites and dissolution of dolomite crystals.

Dissolution of fossil grains occurred deriving early diagenesis, possibly from the infiltration of meteoric water. This is consistent with the presence of solution-collapse

breccias, which are indicative of paleoexposure. Fossils originally composed of aragonite and high-Mg calcite (Tucker, 1981) were dissolved, leaving voids which were later filled by dolomite spar, as evidenced by the presence of a geopetal textures, indicating that dissolution might have occurred before dolomite cements.

Formation of stylolites develops because of the difference in the relative solubility of components when subjected to increased pressure during burial (Choquette and James, 1990). In the Rock Canyon Creek rocks, stylolites crosscut the microdolomites, suggesting that pressure solution postdated microdolomitization.

The presence of intraformational dissolution-collapse breccias with dolomite cements and subsequent fluorite mineralization show that dissolution events predate dolomite cements and fluorite mineralization.

Brecciation

The first generation of brecciation is represented by the intraformational solution-collapse breccias. The fragments in these breccias are poorly-sorted, not rotated, and showing little dissolution. In a few cases, however, there are some rounded fragments in vugs showing evidence of dissolution. No obvious offsetting of existing fractures and veins have been observed, this indicates that the brecciation might not have been caused by faulting. Although no evidence of evaporation and solution such as speleothem or red beds are present in the Rock Canyon Creek area, some evaporites and solution-collapse breccias have been reported (Dix, 1990). Dissolution of evaporite beds will cause collapse of overlying units, producing collapse breccias.

Along the west slope of the creek west of Candy Creek, there is a well-exposed basal conglomerate. Dix (1991) ascribed the conglomerate to a channel filling on an irregular paleotopography. Similar channelling characterizes the Owen Creek base (Norsford, 1969), but also the base of the Middle Devonian (Yahatinda Formation) along the east margin of the West Alberta Arch. This unconformity might also cause solution-collapse breccia formation.

The breccia fragments are surrounded by isopachous dolomite cements, which are coated by saddle dolomite, quartz and fluorite. These textures show that the brecciation

predates the fluorite mineralization and is relatively early in the diagenetic history of the sequence because it predates the formation of the dolomite cements.

Dolomite Cements

Dolomite cements occur as open space fill such as in veins, vugs and in the matrices of intraformational solution-collapse breccias. It also occurs as isopachous rims around microdolomite clasts in intraformational breccia and conglomerate, which indicates that the dolomite cements postdate the microdolomites, but predate the mineralization because these dolomite cements are replaced by fluorite. Under cathodoluminescence, these dolomites are all nonluminescent, which indicates that trace element activators (eg. Fe^{2+}) were not incorporated into the cements, which is consistent with the staining analysis of these dolomite. This is generally the case for cements precipitated by fluids in a marine environment (Steinhauff, 1989) where these elements would be oxidized and thus unavailable for incorporation into the cements (Tucker and Wright, 1990).

Saddle Dolomite I

Saddle dolomite I predates the mineralization, as it is replaced by fluorite. Saddle dolomite I exhibits dull-red CL, but, in some cases, shows CL zonation with red to bright red cores and several outer bands that alternate between being nonluminescent and exhibiting a red CL. These zoned dolomites occur at the boundaries of open space such as veins and vugs, and are followed by non-luminescent saddle dolomite.

Replacement Non-ferroan Dolomite

The replacement non-ferroan dolomites selectively to pervasively replace wackestone and packstone facies. Some of these dolomites have inclusion-rich cores and clear, inclusion-free rims, indicating recrystallization (Tucker and Wright, 1990). The contact between fragments of replacement non-ferroan dolomite and the matrix of fluorite in breccia-matrix style rocks is sharp. Some non-ferroan dolomite relicts floating in the fluorite matrix were replaced by the fluorite, indicating that formation of replacement non-ferroan dolomite predates the fluorite mineralization.

Silicification

As described previously, there are several stages of silicification. The first generation of silica includes microquartz laminae in laminated mudstone, chert nodules in siliceous dolostone and some megaquartz in pores left by fossil fragment dissolution. The megaquartz is normally associated with dolomite cements, indicating that the first silicification is syn- to postdate dolomite cement precipitation. The source of silica could either be biogenic or nonbiogenic. The presence of chert nodules may be taken to indicate the redistribution of biogenic silica (Hesse, 1989), although the siliceous organisms may not be abundant enough in shallow-water carbonates to form the chert nodules (Dapples, 1959). A nonbiogenic source of silica that is reasonable for burial environments is from the conversion of smectite to illite (Hesse, 1989) within the nearby shale basin west of the deposit (Yao et al., 1997), which is consistent with more extensive silicification west of the deposit than east of the deposit.

6.1.2 Mineralization

Petrographic relationships indicate that the mineralization was the result of several stages of hydrothermal activity. In order to evaluate the relationship between the dolomitization and fluorite-REE mineralization, a detailed discussion of the paragenetic sequence for the mineralization stage is presented in this section. These paragenetic studies show that coarse-ferroan dolomites and saddle dolomites are closely associated with the F-REE-rich hydrothermal mineralization, as well as extensive brecciation and silicification. A detailed paragenetic sequence is presented in Figure. 6.2.

Coarse Ferroan Dolomite

Coarse ferroan dolomites are principally found in rocks from the main mineralized zone and are the principal hosts to the mineralization. The spatial distribution of coarse ferroan dolomite along the fluorite-REE mineralization zone indicates that ferroan dolomitization is the product of hydrothermal activity that cause the F-REE minerals. Paragenetically, coarse ferroan dolomites are coeval with the fluorite-REE mineralization, as they are integrown with REE minerals. In most cases, however, the REE minerals and fluorite are disseminated in, and replace, the coarse ferroan dolomites. As noted in section 3.2.2.3, the REE minerals predate saddle dolomite II. These probably

indicate that the formation of coarse ferroan dolomite is coeval to the formation of REE minerals, but that the deposition of fluorite and saddle dolomite II largely postdate the formation of coarse ferroan dolomite.

Saddle Dolomite II

Saddle dolomite II occurs as a replacement and as a cement phase and is closely associated with fluorite-REE mineralization. As noted previously, replacement saddle dolomite crystals only occur where fine-grained, disseminated purple fluorite is present, and are replaced by this fluorite. Most saddle dolomite II occurs around the edges of veins and vugs in ferroan dolostone and may line the cavities along with minor quartz and abundant fluorite. The saddle dolomite is clearer and is coarser grained than the surrounded coarse ferroan dolomite. The textures described previously show that saddle dolomite II is associated with the mineralization and postdates coarse ferroan dolomite and REE mineral deposition, and predates colourless fluorite I.

Fluorite-REE mineralization

Textural relationships indicate that the mineralization was the result of several stages of hydrothermal activity. The formation of some REE minerals are coeval with coarse ferroan dolomite, but the major formation event of REE minerals postdate the coarse ferroan dolomite and predate saddle dolomite II. In rocks containing disseminated mineralization, there is an early disseminated colourless fluorite (I, II) with minor purple fluorite and barite that occurs as a replacement of coarse ferroan dolomite and saddle dolomite II. Luminescence spectra of disseminated colourless fluorite (I and II) indicate low REE concentrations (Kerr, 1995; Samson et al., 1999). The euhedral zoned fluorite crystals postdate colourless fluorite, as these zoned crystals appear to have grown in vugs in colourless fluorite. These crystals have colourless or purple cores surrounded by alternating colourless and purple zones, and are coated by purple rims. Luminescence spectra indicate that the cores have high REE concentrations and the rims low REE concentrations (Kerr, 1995; Samson et al., 1999). The zonation is also visible under CL. This pattern of colour, REE and CL zonation is the same as that of zoned fluorite in breccia-matrices. This suggests that the colourless, disseminated fluorite and the zoned fluorite in breccia-matrices probably precipitated from the same fluid.

The float samples from the southeastern part of the property consist of a very distinctive style of mineralization that is characterized by the alumino-fluorides prosopite and cryolite. No REE fluorocarbonates has been found in this type of rock. The earliest minerals appear to be cryolite, phlogopite and barite. There are at least three separate stages of fluorite. Luminescence spectra indicate a low REE concentrations of fluorite (Kerr, 1995; Samson et al., 1999), and the cathodoluminescence colour is dark blue.

6.1.3 Post-Mineralization

Post mineralization events include late calcite precipitation, silicification and brecciation.

Late Calcitization

Late calcite occludes veins, vugs or breccia-matrices, or occurs as a replacement phase. Petrographically, all these calcites postdate the fluorite-REE mineralization. In rocks containing disseminated fluorite, coarse calcite normally occurs in veins and vugs where it replaces fluorite, saddle dolomite II, barite and quartz. In some breccias, calcite occurs in the matrix and replaces fluorite fragments. All these calcite types have similar isotopic composition, the detailed nature and source of fluids which precipitated these calcite will be discussed in next section.

Silicification

In rocks containing disseminated fluorite, late silicification occurs as aggregates of very fine-grained quartz and length fast chalcedony, which replace fluorite and associated minerals. This silicification represents the latest stage of silicification in the study area. However, the relationship between this silicification and late calcite is still unknown due to a lack of contact between these two minerals.

Brecciation

The latest stage of brecciation is associated with late calcitization. Dix (1991) suggested that there were some fault breccias along the western margin of the property area just south of the Rock Canyon Creek. These breccias are mineralized and polymictic. The clasts are derived from a variety of Ordovician units and fragments of Burnais Formation are present as well (Dix, 1991). Dix (1991) also suggested that this
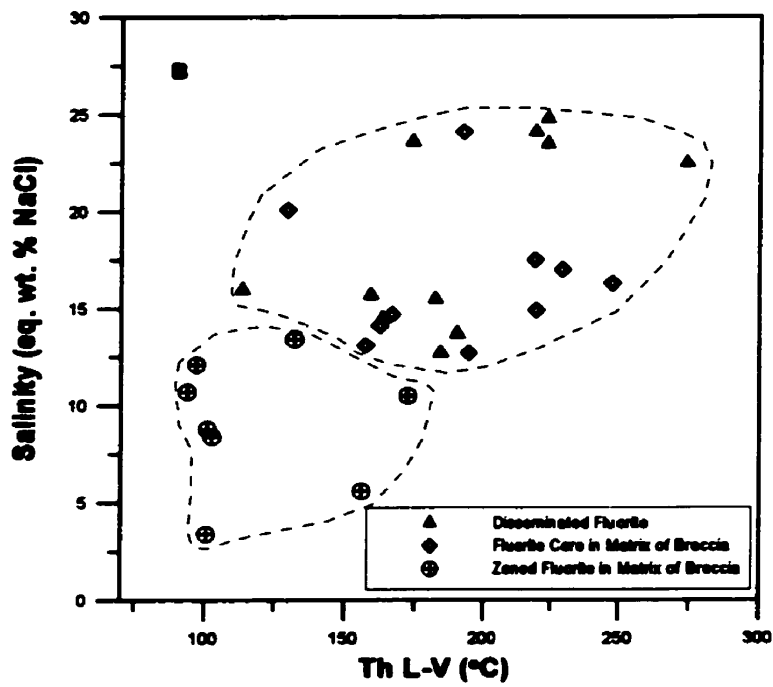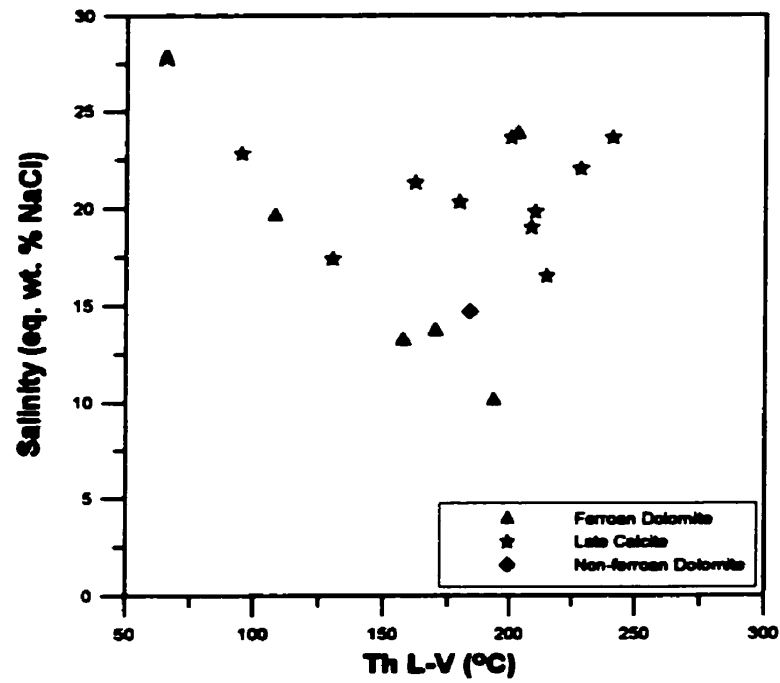
**Fig 6.3 Crossplot of homogenization temperature (Th L-V) to salinty.
A: for different carbonates; B: for variety of fluorites.**

70

breccia is fault bound and is associated with mineralization. Observations reported here show that the matrix is mainly late, coarse calcite (up to 95% of the matrix). In a few cases, the matrix does have minor fluorite (up to 5%), however, the fluorites were replaced by late, coarse calcite (Plate G-D), and probably were, originally, fragments. Some other breccias occur along the western side of the mineralized zone (Plate G-C). These breccias only have late, coarse calcite in the matrix, and fluorite is only present as fragments. These textures suggest that this generation of brecciation postdate the mineralization.

6.2 Nature and Evolution of Fluids

In this section, a discussion of the nature and evolution of fluids responsible for the various diagenetic and hydrothermal events will be presented, using fluid inclusion data.

6.2.1 Pre-mineralization

Replacement non-ferroan dolomite predates the fluorite-REE mineralization. Not much data are available for replacement non-ferroan dolomite because of the yellow colour of the host crystals and small size of the inclusions. Fluid inclusions from non-ferroan dolomites yielded homogenization temperatures ranging from 182 to 233 °C with the mode at approximately 195 °C and final ice-melting temperature at −10.7 °C, indicating that the pre-mineralization fluid was high temperature (195 °C) and of moderately salinity (14.7 wt % NaCl+CaCl₂, equiv) (Fig. 5.3, Fig. 6.3A).

6.2.2 Mineralization

As noted in the previous section, coarse ferroan dolomite and saddle dolomite II are associated with the mineralization stage but in detail predate fluorite deposition. Fluid inclusions from ferroan dolomite and saddle dolomite II have homogenization temperature that average 180 °C and salinity with average of 16 wt % NaCl+CaCl₂, equiv (Fig.6.3A).

As shown in Figure 5.4, based on the salinity of inclusions in fluorites, there are three identifiable groups of inclusions which are represented by modes at 25 (Group I), 11.3 (Group II) and 6.5 (Group III) eq. wt % NaCl+CaCl$_2$. Group I and II are restricted to disseminated fluorite and yellow fluorite cores in the breccia matrices, and there is no correlative relationship between salinity and homogenization temperature. As shown in Figure 6.3, inclusions in disseminated fluorite and the yellow fluorite cores in the breccia matrices show the same range of salinity and homogenization temperature. This might indicate that these two types of fluorites are formed from same fluids and at the same time, which is consistent with petrographic evidence (see section 6.1.2). Group III inclusions with lower salinity are restricted to zoned breccia matrix fluorite, and these inclusions also have lower homogenization temperature (Fig.6.3B).

In summary, fluid inclusions from coarse ferroan dolomite, saddle dolomite and disseminated fluorite are indistinguishable. This might indicate that they are formed from the same fluid, or the mineralizing fluid did not change much during the early stage of the mineralization. From the disseminated fluorite and yellow fluorite cores to the zoned fluorite, the fluids evolved to have lower salinities and lower temperatures.

6.2.3 Post-mineralization

Late calcite, which postdates the mineralization, yielded an average temperature of 183 °C and an average salinity of 20 wt % NaCl+CaCl$_2$, equiv (Fig.6.3A), which indicates that the post-mineralization fluid is high temperature and high salinity. Basically, the post-mineralization fluid has the same temperature as that of pre-mineralization and mineralization, but the salinity is somewhat higher than many of the inclusions that represent the mineralizing fluid.

6.3 Isotopic Composition of Limestone and Microdolomite

As noted in section 4.1.2, Ordovician limestones have isotopic values which are somewhat depleted in ^{18}O relative to typical data for Ordovician calcite (Fig. 4.1A). Samples from Devonian mudstone facies rocks are also somewhat depleted in ^{18}O relative to typical values of Devonian calcite (Fig. 4.1A), whereas the carbon isotopic

values fall in the range of typical value of Devonian calcite. Strontium ($^{87}Sr/^{86}Sr$) isotopic composition shows slightly more radiogenic values of 0.7086 with respect to Middle Devonian seawater (Fig.4.3). The $\delta^{18}O$ and $\delta^{13}C$ values of the microdolomites cover a wide range, and only a few display an original marine carbonate composition (Fig. 4.1A). One sample, which has $\delta^{18}O$ and $\delta^{13}C$ values similar to those of pristine marine carbonates, has $^{87}Sr/^{86}Sr$ ratio of 0.70809 also indicating a marine origin. Other samples show a progressive depletion in both oxygen and carbon with increasing size of crystals. One potential explanation for this depletion is the resetting of oxygen and carbon isotopes during subsequent recrystallization and diagenesis (Packard et al., 1990; White and Al-Aasm, 1997), which is consistent with petrographic evidence of clear overgrowth rims around cloudy cores.

6.4 Source of Fluids

In order to evaluate the source of different fluids at Rock Canyon Creek, several possible models and comparisons to previous data for the Southern Rocky Mountains must be considered.

6.4.1 Previous Work and Possible Models

In recent years, fluid flow models in Western Canada have been the subject of study for many researchers. Integrated geological and geochemical investigations on carbonates, especially dolomites, provide important information for the understanding of the origins, nature and movement of fluids. As indicated in the introduction, such studies have been widely reported from Western Canada.

Dolomitization in Western Canada has also been an intensively studied topic for researchers. It has been suggested that dolomites could have precipitated from the injection of hydrothermal fluids (Qing and Mountjoy, 1994, Packard et al., 1990, Morrow et al., 1986, Aulstead and Spencer, 1985, White and Al-Aasm, 1997). The slow infiltration of basinal fluids into permeable strata during burial is another model for dolomitization (Machel, 1985, 1986, Machel and Mountjoy, 1987). Other proposed models for dolomitization in Western Canada include: dolomitization due to sulphate

reduction (Machel 1987) for the Devonian Nisku reef trend, and precipitation of fine-crystalline microdolomites via the seepage-reflux mechanism (Packard and Al-Aasm, 1993; Qing, 1991). Hypersaline, seawater, and meteoric marine mixing are also popular models for dolomitization.

Two major fluid flow events, which have affected the Rockies, have been reported. One is a high temperature, high salinity fluid flow event (Antler), and the other is a high temperature, low salinity (Laramide) fluid flow event. Several isotopic and fluid studies of dolomites in the Southern Rocky Mountain have been reported (Nesbitt and Muehlenbaches, 1991, 1993, 1994, 1995, 1997; Yao and Demicco, 1997).

Nesbitt et al. (1994) presented a detailed study of epigenetic dolomites in Cambrian carbonate units in the southern Canadian Rocky Mountains. On the basis of fluid inclusion and isotopic studies, they ascribed the dolomitization and MVT mineralization to a large-scale, moderately-saline hydrothermal fluid that emanated from the shale units to the west. This fluid had a temperature of 150 ± 25 °C and a salinity of 20 to 25 equivalent wt % NaCl+CaCl$_2$. The epigenetic dolomites have isotopic values of $\delta^{18}O = -20$ to -10‰ VPDB, $\delta^{13}C = -1 \pm 2$‰ VPDB (Fig. 6.4), and $^{87}Sr/^{86}Sr > 0.710$. From west to east, the fluid temperatures and abundance of epigenetic dolomite, magnesite and Pb-Zn mineralization decrease, the $\delta^{18}O$ of epigenetic dolomite increases. This indicates that the fluids flowed from west to east. A Late Devonian to Early Mississippian age hydrothermal fluid was suggested, which is consistent with the basinal brine associated with the Middle Devonian Golden embayment (Fritz et al., 1991).

Yao and Demico (1997) reported a study of saddle dolomite in Cambrian carbonate rocks in the southern Canadian Rocky Mountains. They proposed that the dolomitization was caused by large-scale fluid flow, and also proposed that the Late Silurian to Late Devonian uplift of western portions of the Alberta Basin produced a west to east topographic gradient that drove flow across the basin. The saddle dolomites studied by Yao and Demico (1997) have $\delta^{18}O$ values of -23 to -18.5‰ VPDB, and $\delta^{13}C$ values of -2 ± 2‰ VPDB (Fig. 6.4). Fluid inclusion studies indicated that the dolomitizing fluid was a hydrothermal brine with homogenization temperature of

δ¹³C (VPDB)

DE

OR

CBT

Epigenetic Dolomite, Southern Rockies
(Nesbit and Muehlenbachs, 1994)

Saddle Dolomite, Middle Devonian, N.E. AB
(Clarke and Al-Aasm, 1999)

Hydrothermal Dolomite, Missi., N.E. BC
(White and Al-Aasm, 1997)

Saddle Dolomite, Cambrian,
Southern Rockies (Yao, 1997)

Carbonatite, Aley (Mader, 1986)

δ¹⁸O (VPDB)
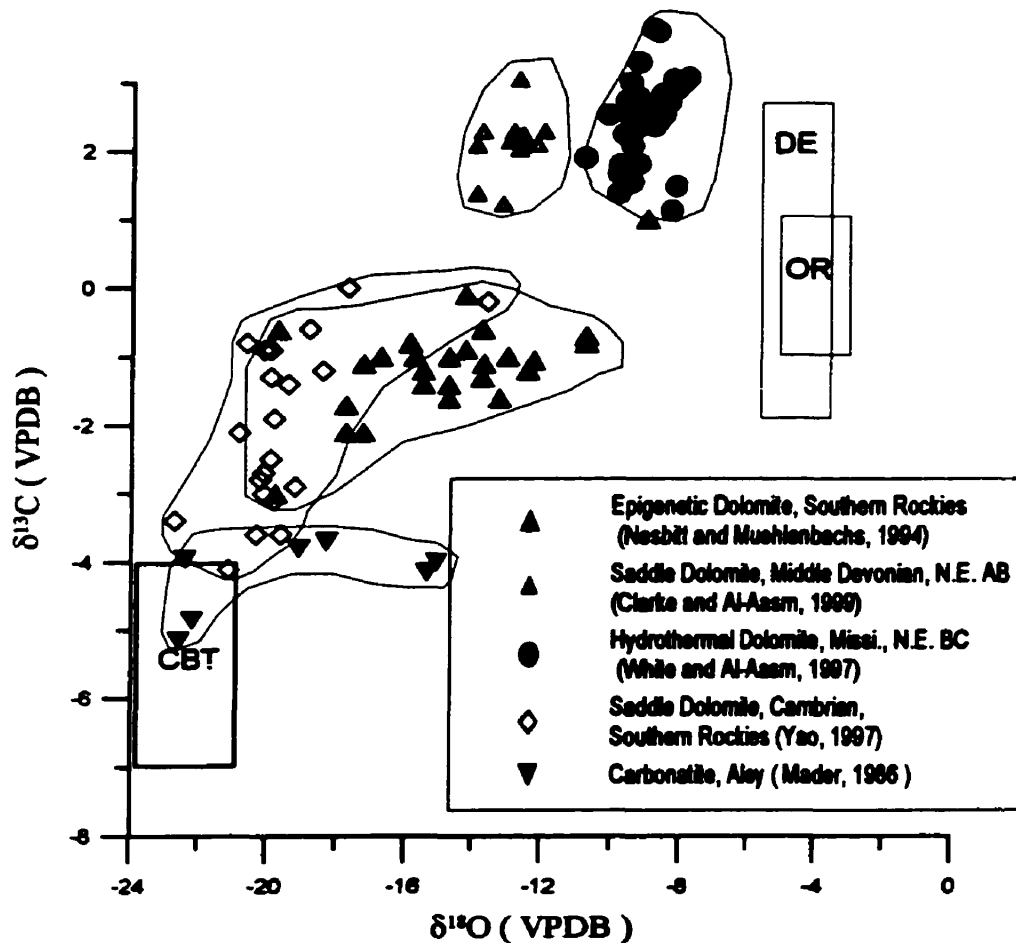
Fig. 6.4 Previous isotopic data for carbonates from southern Rocky mountains.

between 100 and 200°C. The salinity of the fluid was between 20 and 50 equivalent wt. % NaCl+CaCl$_2$.

Based on fluid inclusion and isotopic data, White and Al-Aasm (1997) infered that hot, slightly saline fluids were responsible for the formation of saddle dolomite and coarse crystalline dolomite in the Mississippian Upper Debolt Formation in northeastern British Columbia. White and Al-Aasm (1997) postulated that Laramide deformation drove fluid flow from west to east. These hydrothermal dolomites have isotopic values of $\delta^{18}O$ = -10.8 to -7.82‰ VPDB, $\delta^{13}C$ = +1 to+4‰ VPDB (Fig. 6.4). The inclusions in these dolomites have homogenization temperatures ranging from 87 to 214 °C, salinities

of about 8 wt % NaCl+CaCl$_2$ equiv and strontium isotopic ratios (^{87}Sr/^{86}Sr) from 0.7086 to 0.7099.

Clarke (1998) ascribe the formation of saddle dolomite in the Middle Devonian Slave Point Formation, Northwestern Alberta, to highly saline, hydrothermal fluid which might have been driven by the topographic gradient caused by the uplift of the Western Canada Sedimentary Basin between the Late Devonian and Mississippian. The saddle dolomites have δ^{18}O values of -14.0 to -112.0‰ VPDB, and δ^{13}C values of +1 to 3‰ VPDB (Fig. 6.4). Inclusions in these dolomites have homogenization temperatures ranging from 125 to 161 °C, salinities vary from 22.2 to 24.7 wt % NaCl+CaCl$_2$ equivalent and strontium isotopic values lies between 0.7086 and 0.7104.

Detailed studies of syn- to post-Laramide vein carbonates in Late Proterozoic units (Nesbitt and Muehlenbachs et al., 1993, 1995, 1997) indicate that a large-scale syn- to post-Laramide fluid flow event in the southern Rocky Mountains was associated with the rise of the Southern Rocky Mountains. The fluid was moderate to low temperature, and had low salinity. A significant portion of this fluid is postulated to have been meteoric in origin (evidenced by δD values, Nesbitt et al., 1993, 1995, 1997) and it is thought to have become radiogenic when passing through deep water sedimentary rocks west of the southern Rocky Mountains. The δ^{13}C values and ^{87}Sr/^{86}Sr ratios show a high degree of regional heterogeneity, and they infer that the heterogeneity is related to variations in the host rock lithology, which indicates relatively rapid reequilibration of the isotopic signatures of dissolved C and Sr, as the fluids moved from one rock unit to another. The low δ^{13}C values (Fig.6.4) also indicate that the precipitating fluid contains a certain amount of carbon derived from organic materials which might come from deep water sedimentary rocks.

6.4.2 Pre-mineralization Fluid

6.4.2.1 Source of Fluid

As noted in section 6.1., saddle dolomite I and non-ferroan dolomite predate the fluorite mineralization. As indicated in section 6.2.1, the fluid responsible for these

dolomites was high temperature (195°C), moderately saline (15 wt. % NaCl+CaCl$_2$), and are depleted in $\delta^{18}O$ and radiogenic $^{87}Sr/^{86}Sr$ ratios relative to typical values of Ordovician and Devonian marine dolomites.

The red colour of the saddle dolomite under CL is an indication of precipitation in a deep-burial reducing environment where Fe^{2+} was available (Boggs, 1992). The coarse crystal size and the presence of two-phase fluid inclusions with high homogenization temperatures excludes the possibility that hypersaline seawater, seawater, or meteoric-marine mixing were the mechanisms of dolomitization because dolomite precipitated in any of these models would only contain single-phase fluid inclusions (Allan and Wiggins, 1993).

Local marine carbonates and evaporites are not the source for the ^{87}Sr because $^{87}Sr/^{86}Sr$ ratio (0.70995) of saddle dolomite I is more radiogenic than Ordovician and Devonian marine carbonates and are indicative of a allochthous source. Brines may incorporate radiogenic ^{87}Sr during passage through clastic sequences (Mountjoy et al., 1992). Saddle dolomite from Rock Canyon Creek has a similar carbon and oxygen isotopic composition to epigenetic dolomites (Yao, 1997; Nesbitt et al., 1994) from the southern Rocky Mountains. $\delta^{18}O$ values of non-ferroan dolomite are slightly higher relative to those of saddle dolomite I and are depleted than the expected range for dolomite precipitated from Ordovician and Devonian seawater (Fig. 6.5). The majority of $\delta^{13}C$ values for saddle dolomite I and non-ferroan dolomite fall in the expected range for Ordovician and Devonian marine dolomites, suggesting that carbon was derived locally from the carbonates. $^{87}Sr/^{86}Sr$ ratios of 0.70995 to 0.71082 for saddle dolomite I and non-ferroan dolomite in Rock Canyon Creek fall in the range of epigenetic dolomites in the southern Rocky Mountains (0.709 to 0.712) (Koffyberg and Nesbitt, 1993). They interpreted those dolomites to have been precipitated from a large-scale fluid flow event involving a saline brine that emanated from the deep water shales to the west. The isotopic composition of saddle dolomite I in Rock Canyon Creek lies between values for epigenetic dolomites in the southern Rocky Mountains (Yao et al., 1997; Nesbitt et al., 1994; Koffyberg et al., 1993) and those of saddle dolomite in northwestern Alberta
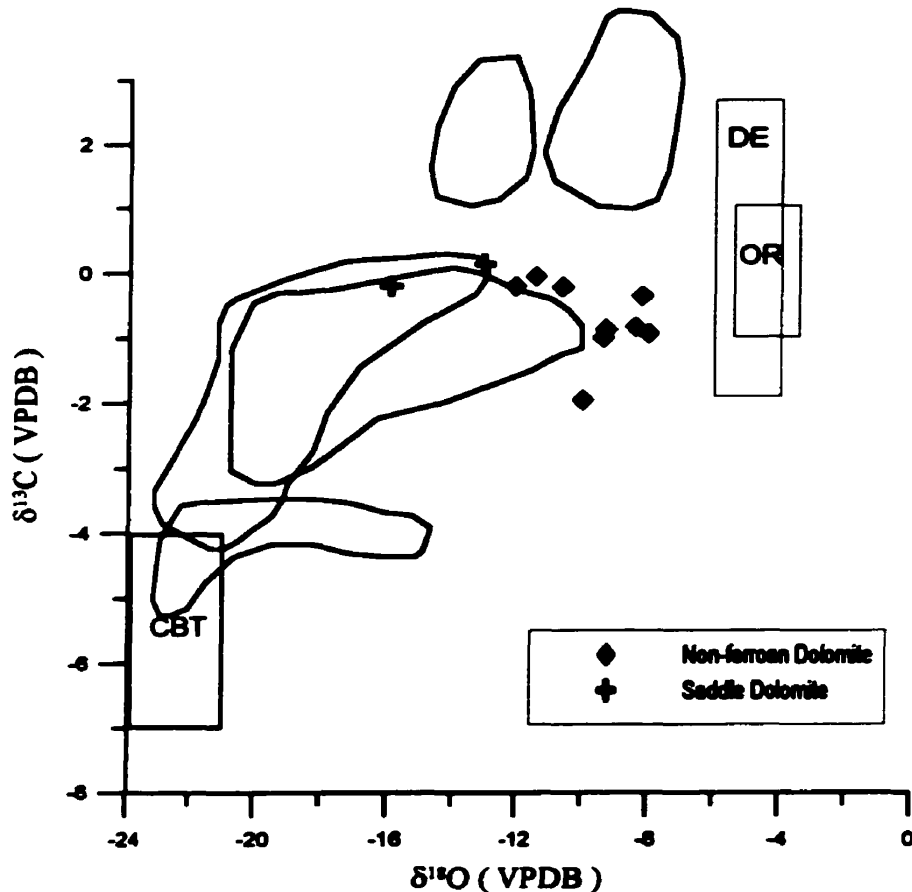
Fig.6.5 Comparison of previous isotopic composition to data of non-ferroan
dolomite and saddle dolomite from this study. The ranges are same as those
in Figure 6.4

(Clarke, 1998) indicate that they might formed from the same fluid related to Antler fluid
flow.

This pre-mineralization fluid flow event caused extensive alteration of carbonate
rocks in the study area. As was noted in section 6.1.1, microdolomite in mudstone and
wackestone facies were recrystallized during the infiltration of a later fluid. Evidence that
support recrystallization include: 1) outer clear rims on crystals; 2) depleted $\delta^{18}O$; and 3)
radiogenic $^{87}Sr/^{86}Sr$ ratios values with respect to postulated Ordovician and Devonian
marine carbonate values. Most of the microdolomites show a progressive depletion in
both oxygen and carbon with increasing crystal size. One potential explanation for this

depletion is the resetting of oxygen and carbon isotopes during subsequent recrystallization and diagenesis (Packard et al., 1990; White and Al-Aasm, 1997).

In summary, the high formation temperature, fluid inclusion salinity, oxygen isotopic composition, and petrographic evidence suggest that saddle dolomite I and non-ferroan dolomite were precipitated during Antler fluid flow. This also may have caused recrystallization of carbonates in the study area. This hypothesis will be tested in the following section using isotopic modeling.

6.4.2.2 Isotopic Modeling

Oxygen and carbon isotopic modeling was performed in order to model the alteration of microdolomite by the fluid which precipitated saddle dolomite I and non-ferroan dolomite, and which cause the recrystallization of microdolomite. The user-defined parameters for this model are as follows: 1) the oxygen and carbon isotopic composition of the microdolomite were chosen to be -3.19 and $0.25‰$ VPDB, respectively, because these values fall within the range expected for dolomite precipitated by Middle Ordovician seawater; 2) the original oxygen and carbon isotopic composition of the fluid that precipitated saddle dolomite I were $+2.44‰$ SMOW and $-0.19‰$ VPDB, respectively; 3) The temperature was assumed to be $195°C$, which represents the mean value for the formation temperature based on fluid inclusion data. As shown in Fig 6.6, this model is consistent with the hypothesis that microdolomite in mudstone and wackestone facies rocks were altered by the Antler large-scale fluid flow event which precipitated saddle dolomite I and non-ferroan dolomite. The higher $\delta^{18}O$ of non-ferroan dolomite compared to saddle dolomite I can be explained by a lower water/rock ratio during the formation of non-ferroan dolomite during the water/rock interaction, which is consistent with petrographic evidence that saddle dolomite I occludes veins and vugs and non-ferroan dolomite is a replacement phase.

6.4.3 Carbonatite-derived, F-REE-rich fluid

The occurrence of the fluorite and related minerals in veinlets, breccia matrices and as a replacement of dolostone indicates that the deposit is hydrothermal and epigenetic. The suggestion has previously been made (Hora and Kwong, 1986; Pell and
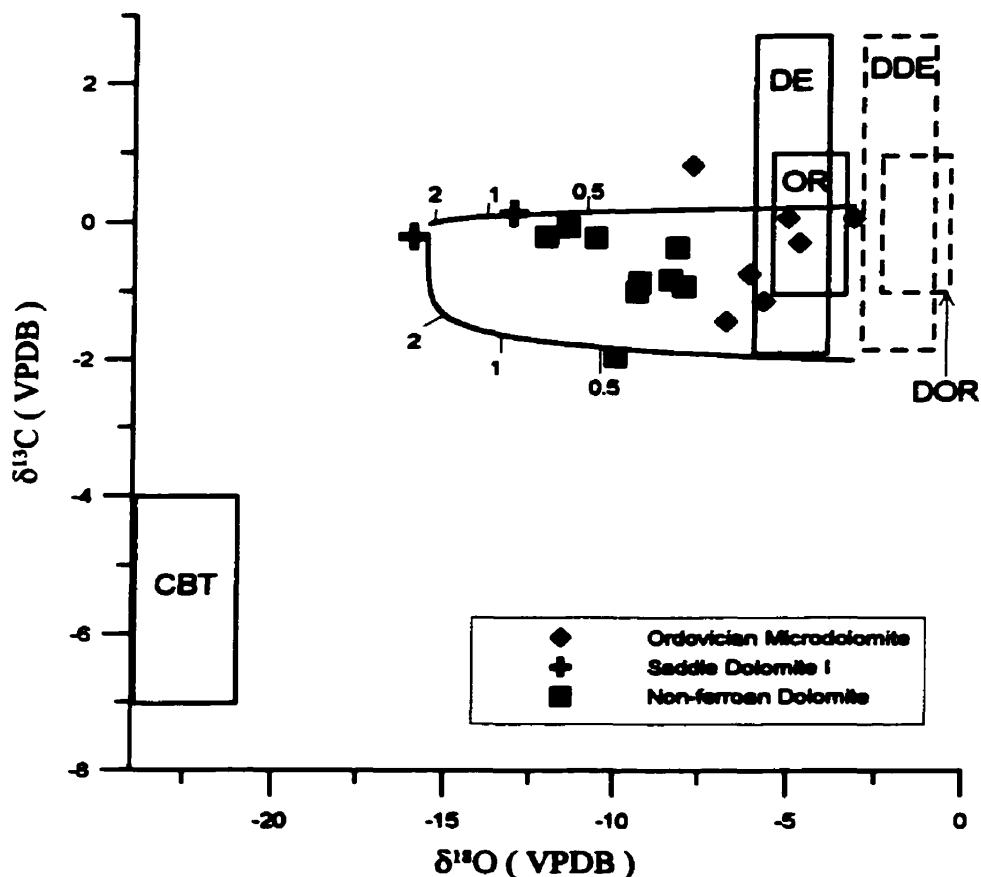
Fig. 6.6 Oxygen and carbon isotopic modeling for pre-mineralization fluid.
Microdolomite react with pre-mineralization fluid which precipitated saddle
dolomite I and non-ferroan dolomite.

Hora, 1987; Pell, 1992) that Rock Canyon Creek was formed by hydrothermal activity related to a hidden carbonatitic intrusion because of the geochemical character of the deposit, most notably the high REE and Nb and the LREE-riched chondrite-normalized REE patterns with no Eu anomaly. Several lines of evidence from this study further support their suggestion.

6.4.3.1 Mineralogy

Several minerals that are common in carbonatites are present in the deposit, notably pyrochlore, apatite (Hogarth, 1989). Although not as distinctive, the REE minerals, fluorite, barite, K-feldspar and Nb-bearing rutile are consistent with a carbonatitic association. These minerals are particularly common in late-stage hydrothermal carbonatites. Dolomites, which host the fluorite-REE mineralization, are ferroan, and ferroan dolomite is a common mineral in late stage carbonatites (Bell, 1989). Cryolite and prosopite are rare and unusual minerals in hydrothermal systems. Cryolite and prosopite are most typically associated with alkaline granites as an accessory

minerals or in pegmatites, veins and alteration zones, and also occurs associated with undersaturated alkalic intrusions (Samson et al., 1999). Phlogopite is rare in sedimentary environments. The presence of these minerals supports the case that the deposit is carbonatite-related.

The cathodoluminescence characteristics of fluorite are quite useful in distinguishing the environment of formation of fluorite. Mariano (1988) noted that fluorite from LREE-dominated carbonatite environment luminesces a strong blue colour with peaks between 405 nm and 430 nm. Cathodoluminescence of fluorite from Rock Canyon Creek shows basically blue CL varying from bright blue to dull blue, which is also consistent with a carbonatite association.

6.4.3.2 Isotopes

As was noted in the introduction, the origin of carbonates become smore complicated when carbonatites are formed among sedimentary carbonate rocks (Barker, 1989). Ferroan dolomites, which host the fluorite-REE mineralization, and associated saddle dolomites have a lack of igneous textures, making it difficult in distinguishing from rocks of sedimentary origin. Oxygen, carbon and strontium isotope analyses provide better evidence of a carbonatitic origin.

The ferroan dolomites have lower $\delta^{18}O$ and $\delta^{13}C$ values (Fig.4.1B) than the pre-mineralization carbonates, and are nearer the primary carbonatite box (CBT, as constructed by Reid and Copper, 1992). The ferroan dolomites show a trend of progressive depletion in both oxygen and carbon isotopes with increasing crystal size. The coarsest ferroan dolomite shows the most depletion in both ^{18}O and ^{13}C. This trend is the same as that for carbonatites in general (Deines, 1989) and in particular for calcite carbonatite, where early coarse carbonate are more depleted in ^{18}O and ^{13}C than later fin-grained carbonates (Reid and Copper, 1992, Clarke et al., 1994). Several models have been proposed to account for such a relationship.

Reid and Cooper (1992) have modeled this trend through crystallization of primary carbonatite at 700°C where CO_2 is the dominant oxygen and carbon carrier, and assuming that the fractionation of carbon and oxygen isotopes occurred between

calcite/dolomite and CO_2 at 700°C. An increase in $\delta^{18}O$ and $\delta^{13}C$ resulted from increasing degrees of fractionation. Adding variable proportions of H_2O as an additional oxygen carrier can reduce the slope of the ^{18}O and ^{13}C enrichment-trend. This trend has also been interpreted as a carbonatite fractionation sequence at high CO_2/H_2O ratios by Neilson and Buchardt (1985), and Knudsen and Buchardt (1991). Although no igneous textures are observed in studied samples, the distinctive strontium isotopic ($^{87}Sr/^{86}Sr$) ratios of ferroan dolomite carries a mantle-like signature. So, the trend observed in this study might also have resulted from the increasing degrees of fractionation.

Strontium-87 is generated naturally by the radioactive decay of ^{87}Rb (Faure, 1986). Early work on the Sr isotopic geochemistry of carbonatites (Powell et al., 1962, Hamilton and Deans, 1963, Powell, 1966, Bell et al., 1973, 1989) showed that most carbonatites have low initial $^{87}Sr/^{86}Sr$ ratios, considerably lower than values for average continental crust. Faure and Powell (1972) quoted a value of 0.7034 ± 0.0006 for typical carbonatites, and pointed out the similarity of this value to values for oceanic basalts, and interpreted the ratio as being consistent with a mantle or deep crustal origin for carbonatitic melts. Exceptions include the high $^{87}Sr/^{86}Sr$ ratios of vein carbonatites, considered to be hydrothermal in origin. These indicate that Sr isotope ratios can serve as useful tracers of fluid sources in hydrothermal systems and help to distinguish carbonatites from sedimentary carbonates.

Although the ferroan dolomite at Rock Canyon Creek has similar oxygen and carbon isotopic compositions to epigenetic dolomites from southern Rocky Mountains (Fig. 6.4 and 6.7) (Nesbitt et al., 1994; Yao et al., 1997), all the ferroan dolomites from Rock Canyon Creek have $^{87}Sr/^{86}Sr$ between 0.703357 and 0.704616 (Fig 4.3). This leaves little doubt that the ferroan dolomite has a mantle-like Sr isotope signature that is similar to that of carbonatites, and that the mineralizing process has not changed the ratio too much.

Saddle dolomite II, which is associated with the mineralization, shows a higher $^{87}Sr/^{86}Sr$ ratio but is slightly lower than those of typical marine carbonates and epigenetic dolomites from the southern Rocky Mountains (Koffyberg, 1993). This might indicate that saddle dolomite II precipitated from a residual fluid which evolved from the fluid
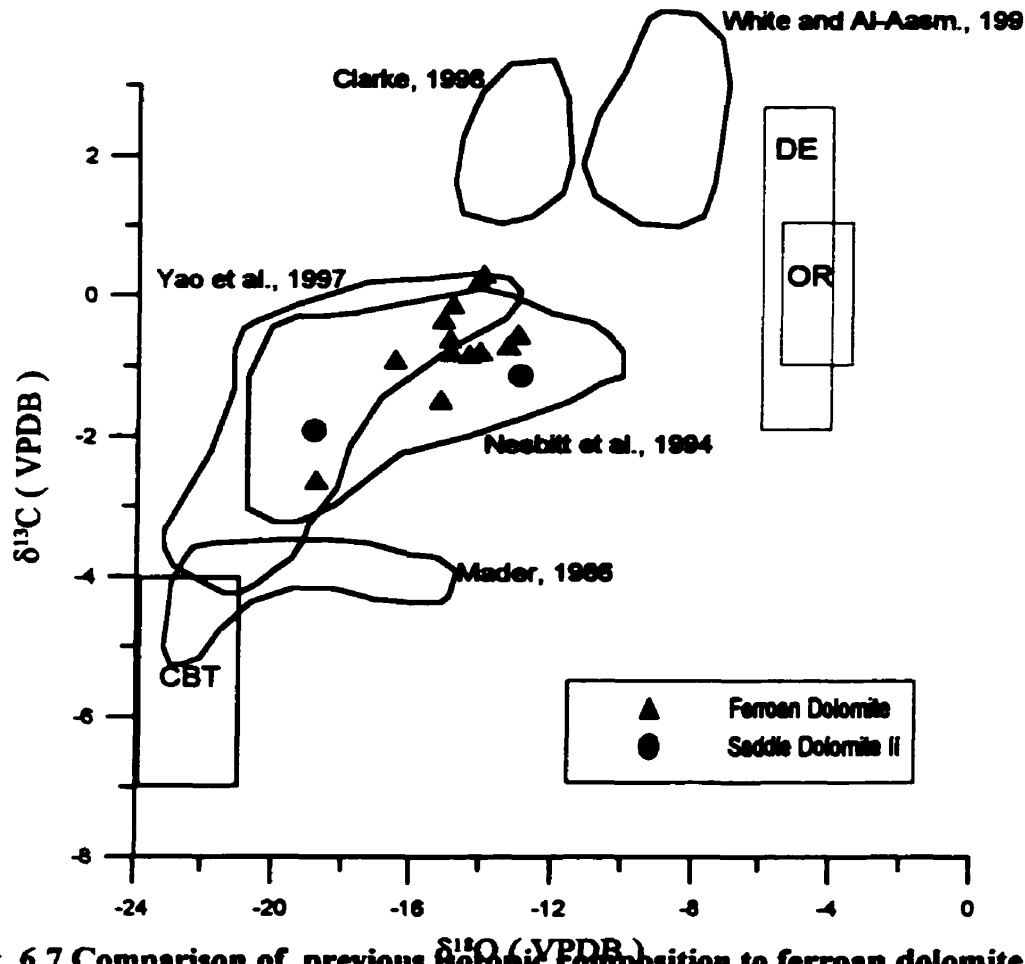
Fig. 6.7 Comparison of previous isotopic composition to ferroan dolomite from this study. The ranges are same as those in Figure 6.4.

that precipitated the ferroan dolomite. If so, the residual fluid inherited the geochemical signature of wall rock. Such a hypothesis is consistent with petrographic evidence that saddle dolomite II postdates ferroan dolomite.

The other possibility is that the fluids responsible for saddle dolomite II and ferroan dolomite could be different. In this scenario, the fluid which precipitated saddle dolomite II has a high $^{87}Sr/^{86}Sr$ ratio. The reaction of this fluid with ferroan dolomite caused the $^{87}Sr/^{86}Sr$ ratio of the fluid to decrease. Therefore, the $^{87}Sr/^{86}Sr$ ratio of saddle dolomite II lies between that of ferroan dolomite and that of precipitating fluid.

6.4.3.3 Isotopic modeling

<u>Carbon and Oxygen Isotopes</u>

As indicated above, it is likely that the ferroan dolomite precipitated from carbonatite-derived fluids via replacement of the sedimentary carbonates. A variety of models of water/rock interaction have been performed based on the reaction of a carbonatite-derived fluid with the carbonate sedimentary rocks. The $\delta^{18}O$ and $\delta^{13}C$ values of the carbonate host rocks were chosen to be -7‰ and 0.5‰ VPDB, respectively, because this value represents the least altered microdolomite in the study area. The porosity was assumed to be 15 % which represents typical values of sedimentary carbonates. The fractionation factors between dolomite and water were calculated using the equation of Land (1983), and the fractionation factors between dolomite and CO_2 were calculated using the equation of Deines (1974). The other parameters were summarized in table 6.1.

In this table, $\delta^{18}O_{fluid}$ (VSMOW) and $\delta^{13}C_{fluid}$ (VPDB) are the values of the carbonatite fluid, calculated using the equations of Land (1983) and Deines (1974) based on a carbonatite equilibration temperature ($T_{Carbonatite}$) of 300°C (Santos et al., 1995). Fractionation factors (α) were calculated based on the water-rock reaction temperature ($T_{reaction}$) modeled. The last column in the table is the carbon concentration in the fluids.

Table 6.1 Parameter Used in Modeling

Model #	$\delta^{18}O_{fluid}$ (SMOW)	$\delta^{13}C_{fluid}$ (PDB)	α (Dolomite-water)	α (Dolomite-CO_2)	$T_{reaction}$ (°C)	$T_{Carbonatite}$ (°C)	Carbon (ppm)
Model 1	-30.3	-4.35	1.0121	1.00153	200	300	44200
Model 2	-30.3	-4.15	1.0121	1.00153	200	300	88400
Model 3	-24.19	-4.15	1.0121	1.00153	200	600	44200
Model 4	-30.3	-4.15	1.00993	1.000907	240	300	88400
Model 5	-30.3	-4.15	1.0147	1.00274	160	300	88400
Model 6	-27.5	-4.15	1.00993	1.000907	240	300	2000

Model 1 and Model 2 basically use the same parameters, but differ in the carbon concentration in the fluid, to test how the carbon concentration affects the model. Model

3 uses a carbonatite formation temperature of 600°C, which resulted in more depleted fluid $\delta^{18}O$ and $\delta^{13}C$, to test how the fluid isotopic composition affects the fluid. Model 4 and model 5 modified the reaction temperature from model 1; Model 4 uses 240°C and Model 5 uses 160°C. Model 6 uses a lower carbon concentration in the fluid and represents marine water, which reacted with microdolomite at temperature of 240°C.

As shown in Figure 6.8, Model 2 fits the actual data well. It requires a high carbon concentration in the original fluid. Compared to Model 1, Model 2 has a higher C concentration in the fluid, and the modeled values are closer to a straight line and fit the actual data better. Normally, carbonatite-derived fluids contain high carbon concentrations, this is confirmed by the gas chromatographic data of the inclusion fluids.

Santos et al. (1995) modeled isotopic exchange between carbonate rocks and carbonatite-derived H_2O-CO_2 fluids at different temperatures and with different H_2O/CO_2 ratios. Their study indicated that large oxygen and carbon isotopic variations in carbonatites can take place at low temperatures (below 300°C) and involves fluids with high carbon concentrations. Model 3 used a fluid with more depleted $\delta^{18}O$ and $\delta^{13}C$ values than the other models because of a higher initial temperature. The modeled values of Model 3 are much higher in ^{18}O than the actual data, which indicates that the temperature of the fluid is not that high and further supports Santos' study.

As shown in Figure 6.8, the modeled values for Model 4 are lower than the actual data in both $\delta^{18}O$ and $\delta^{13}C$ values and the modeled values for Model 5 are higher than the actual data. Comparing Model 2 to Models 4 and 5, the reaction temperature of 200°C is more reasonable than 160 and 240°C. This temperature is consistent with homogenization temperatures of inclusions in ferroan dolomite which have a mode at about 200°C.

Model 6 represent marine water reacting with carbonates. The effect of the low C concentration of marine water (normally between 20 and 2000 ppm) is to only allow significant modification of $\delta^{13}C$ at very high water/rock ratio. Consequently, the model does not fit the actual data.
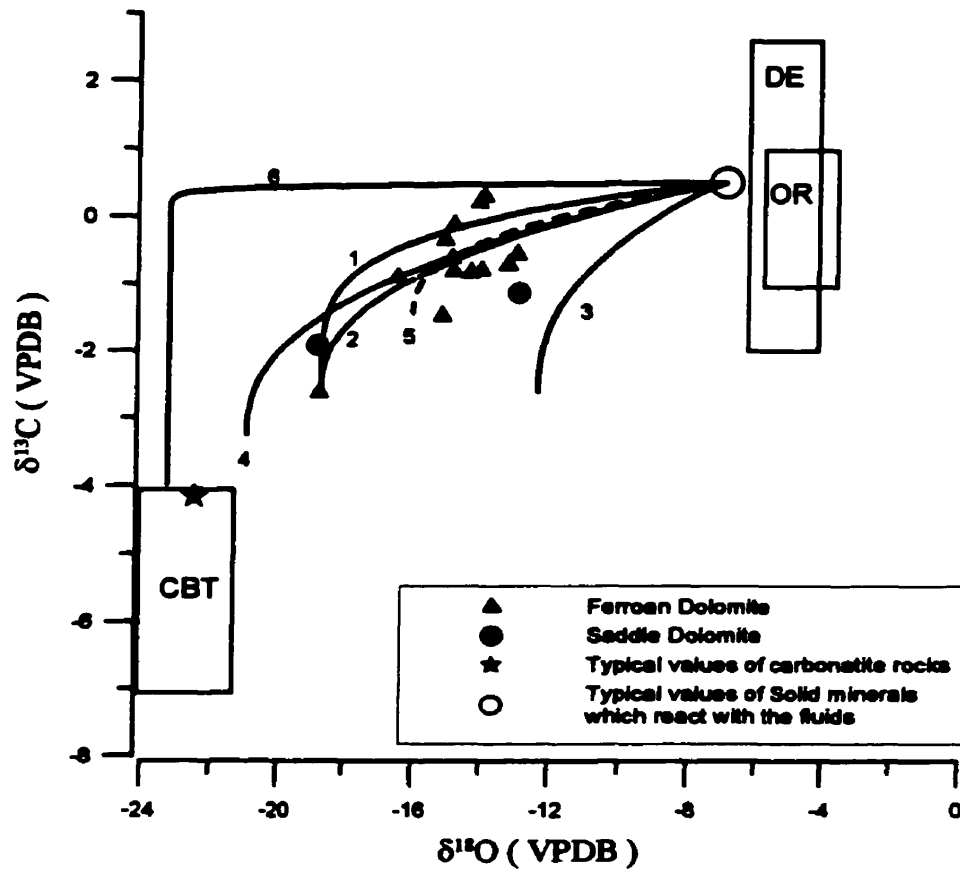
Fig. 6.8 Oxygen and carbon isotopic modeling for ferroan dolomite. Digital numbers label the model number.

In summary, Model 2 is consistent with the actual data and shows that the $\delta^{18}O$ and $\delta^{13}C$ composition of the host rocks are consistent with precipitation of the ferroan dolomite from carbonatite-derived fluids reacting with sedimentary carbonates at a temperature of about 200°C.

Strontium Isotopes

Strontium isotopes and strontium concentrations also can be used to model the same process as was evaluated with the carbon and oxygen isotopic modeling. To model the strontium isotope values for ferroan dolomite and saddle dolomite II, the following parameters were used: 1) an initial Sr^{2+} concentration in the host rock of 350 ppm; 2) a Sr^{2+} concentration in the fluid of 10 000 ppm, based on high concentration of Sr in carbonatite rocks (5000 to 15000 ppm) (Bell, 1989); 3) a strontium $^{87}Sr/^{86}Sr$ value for the
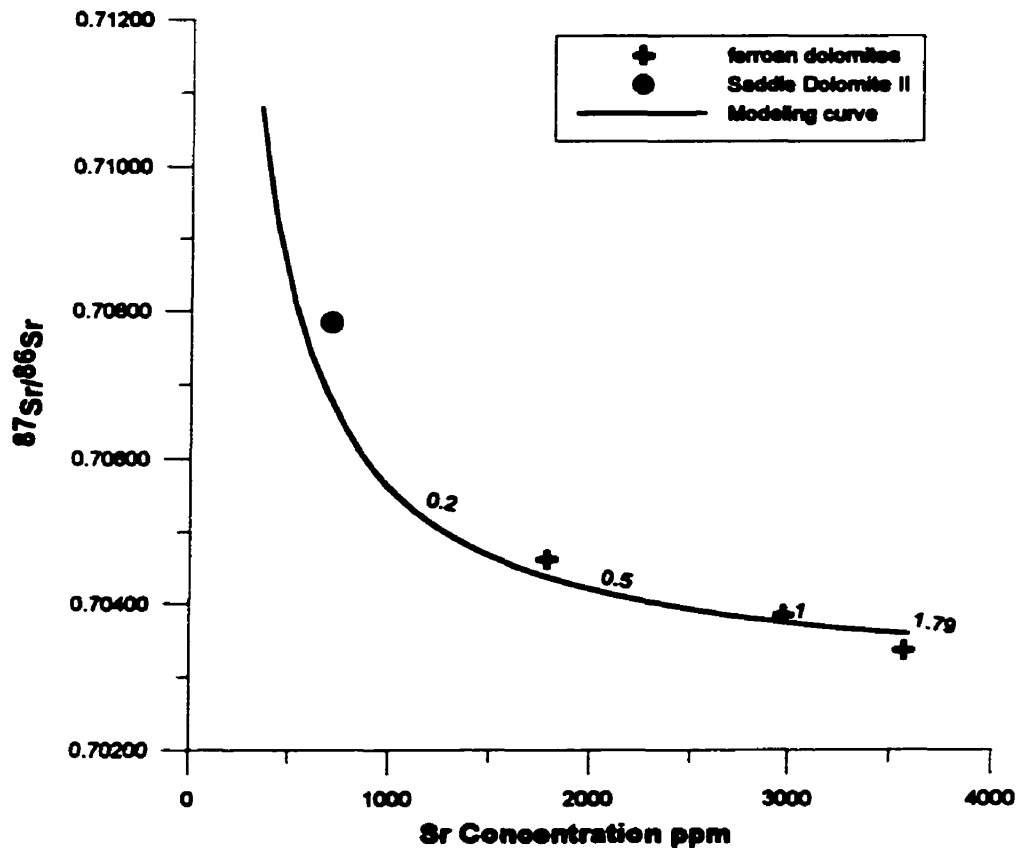
Fig. 6.9 Strontium concentration and strontium isotopic modeling curve. The digital numbers near the curve represent the water/rock ratio.

fluid of 0.7025, which represent the typical value for carbonatites (Bell, 1989); and 4) an original $^{87}Sr/^{86}Sr$ ratio of the host rock of 0.7108, which is the value of analyzed non-ferroan dolomite. Basically, as shown in Figure 6.9, the model shows a good fit to the actual data for ferroan and saddle dolomite and shows the progressive Sr^{2+} enrichment and $^{87}Sr/^{86}Sr$ depletion with increasing fluid/rock ratio, which is consistent with the increasing crystal size of host ferroan dolomite. The model requires the Sr^{2+} concentration in the host rocks to be about 350 ppm, which is somewhat higher than that of the host rock. Nevertheless, the model provides further support for the proposed model. Saddle dolomite II has a lower Sr^{2+} concentration and higher $^{87}Sr/^{86}Sr$ ratio than the ferroan dolomite, and equilibrated at a lower water/rock ratio. This might indicate that the saddle dolomite II precipitated from the residue of the fluid which precipitated the

ferroan dolomite, which is consistent with the petrographic evidence that the saddle dolomite II postdates the ferroan dolomite.

6.4.4 Post-mineralization Fluid

6.4.4.1 Source of Fluid

Late calcites (post-mineralization) are widespread and abundant in the study area. Isotopic ($\delta^{18}O$ = -20.71 to –13.83‰ VPDB, $\delta^{13}C$ = -7.14 to –0.73‰ VPDB) and fluid inclusion evidence (Th L-V = 130 to 240°C with salinities of 16.5 to 23.6 wt % $NaCl+CaCl_2$) imply precipitation from saline brines at elevated temperatures. These carbonates are more depleted in $\delta^{13}C$ than other carbonates in the study area. The Sr^{2+} concentrations in these calcites is much higher than typical marine carbonates and the $^{87}Sr/^{86}Sr$ ratios of 0.708221 and 0.709984 are radiogenic with respect to Ordovician and Devonian marine carbonates. As shown in Figure 6.4 and Figure 6.10, the isotopic composition of the late, coarse calcite from this study is comparable to the composition of calcite from syn- to post-Laramide veins in the Rocky Mountains (Nesbitt and Muehlenbachs, 1993, 1995, 1997), although the Laramide vein values extend to much lower $\delta^{13}C$ values. Nesbitt et al. (1994) ascribed the syn- to post-Laramide veining to be the result of a regional fluid flow from west to east. From the high formation temperature, oxygen isotopic composition of the precipitating fluid and petrographic evidence, it is suggested that the late, coarse calcite at Rock Canyon Creek might have precipitated from equivalent syn- to post-Laramide fluids. A significant portion of this fluid would have been meteoric in origin (as evidenced by δD values, Nesbitt et al., 1993, 1995, 1997) and it would have become more radiogenic when passing through deep-water sedimentary rocks west of the study area. The low $\delta^{13}C$ values also indicate that the fluid contained a certain amount of C derived from organic material which might also have come from deep water sedimentary rocks. On the other hand, fluid inclusion salinities in the late calcites from Rock Canyon Creek are a high, which differs from the low salinities of Laramide fluids. It is possible that the fluid came from a deeper source, which is reasonable because the study area lies immediately east of a basal thrust which could have provided a conduit to transfer the fluid upward.
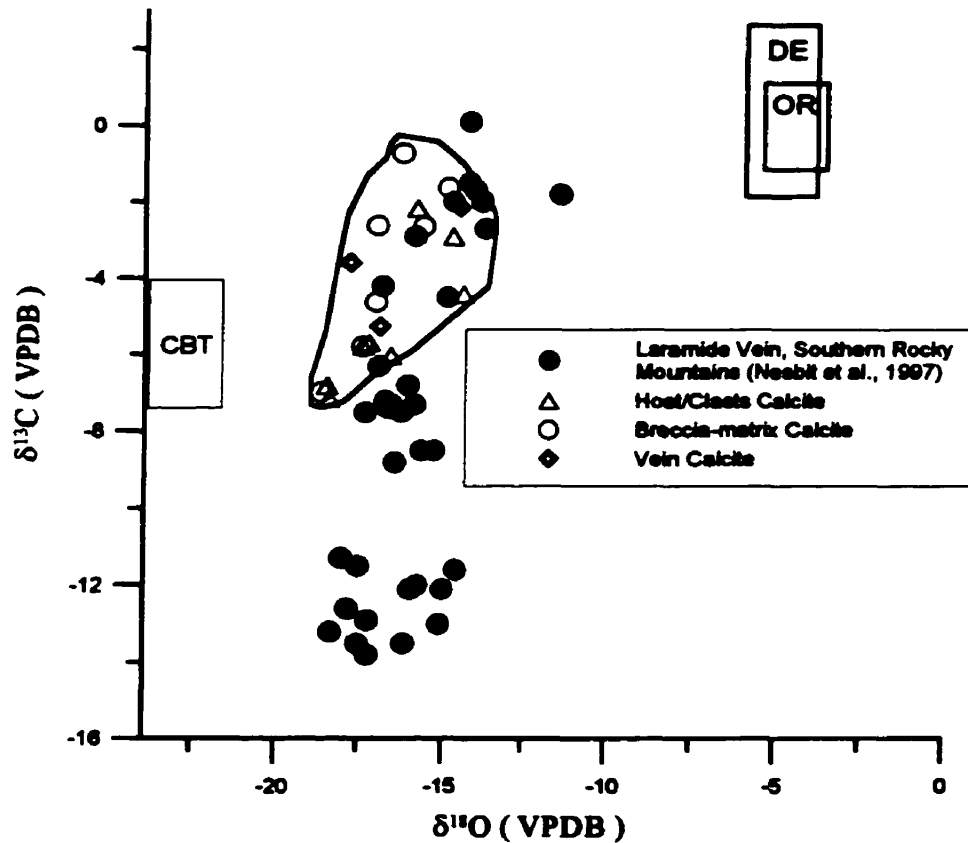
Fig.6.10 Comparison of previous isotopic composition to late calcites from this study. The ranges are same in the Fig.6.4.

This large-scale orogenic fluid flow event may also have caused alteration of pre-existing carbonates in the study area. As was noted in section 6.1.1, some calcite micrite in mudstone and wackestone facies were recrystallized during the infiltration of later diagenetic fluid. Evidence that support recrystallization includes: 1) depleted $\delta^{18}O$ and $\delta^{13}C$ values with respect to postulated values for Ordovician and Devonian calcites; 2) radiogenic $^{87}Sr/^{86}Sr$ ratios. The recrystallization of calcite by the large-scale orogenic fluid which cause the precipitation of late calcites. In order to test this hypothesis, we can model the oxygen and carbon isotopic composition of calcite.

6.4.4.2 Isotopic Modeling

The parameters used in this modeling include: 1) the oxygen and carbon isotopic compositions of calcite micrite were chosen to be –6.19 and 0.08‰ VPDB, respectively, because these values fall within that range expected for calcite precipitated from
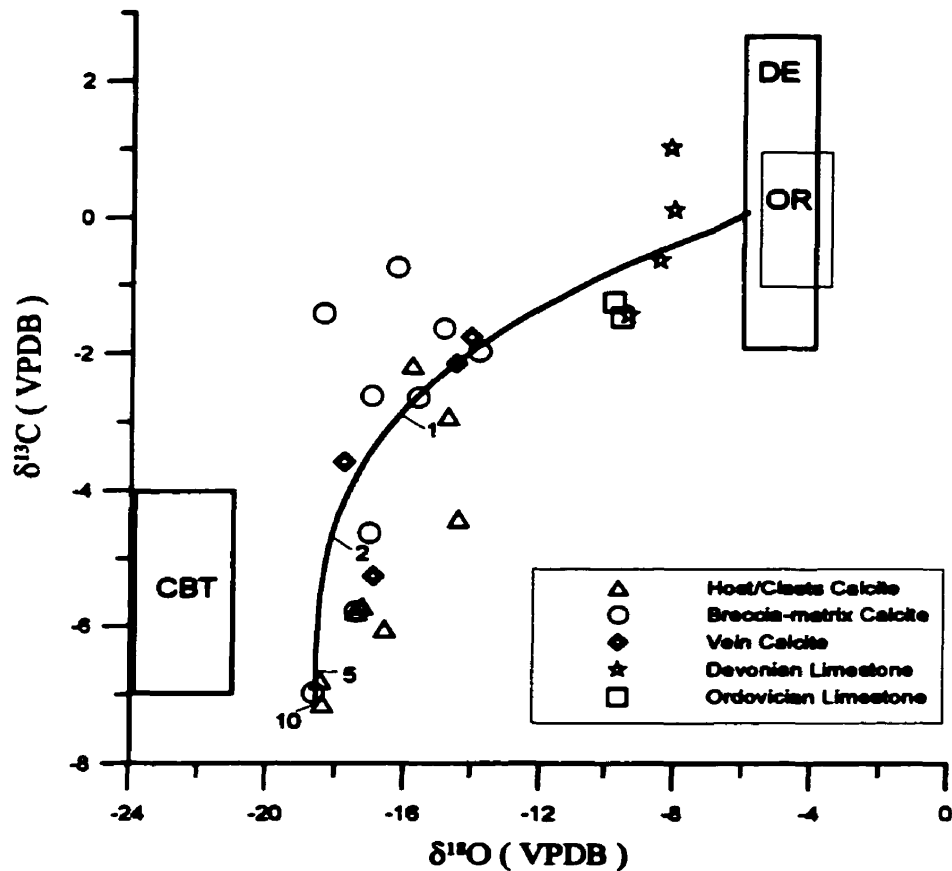
Fig.6.11 Oxygen and carbon isotopic modeling for late calcite. The digital numbers near the curve are water/rock ratios.

Devonian seawater; 2) the original oxygen and carbon isotopic composition of the fluid that precipitated the late calcite were –0.06‰ SMOW and –7.13‰ VPDB, respectively, based on calculations using the equations of Land (1983) and Deines et al. (1974); 3) The temperature is assumed to be 200°C, which represents the mean value for homogenization temperature of late calcites. The model fits the actual data well (Fig.6.11), and so this model confirms that some calcite may have been altered by large-scale orogenic fluid which precipitated late calcites.

6.5 Age Constraints of the Host Rock and Mineralization

As noted in Chapter I, the age of the rocks immediately east of the (basal) thrust, and which host the deposit, is still controversial. As shown in Fig. 2, Dix (1991) interpreted these rocks to be Ordovician in age, because he thought the lithologies are similar to

90

those west of the basal thrust. In this study, samples west of the basal thrust are mainly fine to medium-grained massive dolostone of mudstone facies, whereas samples immediately east of the basal thrust are mainly siliceous coarse-grained dolostone which are brown in hand sample. As mentioned earlier, the host rocks to the mineralization are mainly altered wackestone facies, which is more similar to the Devonian limestone east of the deposit than to the McKay Group dolostone. In other words, these rocks are probably Devonian in age rather than Ordovician.

As discussed in the previous section, a carbonatite-related origin has been proposed for the Rock Canyon Creek fluorite-REE mineralization. Several authors have suggested that the mineralization is stratabound and apparently occurred prior to the Jura-Cretaceous deformation (Laramide Orogeny), as no fluorite is observed west of the basal thrust, and the mineralization postdates the deposition of the basal Devonian unit. Another age have been suggested as most other carbonatites in British Columbia are Devo-Mississippian to Early Mississippian in age (Pell, 1987). Dix (1991) suggested that the mineralization is associated with high-angle faulting. Since some fluorite occurrences have been found west of the thrust, the fluorite-REE mineralization occurred during or after syn to post-Laramide deformation (thrusting), and the mineralization is not bound to a single stratigraphic unit. As discussed in Section 6.1, fault breccias, which Dix suggested are a product of faulting associated with mineralization, are suggested here to postdate the mineralization. So, it is most likely that the mineralization occurred during the Laramide Orogeny, but earlier than the formation of late calcite.

CHAPTER VII
CONCLUSIONS

The following conclusions are based on detailed petrographic and geochemical analysis of samples from Rock Canyon Creek fluorite-REE deposit, southeastern British Columbia.

(1) Three major mineralization styles are identified in the study area: disseminated fluorite, breccia-matrix fluorite, and massive fluorite.

(2) Five major types of dolomite have been identified: massive microdolomite, non-ferroan dolomite, saddle dolomite I, coarse ferroan dolomite, and saddle dolomite II.

(3) Three major fluid events have occurred in the study area. Geochemical and petrographic evidence suggest that saddle dolomite I and non-ferroan dolomite were precipitated from a hot, slightly saline fluid that altered the microdolomite, and which represents a pre-mineralization fluid.

(4) Ferroan dolomite and saddle dolomite II are closely associated with the mineralization. Isotopic evidence suggests that they were precipitated from carbonatite-derived F-REE-rich fluids. Both the temperature and the salinity of the fluid decreased with time.

(5) Late calcite, which postdates mineralization, typically has low $\delta^{13}C$ values and radiogenic $^{87}Sr/^{86}Sr$ ratios. These values are similar to those of Laramide vein carbonates in the southern Rocky Mountains suggesting that late calcite was precipitated from the same fluids that formed late- to post-Laramide veins elsewhere in the Rocky Mountains. The recrystallization of limestone is thought to have resulted from the passage of this fluid through the study area

(6) The occurrence of fluorite to the west of the thrust fault indicates that the mineralization postdates Laramide thrusting. This contradicts the previous suggestion that the mineralization is Devonian-Mississippian to early Mississippian in age.

REFERENCES

Al-Aasm, I.S., Taylor, B.E. and South, B., 1990. Stable Isotope Analysis of Multiple Carbonate Samples Using Selective Acid Extraction. *Chemical Geology (Isotope Geoscience Section)*, V.80: 119-125.

Allan. J.R.; Wiggins, W.D.; 1993. *Dolomite Reservoirs, Geochemical Techniques for Evaluating Origin and Distribution*; American Association of Petroleum Geologists, continuing education course note series #36, SPE,1987; pp. 129.

Anderson, G.M; and Macqueen, R.W., 1982, ore deposit models-6. *Mississippi Valley-type lead-zinc deposits: Geoscience Canada*, V.9, p.108-117.

Aulstead, K.L., and Spencer, R.J., 1985; Diagenesis of the Keg River Formation, northwestern Alberta: fluid inclusion evidence. Bulletin of Canadian Petroleum Geology. V. 33, pp.136-183.

Baldock, J. W., 1973, Potassic fenitisation, trachytes and agglomerates at the Bukusu carbonatite complex, Uganda. *Overseas Geology & Mineral Resources*, Vol. 42, pp. 1-24

Bally, A.W., Gordy, P.L., and Stewart, G.A., 1966, Structure, seismic data, and orogenic evolution of the southern Canadian Rocky Mountains. Bulletin of Canadian Petroleum Geology. V.14, pp.337-381.

Banner, J.L. 1995, Application of the trace element and isotope geochemistry of strontium to studies of carbonate diagenesis. *Sedimentology*. V.42, pp.805-824.

Banner, J.L., and Hanson, G.N. 1990. Calculation of simultaneous isotopic and trace element variations during water-rock interaction with applications to carbonate diagenesis. *Geochimica et Cosmochimica Acta*. V.54, pp.3123-3137.

Barber, C., 1974; The geochemistry of carbonbatites and related rocks from two carbonatite complexes, South Nyonza, Kenya. *Lithos*. V.7, p.53-63.

Barker, D.S., 1989, Field relations of carbonatites. In: Bell, K. (Ed.), *Carbonatites: Genesis and Evolution*. Unwin Hyman, London, pp. 38-69.

Bell, K., Dawson, J.B., Farquhar, R.M., 1973. Strontium isotope studies of alkalic rocks: The active carbonatite volcano Oldoinyo Lengai. *Geological Soceity of America*, Vol. 84, pp. 99-102.

Bell, K., Blenkinsop, J., 1989. In: Bell, K. (Ed.), *Carbonatites: Genesis and Evolution*. Unwin Hyman, London, pp. 278-300.

Bending, D.,1978, Flouorite claims, Golden Mining Division. B.C. *Ministry of Engergy, Mines,and Petroleum Resources*, Assessment Report 6978.

Bodnar, R.J., 1993. Revised equation and table for determing the freezing point depression of H_2O-NaCl solutions. *Geochimica et Cosmochimica Acta*, Vol. 57, 683-684.

Boggs, S. 1992. Petrology of Sedimentary Rocks. Macmillan Publishing Company, New York. 707p.

Braithwaite, C.J.R., and Rizzi, G., 1997, The geometry and petrogenesis of hydrothermal dolomites at Navan, Ireland, *Sedimentology*, V.44, p.421-440.

Burruss, R.C., Ging, T.G., Eppinger,R.G., and Samson, I.M., 1992, Laser excited flourescence of REE in flourite: Initial observations with a laser Raman microporobe. *Geochim. Cosmochim. Acta.*, v.56, 2713-2723.

Choquette, P.W., and James, N.P., 1987. Diagenesis 12. Diagenesis in limestones -3. The deep burial environment. *Geoscience Canada*. V.14, pp.3-35.

Clarke, L.B., Le Bas, M.J., and Spiro, B., 1994. Rare earth, trace element and stable isotope fractionation of carbonatites at Kruidfontein, Transvaal, S. Africa. Proceedings of the 5th Kimberlite Conference, V.1., Kimberlite, related rocks and mantle xenoliths. p.263-251.

Clarke, D.J., 1998. Petrology, geochemistry and diagenesis of the Middle Devonian Slave Point Formation, Hamburg Sield, northwestern Alberta. [M.Sc. thesis]:Windsor, Ontario, University of Windsor. 126p.

Dapples, E.C., 1959. The behaviour of silica in diagenesis. In H.A. Ireland (e.d.), Silica in Sediments. Society Economy of Paleotology Mineralogy, Special Publication. #7, pp.36-54.

Deines, P., 1989, Stable isotope variations in carbonatites. In: Bell, K., (Ed.) *Carbonatites: Genesis and Evolution*. Unwin Hyman, London, pp. 301-359

Deines, P., Gold, D.P., 1973, The isotopic composition of carbonatites and kimberlite carbonates and their bearing on the isotopic composition of deep-seated carbon. *Geochimica et Cosmochimica Acta*, Vol. 37, 1709-1733.

Deines, P., Langmuir D., Harmon R.S., 1974. Stable carbon isotope ratios and the existence of a gas phase in the evolution of carbonate ground waters. Geochimica et Cosmochimica Acta. V.38, No. 7, pp1147-1164.

Dickson, J.A., 1965, Carbonate identification and genesis as revealed by staining. Journal of Sedimentary Petrology. V.27, pp.107-118.

Dix, G.R., 1991, Report on the stratigraphy, structure and soil geochemistry of the flourite-REE prospect on the Deep Purple - Candy claims (Minfile 082JSW018), Southeastern British Columbia. Unpublished Report, Active Minerals Ltd.

Dunham, R.J., 1962. Classification of carbonate rocks. *In* Classification of carbonate rocks, a symposium. *Editedy by* W.E. Ham. American Association of Petroleum Geologists, Memoir 1, pp.108-121.

Eby, G. H., 1975; Abundance and distribution of the rare earth elements and yttrium in the rocks and minerals of the Oka carbonatite complex, Quebec. *Geochimica et Cosmochimica Acta*, Vol. 39, 597-620.

Faure, G., Powell, J.L., 1972. *Strontium Isotope Geology*. Berlin: Springer.

Faure, G., 1986. *Principle of isotope geology*. Second edition, John Wiley & Sons, New York, 589p.

Fritz, W.H., Cecile, M.P., Norford, B.S., Morrow, D., Geldsetzer, H.H.J., 1991, Cambrian to Middle Devonian assemblages, in Gabrielse, H., and Yorath, C.J., editors, *Geology of the Cordilleran Orogen in Canada: Geological Survey of Canada*, Geology of Canada, no.4, pp.151-218.

Gammons, C., Wood, S.A., and Williams-Jones,A.E., 1996, The aqueous geochemistry of the rare earth elements and yttrium: VI. Stability of neodynium chloride complexes from 25 to 300 °C: *Geochimica et Cosmochimica Acta*, V. 60, p. 4615-4630.

Graf, C., 1981, Geochemical report, Candy Claims, Golden Mining Division NTS 82J/3E. British Columbia Ministry of Energy, Mines and Petroleum Resources, Assessment report 9960.

Graf, C., 1985. Geological report on the DP 1,2,3 and Candy Claims, Rare-earth element-fluorite prospect. British Columbia Ministry of Energy, Mines and Petroleum Resoureces, Assessment report 14677.

Graven, G., Sverjensky, D.A.; 1994; Paleohydrogeology of the Canadian Rockies and Origins of brines, Pb-Zn Deposits and Dolomitization in the Western Canada Sedimentary Basin: Comment; *Geology*; Vol. 297, pp.1149-1150

Gregg, J.M.; and Sibleyu, D.F.; 1984, Epigenetic dolomitization and the origin of xenotopic dolomite texture: *Journal of Sedimentary Petrology.*, V.54, p.908-931.

Gregg, J.M; 1985, regional epigenetic dolomitization in the Bonnetterre dolomite (Cambrian), Southeastern Missouri; *Geology*, V. 13, p.503.

Haas, J.R., Shock,E.L., and Sassani,D.C., 1995, Rare earth elements in hydrothermal systems: Estimates of standard partial molar thermodynamic properties of aqueous complexes of the rare earth elements at high pressures and temperatures: *Geochimica et Cosmochimica Acta.*, V. 59, P. 4329-4350.

Hamilton, E.I., Deans, T., 1963. Isotopic composition of strontium in some African Carbonatites and Limestones and in strontium minerals. *Nature*, Vol. 198, pp.776-777.

Heinrich, E.W., 1966. The geology of carbonatites. Chicago: Randy Mcnally.

Hesse, R., 1989. Silica Diagenesis: origin of inorganic and replacement cherts. *Earth Science Review*. V.26, pp.253-284.

Hogarth, D.D., 1989. Pyrochlore, apatite and amphibole: distinctive minerals in carbonatite. *In*: Bell, K. (Ed.), *Carbonatites: Genesis and Evolution*. Unwin Hyman, London, pp. 105-148.

Hora, Z.D. and Kwong, Y.D.J., 1986, Anomalous rare earth elements (REE) in the Deep Purple and Candy claims. B.C. Ministry of Energy, Mines, and Petroleum Resources, *Geological Fieldwork 1985*, Paper 1986-1,p. 241-242.

Kapustin, K. L., 1966; Geochemistry of rare earth elements in carbonatites. *Geochemistry. International*, V.3: 1054.

Kerr, I.D., 1995, Mineralogic and paragenetic studies of the Rock Canyon Creek fluorite-rare earth element deposit, British Columbia. Unpublished Bsc thesis, University of Windsor, 33p.

Knudsen, C., Buchardt, B., 1991. Carbon and oxygen isotope composition of carbonates from the Qaquarssuk Carbonatite Complex, Southern West Greenland. *Chemical Geology*. Vol. 12, 263-274.

Koffyberg, A., 1993, Strontium isotopic constraints on the geochemistry and origins of regional vein-forming fluids in the southern Canadian Cordillera [M.Sc. thesis]: Edmonton, Alberta, University of Alberta, 102p.

Krause, 1988, chemical and isotopic evidence of thermalchemical sulfate reduction by light hydrocarbon gases in deep carbonate reservoirs; *nature*, V.333, p.415-419.

Land, L.S., 1983. The application of stable isotopes to studies of the origin of dolomite and to problems of diagenesis of clastic sediments. *In* Stable isotopes in sedimentary geology. *Society of Economic Paleontologists and Mineralogists*, Short Course #10, 4-1 to 4-22.

Leach, D.L., Plumlee, G.S., et al., 1991, Origion of late cement by CO2 saturated deep basin brines: evidence from the Ozark region, central U.S., *Geology*, V.19, p.384-351.

Leach, D.L, 1979, Temperature and salinity of the fluids responsible for minor occurences of sphalerite in the Ozark region of Missouri, *Ecnomic Geology*, v.74, p.931-937.

Le Bas, M.J., Spiro, B., Yang, X.M., 1997, Oxygen, carbon and strontium isotope study of the carbonatitic dolomite host of the Bayan Obo Fe-Nb-REE deposit, Inner Mongolia, N CHINA. *Mineralogical Magazine*, Vol. 61, pp. 531-541.

Leech,G.B., 1979, Kananaskis Lakes map area,NTS 82J,*Geological Survey of Canada,Open file 634*.

Machel, H.G., 1987. Saddle dolomite as a by-product of chemical compaction and thermochemical sulphate reduction. *Geology*. V.15, pp.936-940.

Machel H.G., and Mountjoy, E.W., 1986. Chemistry and environments of dolomitization a reappraisal. Earth Science Reviews. V.23, pp.175-222.

Mariano, A.N., 1988. Some further geological applications of cathodoluminescence. *In* Cathodoluminescence of Geological Materials. Edited by D.J. Marshal. Boston UNWIN HYMAN.

Mattes, B.W., and Mountjoy, E.W., 1980, Burial dolomitization of the Upper Devonian Miette buildup, Jasper National Park, Alberta, in Zenger, D.H., Dunham, J.B., and Ehington, R.L., eds., *Concepts and models of dolomitization*: Society of Economic Paleontologists and Mineralogists. Special Publication. V.28, p.269-297.

Mitchel, R. H., and Brunfelt, A. O., 1975; Rare earth geochemistry of the Fen alkaline complex, Norway. Contribution Mineral. *Petrology*. V.52, pp.247-259.

Morrow, D. W., Cumming, G. L., Koepnick, R.B., 1986. Manetoe facies – a gas-bearing, megacrystalline, Devonian dolomite, Yukon and Northwest Territories, *Canada*. *American Association of Petroleum Geologists Bulletin*, V.70, pp.702-720.

Morrow, D.W., 1982. Descriptive filed classification of sedimentary and diagenetic breccia fabrics in carbonate rocks. *Bulletin of Canadian Petroleum Geology*. V.30, pp.227-229.

Mott. J.A., Dixon, J. M., and Helmstaedt, H., 1986, Ordovician stratigraphy and the structural style at the Main Ranges-Front Ranges boundary near Smith Peak, British Columbia. In Current Research, Part B, *Geological Survey of Canada*, Paper 86-1B, p. 457-465.

Mountjoy, E.W., Qing, H., and McNutt, R.H., 1992. Strontium isotopic composition of Devonian dolomites, Western Canada Sedimentary Basin: significance of sources of dolomitizing fluids. Applied Geochemistry. V.7, pp.59-75.

Mueller, W., 1986, *Internal* Newmont petrograhic report,

Neilson, T.F.D., Buchardt, B., 1985, Sr-C-O isotope in nephelinitic rocks and carbonatites, Gardiner complex, Tertiary of East Greenland. *Chemical Geology*, Vol. 53, pp.207-217.

Nesbitt, B. E., Muehlenbachs, K.; 1994; Paleohydrogeology of the Canadian Rockies and Origins of Brines, Pb-Zn Deposits and Dolomitization in the Western Canada Sedimentary Basin; *Geology*, Vol.22, pp.243-246.

Nesbitt, B. E., Muehlenbachs, K.; 1994; Paleohydrogeology of the Canadian ROckies and Origins of brines, Pb-Zn Deposits and Dolomitization in the Western Canada Sedimentary Basin: Reply; *Geology*; Vol. 297, pp.1150-1151

Nesbitt, B. E., Muehlenbachs, K.; 1991; Stable Isotopic Constraints on the Nature of the Syntectonic Fluid Regime of the Canadian Cordillera; *Geophysical Research Letters*; Vol. 18, No. 5, pp. 963-966.

Nesbitt, B.E., and Muehlenbachs, K., 1997. Paleo-hydrogeology of Late Proterozoic units of southeastern Canadian Cordillera. *American Journal of Science*. V.297, pp.359-392.

Nesbitt, B.E., and Muehlenbachs, K., 1995. Geochemical studies of the origins and effects of synorogenic crustal fluid in the southern Omineca Belt of British Columbia, Canada. *Geological Society of America Bulletin*. V.107, pp.1033-1050.

Nesbitt, B.E., and Muehlenbachs, K., 1993. Crustal hydrogeology of the Rockies: Implications to the origins of brines and Pb-Zn mineralization in the Western Canada Sedimentary Basin. Geological Association of Canada Annual Meeting Programme with Abstracts, V.18, p.A-76.

Norford, B. S.; 1981; Devonian Stratigraphy ar the Margins of the Rocky Mountain Trench, Columbia River, Southeastern British Columbia; *Bulletin of Canadian Petroleum Geology*; Vol. 29, No.4, pp.540-560.

Packard, J. J., Pellegrin, G. J., Al-Aasm, I.S., Samson, I.M., and Gagnon, J., 1990. Daigenesis and dolomitization associated with hydrothermal karst in Famennian Upper Vabmun ramp sediments, northwestern Alberta. *In* The development of porosity in carbonate reservoirs. Edited by G. R. Bloy and Mo G. Hadley. *Canadian Society of Petroleum Geologists, Short Course Notes*, pp. 9-1 to 9-19.

Pell, J. 1987, Alkaline ultrabasic rocks in British Columbia: Carbonatites, nepheline syenites, kimberlites, ultramafic lamprophyres and related rocks. B.C. Ministry of Energy, Mines and Petroleum Resources, Open File 1987-17, 109 p.

Pell, J., 1992, Flourspar and flourine in British Columbia. B.C. Ministry of Energy, Mines and Petroleum Resources, Open File 1992-16, 81 p.

Pell, J., Culbert, R. and Fox, M., 1989, The Kechika yttrium and rare-earth prospect. B.C. ministry of Energy, Mines and Petroleum Resources, *Geological Fieldwork 1988*, Paper 1989-1, p. 417-421.

Pell, J. and Hora, Z. D., 1987, Geology of the Rock Canyon Creek fluorite/rare earth element showing, southern Rocky Mountains. B.C. Ministry of Energy, Mines and Petroleum Resources, *Geological Filework 1986*, Paper 1987-1, p. 255-261.

Pell, J., and Fontaine, 1988, Fluorspar in British Columbia. In British Columbia Ministry of Energy, Mines and Petroleum Resources, *Geological Fieldwork 1987*, Paper 1988-1, p.469-482.

Plumlee, G. S., Leach, D. L., et al., 1994, Chemical Path Modeling of ore deposition in Mississippi Valley-type Pb-Zn deposits of the Ozark region, U.S. Midcontinent, *Economic Geology*, V.89, pp.1361-1383.

Powell, J. L., Hurley, P.M., Fairbairn, H. W., 1962. The isotopic composition of strontium in carbonatites. *Nature*, Vol. 196, pp.1085-1086.

Powell, J. L., 1966. Isotopic composition of strontium in carbonatites and kimberlites. In: *International Mineralogical Association Fourth General Meeting Papers and proceedings*, P.R.J., Naidu & M.N., Viswanathiah (eds), pp.58-66. Mysore: Mineralogical Soceity of India.

Price, R.A., 1981, The Cordillerian thrust and fold belt in the southern Canadian Rocky Mountains. *In* McClay, K.R., Price, N.J., editors, *Trust and Nappe Tectonics*: Geological Society of London, Special Publication. V.9, pp.427-338.

Price, R.A., and Mountjoy, E.W., 1970, Geologic structures of the Canadian Rocky mountains between Bow and Athabaska rivers-a progress report, *in* Wheeler, J.O., editor, Structure of the Southern Canadian Cordilelra: *Geological Association of Canada, Special Paper*, v.6, pp.7-25.

Qing, H., and Mountjoy, E.W., 1994, Formation of Coarsely crystalline, hydrothermal dolomite reservoirs in the Presqu'ile Barrier, Western Canada Sedimentary Basin, *AAPG Bulletin*, V.78, No.1, p.55-77.

Qing, H., Mountjoy, E.W., 1992; Large-scale fluid flow in the Middle Devonian Presqu'ile Barrier, Western Canada Sedimentary Basin; *Geology*; Vol. 20, pp.903-906.

Reading, H.G., 1986, *Facies. In* Sedimentary environments and facies. *Edited by* H.G. Reading. Blackwell Scientific publications, Oxford, pp.4-19.

Reid, D.L., Cooper, A. F., 1992, Oxygen and carbon isotope patterns in the Dicker Willem carbonatite complex, southern Namibia. *Chemical Geology*. Vol. 94, pp.293-305.

Ricketts, B.D., ed., 1989, Western Canada Sedimentary Basin: A case history: Calgary, Alberta. *Canadian Society of Petroleum Geologists*. 320p.

Robinson, R.A., 1964, Upper Middle Cambrian stratigraphy of western Utah; *Bulletin of Geological Society of America*, Vol. 75, pp. 995-1010.

Roedder, E., 1977, Fluid inclusion studies of ore deposits in the Viburnum Trend, Southeast Missouri, *Economic Geology*, V.72, pp.474-479.

Roedder, E., 1984. Fluid inclusion. Reviews in mineralogy. Mineralogical Society of America. Vol.12, 644p.

Rowan E.L., and Leach, D.L., 1989, Constraints from fluid inclusion on sulfide precipitation mechanism and ore fluid migration in the Viburnum Trend Lead Districts, Missouri., *Economic Geology*, V.84, pp.1948-1965.

Salvi, S. and William-Jones, A.E., 1997. Fluid inclusion volatile analysis by gas chromatography: Application of a wide-bore porous-polymer capillary column to the separation of organic and inorganic compounds. *The Canadian Mineralogists*. V.35, pp.1391-1414.

Santos, R.V., and Clayton, R.N., 1995, variation of O and C isotopes in carbonatities: A study of Brazilian alkaline complexes, *Geochimica et Cosmochimica Acta*, V.59, No.7, pp.1339-1352.

Schofield, A., and Haskin, L., 1964; Rare –earth distribution pattern in eight terrestrial materials. *Geochimica et Cosmochimica Acta*. V.28, pp.437-446.

Shelton, K.L., Bauer, R.M., Gregg, J.M., 1992, fluid inclusion studies of regionally epigenetic dolomites, Bonetterre Dolomite (Cambiran), Southeast Missouri: Evidence of Multiple fluids during dolomitization and lead-zinc mineralization, *Geological Society of America bulletin*, V.104, p.675-683.

Shinn, E.A., and Robbin, D.M., 1983. Mechanical and chemical compaction in fine-grained shallow water limestone. *Journal of Sedimentary Petrology*. V.53, pp.595-618.

Sibley, D.F., and Greg, J.M., 1987, Classification of dolomite rock textures. *Journal of Sedimentary Geology*. V.57, pp.967-975.

Steinhauf, D.M., 1989. Marine cements. *In* The fabric of cements in Paleozoic limestones. *Edited by* K.R. Walker. Geological Society of America, Short Course #20, 37-53.

Sutherland, D.S., 1965, Nomenclature of potassic feldspathic rocks associated with carbonatite. *Geological Society of America, Bulletin.* Vol. 76, pp.1409-1412.

Taylor, H. P., Jr., French J., Degens, E. T., 1967, Oxygen and carbon isotope studies of carbonatites from the Laacher See District, West Germany and Alnꞓ district, Sweden. *Geochimica et Cosmochimica Acta*, Vol.31, 407-430.

Tucker, M.E., 1981. Sedimentary Petrology, an introduction. Blackwell Scientific Publicarions, Oxford, 252p.

Tucker, M.E., and Wright, V.P., 1990. *Carbonate sedimentology*. Blackwell Scientific Publications, Oxford, 482p.

Veizer, J., Brunckschen, P., Pawellek, F., Diener, A., Podlaha, O.G., Carden G.A.F., Jasper, T., Korte, C., Strauss, H., Azmy, K., Ala, D., 1997. Oxygen isotope evolution of Phanerozoic seawater. *Plaeo*, Elsevier, V.132, pp.159-172.

Viets, J. G., Leach, D. L., 1990, genetic implications of regional and temporal trends in ore fluid geochemistry of Mississippi Valley-type deposits in the Ozark region, *Economic Geology*, V.85, pp.842-861.

White, T., and Al-Aasm, I.S., 1997; Hydrothermal dolomitization of the Mississippian Upper Debolt Formation, Sikanni gas field, northeastern British Columbia, Canada. *Bulletin of Canadian Petroleum Geology*, V.45, pp.297-316.

Williams-Jones, A. E., Samson, I. M. and Olivo, G. R., The Genesis of Hydrothermal Fluorite-REE Deposits in the Gallinas Mountains, New Mexico. Submits to Economic *Geological Fieldwork 1986*, Paper 1987-1, p.255-261.

Wood, S. A., 1990, The aqueous geochemistry of the rare-earth elements and yttrium 2. Theoretical predictions of speciation in hydrothermal solutions to $350\,^{0}C$ at saturation vapor pressure: *Chemical Geology*, v. 88, p. 99-125.

Woolley, A. R., Kempe, D. R. C., 1989, Carbonatites: nomenclature, average chemical compositions, and element distribution. In: Bell, K. (Ed.), *Carbonatites: Genesis and Evolution.* Unwin Hyman, London, pp. 1-37.

Wright, V.P., 1992, A revised classification of limestones. *Sedimentary Geology.* V.76, pp.177-185.

Yang, W., 1995; Stable Isotope and Major Element Compositions of Fluid Inclusions in Devonian and Cambrian Cements, Western Canada; *Geochimica et Cosmochimica Acta*, Vol. 59, No. 15, pp. 3159-3172

Yao, Q., Demico, R. V., 1997; Dolomitization of the Cambrian Carbonate Platform, Southern Canadian ROcky Mountains:Dolomite Front Geometry, Fluid Inclusion Geochemistry, Isotopic Signature, and Hydrogeologic Modelling Studies; *American Journal of Science*; Vol. 297, November, 1997, pp.892-938.

Zhu, L., Samson, I.M., and Al-Aasm, I.S., 1999, Hydrothermal carbonates associated with the Rock Canyon Creek fluorite-REE deposit, B.C.: Petrographic and stable isotopic charactertistics: Abstract volume 24, GAC-MAC annual meeting, Sudbury, May, 1999. P.140.

APPENDIX I

Oxygen, Carbon and Strontium Isotope Results

Sample	Description	$\delta^{18}O$ (SMOW)	$\delta^{18}O$ (PDB)	$\delta^{13}C$ (PDB)	$^{87}Sr/^{86}Sr$	Sr^{2+} (ppm)
RCC95-15	cc clast, recrystallized	13.15	-17.23	-5.7		
RCC97-10	cc clast, recrystallized	11.97	-18.37	-7.14		
RCC95-3b-1	cc clast, recrystallized	12.95	-17.42	-5.78	0.70822±19	1488.0
RCC29-1	cc host, recrystallized	14.62	-15.81	-2.17		
RCC95-4	cc host, recrystallized	15.7	-14.72	-2.91		
RCC95-3a	cc host, recrystallized	12.11	-18.43	-6.8		
RCC95-14-1	cc host, recrystallized	16.01	-14.4	-4.41		
RCC95-13	cc host, recrystallized	13.82	-16.58	-6.04		
Average		13.79	-16.62	-5.12		
σ		1.54	1.54	1.79		
RCC32b	cc matrix	14.15	-16.26	-0.73		
RCC95-3b-3	cc matrix	12.95	-17.42	-5.78		
RCC97-11	cc matrix	13.35	-17.03	-4.62	0.70998±21	2069.0
RCC97-26	cc matrix	14.8	-15.62	-2.64		
RCC41-1	cc matrix	11.94	-18.4	-1.41		
RCC97-16	cc matrix	9.56	-20.71	-1.73		
RCC97-10-1	cc matrix	11.7	-18.63	-6.98		
RCC97-25-1	cc matrix	13.39	-16.99	-2.62		
RCC97-23	cc matrix	15.57	-14.88	-1.63		
RCC27	cc matrix	16.57	-13.83	-1.97		
Average		13.39	-16.98	-3.01		
σ		2.034	1.99	2.07		
RCC97-13	Late cc vein	16.42	-14.06	-1.76		
RCC95-14-2	Late cc vein	13.48	-16.91	-5.26		
RCC97-19-1	Late cc vein	15.96	-14.51	-2.14		
RCC97-9	Late cc vein	12.58	-17.78	-3.58		
Average		14.61	-15.82	-3.19		
σ		1.87	1.81	1.59		

Oxygen, Carbon and Strontium Isotope Results (cont'd)

Sample	Description	$\delta^{18}O$ (SMOW)	$\delta^{18}O$ (PDB)	$\delta^{13}C$ (PDB)	$^{87}Sr/^{86}Sr$	Sr^{2+} (ppm)
RCC97-6	Mass cc, Ordovician	20.81	-9.8	-1.24		
RCC23	Mass cc, Ordovician	21.03	-9.59	-1.46		
Average		20.92	-9.69	-1.35		
σ		0.156	0.148	0.156		
RCC95-16	Limestone, Devonian	21.23	-9.39	-1.43		
RCC97-20	Limestone, Devonian	22.58	-8.08	0.12		
RCC95-8	Limestone, Devonian	21.76	-8.48	-0.62	0.70862±14	267.7
RCC97-28	Limestone, Devonian	22.48	-8.18	1.03		
Average		22.01	-8.53	-0.23		
σ		0.64	0.59	1.05		
RCC97-5	Microdolomtie	24.98	-5.75	-1.13		
RCC97-3c	Microdolomite	26.01	-4.75	-0.28	0.70809±28	161.9
RCC97-2	Microdolomite	23.9	-6.8	-1.42		
RCC97-3a	Microdolomite	22.88	-7.79	0.84		
RCC97-1-1	Microdolomite	27.62	-3.19	0.08		
RCC97-1-2	Dolomite Cement	25.68	-5.07	0.08		
RCC97-4a	Microdolomite	24.58	-6.14	-0.74		
Average		25.09	-5.64	-0.37		
σ		1.53	1.49	0.78		
RCC97-15-1	Ferroan Dolomite	17.49	-13.02	-0.55		
RCC95-1	Ferroan Dolomite	16.42	-14.06	-0.79	0.70462±14	1785.0
RCC95-2	Ferroan Dolomite	15.56	-14.89	-0.8		
RCC33c	Ferroan Dolomite	15.51	-14.94	-0.61	0.70384±22	2977.0
RCC44	Ferroan Dolomite	15.23	-15.21	-1.47		
RCC41-2	Ferroan Dolomite	16.08	-14.38	-0.82		
RCC42	Ferroan Dolomite	11.51	-18.81	-2.62	0.70336±11	3571.0
RCC33b-1	Ferroan Dolomite	16.48	-13.99	0.3		
RCC34-1	Ferroan Dolomite	13.88	-16.52	-0.9		
RCC32a	Ferroan Dolomite	16.35	-14.13	0.21		

103

Oxygen, Carbon and Strontium Isotope Results (cont'd)

Sample	Description	$\delta^{18}O$ (SMOW)	$\delta^{18}O$ (PDB)	$\delta^{13}C$ (PDB)	$^{87}Sr/^{86}Sr$	Sr^{2+} (ppm)
RCC95-12	Ferroan Dolomite	15.57	-14.88	-0.12		
RCC95-6	Ferroan Dolomite	15.32	-15.13	-0.34		
RCC43	Ferroan Dolomite	17.22	-13.28	-0.71		
Average		15.59	-14.86	-0.71		
σ		1.54	1.49	0.75		
RCC29-2	saddle dolomite II	11.45	-18.88	-1.91	0.70784±22	703.6
RCC35-2	saddle dolomite II	17.93	-12.95	-1.13		
RCC97-15	saddle dolomite I	14.47	-15.95	-0.2	0.70995±12	539.9
RCC97-5-2	saddle dolomite I	17.43	-13.08	0.14		
Average		15.32	-15.22	-0.78		
σ		2.99	2.81	0.93		
RCC97-13-1	Non-ferroan Dolomite	18.44	-12.1	-0.2		
RCC97-14-2	Non-ferroan Dolomite	19.09	-11.46	-0.05		
RCC95-3b-2	Non-ferroan Dolomite	20.26	-10.02	-1.95		
RCC35-1	Non-ferroan Dolomite	21.22	-9.4	-0.99		
RCC37	Non-ferroan Dolomite	19.94	-10.65	-0.21		
RCC36	Non-ferroan Dolomite	22.44	-8.22	-0.35	0.71082±15	185.5
RCC97-7	Non-ferroan Dolomite	22.23	-8.42	-0.82		
RCC97-21	Non-ferroan Dolomite	22.63	-8.03	-0.92		
RCC97-25	Non-ferroan Dolomite	21.3	-9.32	-0.86		
Average		20.84	-9.74	-0.71		
σ		1.50	1.44	0.59		

Note: CC: Calcite; ±: variations caused by machine.

APPENDIX II

Fluid Inclusion Data

Sample	Host Minerals	Group #	Inclusion #	Origin	Phases	Tn (°C)	Te (°C)	TmICE (°C)	TmHH (°C)	ThLV (°C)	TD (°C)	Salinity wt % NaCl+CaCl₂
Rcc95-1	FDO	1-1-4	1	P	LV	-47.6	-21.4	-9.8		170		13.7
Rcc95-1	FDO	1-1-5	1	P	LV	-58.3	-20.8	-16.2		108		19.6
Rcc95-1	FDO	1-4-5	2	P	LV					183.5		
Rcc95-1	FDO	1-4-5	1	P	LV					183.5		
Rcc95-1	FDO	1-7-1	2	P?	LV						242.7	
Rcc95-1	FDO	1-7-1	1	P	LV			-6.7		193.3		10.1
Rcc95-1	FDO	1-8-1	1	P?	LV						152.5	
Rcc95-1	FDO	1-9-1	1	P	LV					116.5		
Rcc95-1	FDO	1-9-1	2	P	LV			-22.1		202.9		23.8
Rcc95-1	FDO	1-9-2	2	P	LV					176.8		
Rcc95-1	FDO	1-9-2	1	P	LV			-9.3		157.5		13.2
Rcc36	CFL	1-1-1	2	P	LV	-44.7				170		
Rcc36	CFL	1-1-1	3	P	LV	-44.7		-9.2		157.4		13.1
Rcc36	CFL	1-1-1	1	P	LV	-44.7		-9.2		157.4		13.1
Rcc36	ZFL	1-2-1	1	P	LV						122.1	
Rcc36	ZFL	1-2-1	2	P	LV	-48.5		-3.4		156.1		5.6
Rcc36	CFL	1-3-1	1	P	LV+S?	-62.1	-34.9	-8.9		194.4		12.7
Rcc36	CFL	1-3-2	3	P	LV	-62.1				195		
Rcc36	CFL	1-3-2	2	P	LV	-62.1		-10.7		166.8		14.7
Rcc36	CFL	1-4-1	1	PS?	LV	-63.1						
Rcc36	CFL	1-4-1	2	PS?	LV	-63.1		-22.6		192.3		24.1
Rcc36	CFL	1-4-1	3	PS?	LV	-63.1		-16.8		129.7		20.1

Fluid Inclusion Data (cont'd)

Sample	Host Minerals	Group #	Inclusion #	Origin	Phases	Tn (°C)	Te (°C)	TmICE (°C)	TmHH (°C)	ThLV (°C)	TD (°C)	Salinity Wt % NaCl+CaCl₂
Rcc36	CFL	1-4-1	4	P	LV					169.9		
Rcc36	CFL	1-5-1	2	P?	LV						119.7	
Rcc36	ZFL	3-1-1	1	P	LV	-34.9	-21.4	-4.2	-2.8	290.1		6.7
Rcc36	CFL	3-2-1	4	P	LV			-12.4		247.6		16.3
Rcc36	ZFL	3-3-1	1	P	LVS			-5.7		101.1		8.8
Rcc36	ZFL	3-4-1	1	P	LV			-7.2		93.9		10.7
Rcc36	CFL	3-4-2	1	P	LV			-25.7		346.8		26
Rcc36	ZFL	3-5-1	1	P	LVS	-47.3		-4.9		229.8		7.7
Rcc36	CFL	3-5-2	1	P	LVS	-57.4		-10.9		219.6		14.9
Rcc36	CFL	3-5-2	2	P	LVS	-65		-13.7		219.1		17.5
Rcc37	CFL	1-1-1	1	P	LV						84.1	
Rcc37	ZFL	1-1-2	1	P?	LV						172.4	
Rcc37	ZFL	1-1-2	2	P?	LV						104.9	
Rcc37	ZFL	1-2-1	1	P	LV	-56.3		-8.34		97.1		12.1
Rcc37	ZFL	1-2-1	2	P	LV	-56.3		-5.4		102.8		8.4
Rcc37	ZFL	1-2-2	1	P?	LV		-27.8			291.4		
Rcc37	CFL	1-3-1	2	P	LV						102.6	
Rcc37	CFL	1-3-1	1	P	LV			-17.7		109.5		20.7
Rcc37	CFL	1-3-3	2	P?	LV							
Rcc37	CFL	1-3-3	1	P	LV	-49.2	-22.8	-13.1		229.3		17
Rcc37	ZFL	1-4-1	1	P	LV					125.3	202.3	
Rcc37	ZFL	1-4-1	2	P	LV						202.3	
Rcc37	ZFL	1-4-2	1	P	LV	-48.3		-9.5		132.3		13.4
Rcc37	ZFL	1-5-1	1	P	LV						159.2	

Fluid Inclusion Data (cont'd)

Sample	Host Minerals	Group #	Inclusion #	Origin	Phases	Tn (°C)	Te (°C)	TmICE (°C)	TmHH (°C)	ThLV (°C)	TD (°C)	Salinity Wt % NaCl+CaCl₂
Rcc37	ZFL	1-5-1	2	P	LV	-48.5		-3.9		249.4		6.3
Rcc37	ZFL	1-6-1	1	P	LV	-50.5	-16.9	-7		172.5		10.5
Rcc37	ZFL	1-7-1	1	P	LV	-37.1		-2		100.7		3.4
Rcc37	CFL	1-7-2	1	P?	LV							
Rcc37	CFL	1-8-1	1	P	LV	-48.5		-10.2		162.5		14.1
Rcc45	DFL	1-1-1	1	PS?	LV							
Rcc45	DFL	1-1-2	1	PS?	LV	-56.3		-20.2		274.1		22.5
Rcc45	DFL	1-2-2	4	P	LV	-64.8		-21.7		223.8		24.8
Rcc45	DFL	1-2-2	1	P	LV	-64.8		-23.8		223.8		23.5
Rcc45	DFL	1-2-2	3	P	LV						271.9	
Rcc45	DFL	1-3-1	1	P	LV	-44.5		-8.9		184.2		12.7
Rcc45	DFL	1-3-2	1	P	LVS	-56.8		-10.5		118.2		14.5
Rcc95-1	DFL	1-1-1	1	PS?	LV	-55.6	-27.2	-10.5		163.4		14.5
Rcc95-1	DFL	1-1-3	3	PS?	LV					190.5		
Rcc95-1	DFL	1-1-3	2	PS?	LVS	-30.1		-2.5		190.5		4.2
Rcc95-1	DFL	1-1-3	1	PS?	LVS	-60.2		-12		113.7		16
Rcc95-1	DFL	1-2-2	1	PS?	LV	-57.3		-13.5				17.3
Rcc95-1	DFL	1-4-1	1	PS?	LVS			-11.74		159.2		15.7
Rcc95-1	DFL	1-4-1	3	PS?	LVS			-11.5		182.3		15.5
Rcc95-1	DFL	1-4-1	2	PS?	LV					119.4	145.7	
Rcc95-1	DFL	1-4-3	1	P?	LVS			-9.8		190.2		13.7
Rcc95-5	DFL	1-2-2	1	P	LV	-68				199.8		
Rcc95-5	DFL	1-3-1	1	P	LVS	-72.6		-21.9		174		23.6

Fluid Inclusion Data (cont'd)

Sample	Host Minerals	Group #	Inclusion #	Origin	Phases	Tn (°C)	Te (°C)	TmICE (°C)	TmHH (°C)	ThLV (°C)	TD (°C)	Salinity wt % NaCl+CaCl₂
Rcc95-5	DFL	1-6-1	1	P	LV			-22.7		219.3		24.1
Rcc95-5	DFL	1-6-1	2	P	LV						209.5	
Rcc97-16	LCC	1-1-1	5	P	LV					209.7		
Rcc97-16	LCC	1-1-1	3	P	LV					208.7		
Rcc97-16	LCC	1-1-1	4	P	LV					154.5		
Rcc97-16	LCC	1-1-1	1	P	LV			-20.6		94.9		22.8
Rcc97-16	LCC	1-1-1	2	P	LV					131.2		
Rcc97-16	LCC	1-2-1	2	P	LV					154.1		
Rcc97-16	LCC	1-2-1	3	P	LV			-15.4		208.4		19
Rcc97-16	LCC	1-3-1	5	P	LV			-21.9		200		23.6
Rcc97-16	LCC	1-3-1	7	P	LV					210		
Rcc97-16	LCC	1-3-1	6	P	LV					174.9		
Rcc97-16	LCC	1-3-1	2	P	LV					161.9		
Rcc97-16	LCC	1-3-1	3	P	LV			-17.1		179.2		20.3
Rcc97-16	LCC	1-3-1	1	P	LV			-18.4		161.9		21.3
Rcc97-16	LCC	1-3-1	4	P	LV					179.2		
Rcc97-16	LCC	1-3-2	1	P	LVS	-54.4		-16.4		209.9	362.2	19.8
Rcc97-16	LCC	1-3-2	2	P	LVS	-60.2		-21.9		240.8		23.6
Rcc97-16	LCC	1-3-3	1	P	LVS	-48.5		-12.6		214.6		16.5
Rcc97-16	LCC	1-4-1	1	P	LV	-59	-23.1	-19.5		228		22
Rcc97-16	LCC	1-4-1	2	P	LV					126		
Rcc97-16	LCC	1-5-1	1	P	LV	-66		-13.6		130.1		17.4
Rcc95-3b	NFD	1-1-5	1	P	LV	-51.5		-10.7		183.5		14.7

Fluid Inclusion Data (cont'd)

Sample	Host Minerals	Group #	Inclusion #	Origin	Phases	Tn (°C)	Te (°C)	TmICE (°C)	TmHH (°C)	ThLV (°C)	TD (°C)	Salinity Wt % NaCl+CaCl$_2$
Rcc95-3b	NFD	1-3-1	2	P	LV					200		
Rcc95-3b	NFD	1-3-1	4	P	LV					193.1		
Rcc95-3b	NFD	1-3-1	1	P	LV					195.7		
Rcc95-3b	NFD	1-3-1	3	P	LV					193.1		
Rcc95-3b	NFD	1-3-2	1	P	LV					209.3		
Rcc95-3b	NFD	1-3-3	2	P	LV					192.6		
Rcc95-3b	NFD	1-3-3	1	P	LV					186.9		
Rcc95-3b	NFD	1-4-1	3	PS?	LV					181.7		
Rcc95-3b	NFD	1-4-2	1	P	LV					233.2		
Rcc97-10	Qz	1-1-1	2	P	LV					386.5		
Rcc97-10	Qz	1-1-1	1	P?	LV						303	
Rcc29	SD	1-1-1	1	P	LV					116.5		
Rcc29	SD	1-1-1	2	P	LV					182.1		
Rcc29	SD	1-1-2	1	P	LV					172.4		
Rcc29	SD	1-2-1	1	P	LV					189.3		

Notes: FDO: Ferroan Dolomite   CFL: Colourless Fluorite   ZFL: Zoned Fluorite
DFL: Disseminated Fluorite   LCC: Late Calcite   NFD: Non-ferroan Dolomite
QZ: quartz   SD: Saddle Dolomite II

APPENDIX III
INTRODUCTION AND FORMULAE FOR
GEOCHEMICAL MODELING

Introduction

Geochemical modeling was used in this study in order to: 1) determine the necessary conditions, especially fluid isotopic compositions, required to chemically alter sedimentary carbonates to various dolomite and calcite phases; 2) compare the results of this modeling with actual geochemical data from Rock Canyon Creek; 3) determine if the precipitating environment proposed for the alteration of the phase are compatiable with fluid composition suggested by the model.

The equations used in the geochemical modeling were taken from Banner and Hanson (1990). Mass balance equations were employed to monitor simultaneous variations in the isotopic composition of the fluid and solid as a function of water/rock ratio during water/rock interaction. The mass balance equations allow comparisons to be made between the proposed water/rock interaction model and the actual geochemical data. The series of equations are summarized below.

The modeling is performed for a porous mineral-fluid system where the fluid passes through the pores of a given volume of rock, and where a particular mineral is altered in increments of fluid. The basic assumption is that mineral and fluid reach isotopic and elemental equilibrium before the next increment of fluid is introduced into the system. Numerous iterations are performed until, at a certain water/rock ratio, the entire system reaches equilibrium.

The variables which control the chemical composition of the carbonate minerals are the isotopic composition of the fluid, the isotopic composition of the original sediments, water/rock ratio, the fractionation factor (temperature dependent), whether open- or closed system behavior is assumed, and porosity. All of these parameters are selected by the user except for the water/rock ratio, which is dependent on the porosity of the original sediment.

Formulae

The following set of equations is taken from Banner and Hanson (1990), and was used for modeling element and isotopic variations during fluid-rock interaction.

The initial concentration of element (I) in the system, C_o^I, is determined by:

$$C_o^I = F \times C_{f,o}^I + (1 - F) \times C_{s,o}^I \qquad (1)$$

Where F is the weight fraction in the system for any iteration, $C_{f,o}^I$ and $C_{s,o}^I$ are the initial concentrations of element (I) in the fluid and solid before interaction, respectively.

F is related to the amount of porosity in the altered rock and the density of the fluid and rock by:

$$F = \frac{P \times \rho_f}{P \times \rho_f + (1 - P)\rho_s} \qquad (2)$$

Where P is porosity in volume fraction or weight fraction, and ρ_s and ρ_f are the densities of the solid and fluid, respectively.

The cumulative fluid/rock ratio, N, at any stage of the modeling process is determined by:

$$N = n \times (F(1 - F)) \qquad (3)$$

Where n is the number of iterations, and $F/(1 - F)$ is the incremental fluid/rock ratio.

The single element distribution coefficient, D^I, is used to calculate the concentration of element (I) in the solid, Cs^I, after the equilibration with the fluid:

$$C_s^I = \frac{C_o^I}{F/D^I + (1 - F)} \qquad (4)$$

Calculation of the change in the composition of the rock upon repeated addition of fluid with the same initial composition simulates open-system fluid-rock interaction. These changes are determined by iterative calculations, using first equation (1) and then equation (4) in which the composition of the rock in equation (1), $C_{s,o}^I$, is derived from the previous calculation of C_s^I using equation (4).

For modeling of the strontium concentration and strontium isotope composition in the fluid/rock system, the initial concentration of the system, C_o^{Sr}, is determined using equation (1), and the concentration of strontium in the solid, C_S^I, following equilibration with the fluid is calculated using equation (4).

The strontium isotope ratio for the system, $(^{87}Sr/^{86}Sr)_o$, prior to any interaction is governed by the following equation:

$$(^{87}Sr/^{86}Sr)_o = \frac{(^{87}Sr/^{86}Sr)_{f.o}(C_{f.o}^{Sr})F + (^{87}Sr/^{86}Sr)_{s.o}(C_{s.o}^{Sr})(1-F)}{C_o^{Sr}} \qquad (5)$$

Where $(^{87}Sr/^{86}Sr)_{f.o}$ represent the strontium isotope ratio of the fluid, and $(^{87}Sr/^{86}Sr)_{s.o}$ the strontium isotope ratio of the solid.

Following calculation of the original strontium isotope ratio, the concentration of strontium in the solid, $C^I s$, is substituted for the original concentration of strontium in the solid, $C^{Sr}_{s.o}$ to calculate successive strontium ratios.

For the oxygen isotopic composition of the system, $\delta^{18}O_o$, for each iteration is calculated by:

$$\delta^{18}O_o = \frac{(\delta^{18}O_{f.o})(C_{f.o}^O)F + (\delta^{18}O_{s.o})(C_{s.o}^O)(1-F)}{C_o^O} \qquad (6)$$

Where $\delta^{18}O_{f.o}$ and $\delta^{18}O_{s.o}$ are the oxygen isotopic composition (SMOW), prior to interaction for the fluid and solid respectively. And C_o^O is constant for a given F, because $C_{f.o}^O$ and $C_{s.o}^O$ are constant. After equilibration, $\delta^{18}O_s$ and $\delta^{18}O_f$ are related by:

$$\delta^{18}O_s = \alpha(\delta^{18}O_f + 1000) - 1000 \qquad (7)$$

and $\delta^{18}O_s$ is given by:

$$\delta^{18}O_s = \frac{(\delta^{18}O_o)C_o^O(\alpha_{s-f}^{18\ 16}) - 1000(C_f^O)F(1 - (\alpha_{s-f}^{18\ 16}))}{C_s^O(1-F)(\alpha_{s-f}^{18\ 16}) + C_f^O(F)} \qquad (8)$$

where $\alpha_{s-f}^{18\ 16}$ is the isotopic fractionation factor for oxygen between the solid and the fluid phase, and is temperature dependent. For the next fluid/rock interaction, $\delta^{18}O_s$ from this

equation is substituted into the previous equation to calculate the new $\delta^{18}O_o$ and the new $\delta^{18}O_s$, and the process is continued until the fluid/rock system reaches the equilibrium, i.e. the fluid can no longer alter the isotopic composition of the solid.

Modeling of the carbon isotopic system can be accomplished by substituting $\delta^{13}C$ for $\delta^{18}O$ in the above equations, and applying the appropriate fractionation factor (α) for carbon in equations (7) and (8).

VITA AUCTORIS

NAME:	Lichun Zhu
PLATE OF BIRTH:	Ji`an, Jiangxi, P.R.CHINA
YEAR OF BIRTH:	1970
EDUCATION:	University of Windsor, Windsor, Ontario, Canada
	1997-2000 M.Sc. (Geology)

Chengdu Institute of Technology, Chengdu, P.R.CHINA

1993-1996 M.Sc. (Petroleum Geology)

Chengdu Institute of Technology, Chengdu, P.R.CHINA

1989-1993 B.Sc. (Geology)